AN ABSTRACT OF THE THESIS OF

Entsung Hsiao for the degree of Doctor of Philosophy in Mechanical Engineering presented on November 20,1990.

Title: An Experimental/Analytical Investigation of Buoyant Jets in Shallow Water.

Abstract approved: Redacted for Privacy
Lorin R. Davis

This thesis presents the results of an experimental and analytical study of single-port buoyant turbulent jets discharged into shallow water. The experimental results include the measured downstream dilution, centerline concentration and trajectory. Independent parameters considered were Froude number, submerged depth, discharge angle and velocity ratio.

Results indicate that decreasing the discharge depth provides earlier occurrence of surface effect and greatly decreases dilution. Dilution increases with decreasing Froude number. Increasing the discharge angle from the horizontal into cross current increases the dilution ratio. The effect of ambient current on dilution depends on the angle of discharge. For cross-flow discharges, the dilution rate decreases with increasing ambient current, while for co-flow discharge the reverse trend was observed. As plumes reach the water surface, the dilution rate increases with increasing ambient velocity. The

jets bend over rapidly for cross-flow discharges when large ambient currents are present.

The analytical portion of this report presents an integral method proposed by Davis (1975) for merging multiple buoyant jets. This merging model was used to simulate the single-port buoyant jet in shallow water. This was done by using an image method where the submerged depth was simulated by the spacing between images. The entrainment function as presented by Kannberg and Davis (1978) was used except for a modification within the zone of merged plumes.

Comparisons of the model prediction were made with experimental data. Results indicate that good predictions are obtained for buoyant jets discharging at 0 and 45 degrees into shallow water by using the image method as long as the Froude number is above 13.5. For lower Froude number and vertical discharges, model predictions are only fair.

An Experimental/Analytical Investigation of Buoyant Jets in Shallow Water

by

Entsung Hsiao

A THESIS

submitted to

Oregon State University

in fulfillment of the
requirements for the
degree of

Doctor of Philosophy

Completed November 20, 1990

Commencement June 1991

APPROVED

Redacted for Privacy

Professor of Mechanical Engineering
in charge of major

Redacted for Privacy

Head of Department Mechanical Engineering

Redacted for Privacy

Dean of Graduate School

Date thesis is presented November 20, 1990

Typed by Entsung Hsiao for Entsung Hsiao

ACKNOWLEDGEMENTS

It is great pleasure that I acknowledge the inspirational guidance, encouragement and continuing advice of my adviser, Dr. Lorin R. Davis, during the completion of this research. Without him this work would not have been possible.

I would also like to express my sincere appreciation to Dr. James R. Welty, Dr. Ronald B. Guenther and Dr. Richard B. Peterson for their advice. Appreciation is also extended to the faculty, staff in the Department of Mechanical Engineering for their advice and help during my years at Oregon State University.

I must also acknowledge my parents for their unending support and my wife Julie for her understanding and patience during my studies in Oregon State University.

TABLE OF CONTENTS

LIST OF FIGURES

LIST OF TABLES

LIST OF APPENDIX FIGURES

LIST OF NOMENDATURE AND SYMBOLS

a	Entrainment coefficient
$a_{0,1,2,..}$	Entrainment coefficients and regression fit coefficients
b	3/2 power profile plume half width
b_1	b/0.53
C	Concentration
C_0	Concentration at discharge
C_∞	Ambient Concentration
$\Delta C/\Delta C_0$	$(C-C_\infty)/(C_0-C_\infty)$
$\Delta C_m/\Delta C_0$	Maximun valus of normalized concentration deficit
c_v	Specific heat
$c_{1,2...}$	Entrainment coefficients for zone of flow establishment
D	Port diameter
E	Entrainment
Fr	Densimetric Froude Number = $U_0 \,/(gD\Delta\rho/\rho)^{1/2}$
g	Graitational constant
H	Submergence depth
k	Thermal conductivity
L	Distance between ports
P	Pressure
R	Velocity ratio = U_∞/U_0 and equivalent resistance measured by conductivity probe
r	Plume radius and plume coordinate
r_c	Species core radius
r_t	Temperature core radius
r_u	Velocity core radius

r_0	Discharge port radius
s	Centerline coordinate
Se	Starting length
T	Temperature
T_∞	Ambient Temperature
T_0	Discharge Temperature
T_c	Centerline Temperature
ΔT_c	$T_c - T_\infty$
ΔT_0	$T_0 - T_\infty$
U_0	Discharge Velocity
U_∞	Ambient Velocity
u	Velocity in the s direction
u_c	Centerline velocity in the s direction
v	Velocity in radial
W	Plume width, vertical or X-sectional
X	Horizontal downstream distance and coordinate
Y	Vertical coordinate and height above port
Z_0	Height of port above the channel bottom
β	Coefficient of thermal expansion
γ	Coefficient of Species concentration expansion
ϵ	Eddy diffusivity
ζ	Merging coordinate along line of jet centerlines
η	Merging coordinate perpendicular to the S plane
θ	Discharge angle
θ_1	Angle of projection of the plume centerline on the X-Z plane from the Z-axis
θ_2	Angle of plume centerline to the X-Z plane

κ_1 and κ_2	Curvature of the plume centerline with respect to θ_1 and θ_2
ν	Kinematic viscosity
ρ	Density
ρ_0	Discharge density
ρ_∞	Ambient density
ω	Uncertainty

AN EXPERIMENTAL/ANALYTICAL INVESTIGATION
OF BUOYANT JETS IN SHALLOW WATER

1. INTRODUCTION

1.1 Background

In recent years the enormous quantities of wastewater discharged into environment from industrial and municipal plants create environmental problems and has been of serious concern to legislators and engineers. The discharge of these waste fluid usually leads to the formation of turbulent jets and plumes. The receiving water quality depends on the characteristics of turbulent mixing between discharged wastewater and receiving water. This mixing process is governed by the characteristics of the resulting jets or plumes and environmental conditions. In most cases, the density of the discharged wastewater is different from the density of the environment due to temperature or concentration difference. The resulting buoyancy forces will have a great effect on the dispersion of pollutants. In order to control and reduce the impact of emission of pollutants, an understanding of the turbulent mixing process which is used to predict the dilution under given conditions of various discharge systems is required.

Wastewater can be disposed of to the receiving ambient in many ways, for example, single submerged diffuser, multi-port submerged diffuser, or surface jet. Submerged discharges provide rapid dilution because of jet induced entrainment of ambient fluid. Thus, small temperature or concentration changes occur in relatively small mixing zones near the discharge sites. In some cases, a single-port discharge may provide adequate dilution while many others require a multi-port diffuser to enhance the dilution. In many multiple port discharges, the spacing is such that the edge of the mixing zone is reached before the plumes merge. As a result, they can be considered as single plumes.

In this study, a fluid discharge is called a jet if its primary source of kinetic energy is discharge momentum. A discharge fluid whose main source of kinetic energy is buoyancy or one that has no momentum, is called a plume. Waste water discharges are usually classified as buoyant jets because they are initially derived from sources of both momentum and buoyancy. The densimetric Froude number is the ratio of these two forces defined as $Fr= U_0/(\Delta\rho g D/\rho)^{1/2}$. The higher the Froude number, the higher is the initial momentum. The resulting flow then resembles a momentum jet. The smaller the Froude number, the more the buoyancy is important. The resulting flow is referred to as plume. When neither the momentum nor the buoyancy dominate the initial mixing process, the Froude number is moderate and the flow is termed buoyant jet.

Discharge Froude numbers for wastewater discharges generally vary between 1 and 30. As a result such flow will begin as buoyant jets.

The buoyant jet issuing from a submerged port can be divided into several flow regimes as shown in Figure 1-1. The four commonly considered regimes are :

1. the zone of flow establishment,
2. the zone of established flow,
3. the zone of surface impingement,
4. the drift zone,

Each of them has its own flow characteristics.

The characteristics of the buoyant jet depend on three classes of parameters :

1. source parameters,
2. environmental parameters, and
3. geometrical factors.

The first group of variables includes the initial velocity distribution, the jet mass flux, the jet momentum flux, and the flux of jet tracer material such as heat or concentration. The influence of these parameters can be represented by source Froude number.

The environmental parameters include ambient factors such as turbulent levels, currents, and density stratification. These factors usually begin to influence jet behavior after some distance from the discharge. The existence of ambient currents can significantly influence

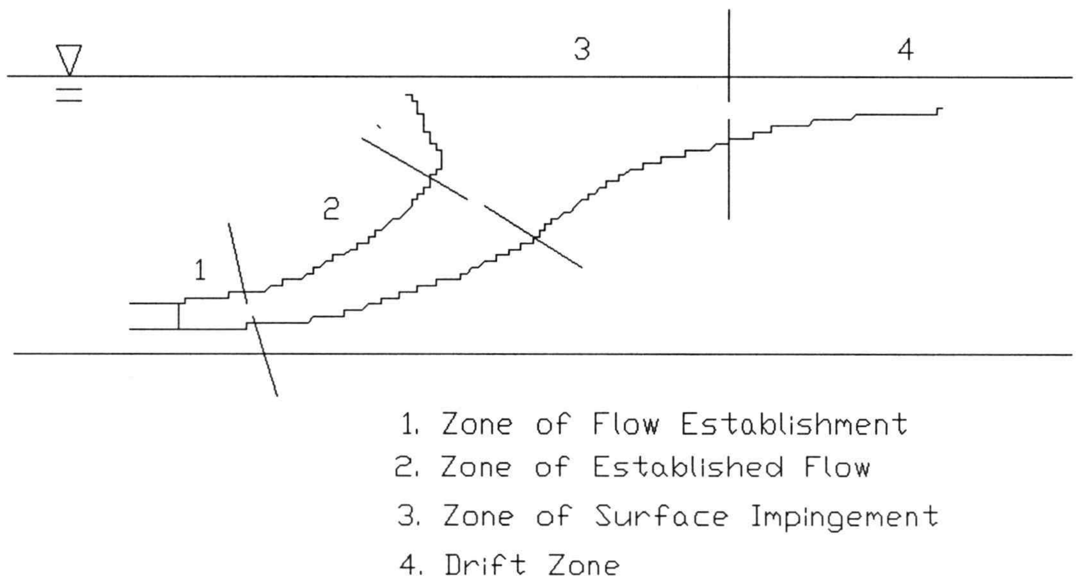

Figure 1-1. Flow regimes for buoyant jets in shallow water.

buoyant jet trajectories, dilution, and plume cross section. Stratification effects within the environment influence the height to which a buoyant discharge will rise. In a stable stratified environment, the vertical motion of buoyant jets can be trapped as the plumes reach a position where buoyancy equals that of the ambient, and becomes a neutral buoyant trapped plume. Thus, dilution is decreased markedly.

The third group of variables includes the size and number of discharge ports, the jet shape, its orientation, and its submergence depth. Multiple numbers of discharges may complicate the mixing process. Merging then needs to be considered and competition for entrainment of ambient fluid by adjacent discharges become very important. The presence of free surface can significantly influence discharge patterns and can markedly reduce dilution and is the focus of the present study.

All of the above factors can enter into a single problem and increase the complexities of the mixing process of buoyant jets. To explain the effect of each of the above factors on dilution of buoyant jets is a complex task that even now is not fully completed.

1.2 Literature Review

The investigation of submerged buoyant jets has been carried out for decades. There is a great deal of literature available which considers submerged buoyant jet theory and experiment. Some excellent reviews on turbulent momentum jets and turbulent buoyant jets are presented by Davis and Shirazi (1978), Davis (1989) (1990), and Baumgartner and Trent (1970). List (1982) also presents a detailed review which deals with basic phenomenon of turbulent jets influenced both by source momentum and buoyancy. An other good review of experimental data on vertical turbulent buoyant jets is presented by Chen and Rodi (1980).

The problems of a turbulent buoyant jet in an infinite environment have received considerable attention in the literature, commensurate with their importance in environmental fluid mechanics. The early study includes the work of Alberson et.al. (1950), Morton (1956), Morton et. al. (1959), Abraham (1960), and many others. Probably the first major practical advance in the calculation of dilutions and trajectories of buoyant jets was made in the paper by Morton et.al. (1959). They introduced the entrainment hypothesis method which relates the rate of the inflow of dilution water to the local properties of the jet, especially its local mean velocity. This method has been used widely by subsequent investigators. By using the fundamental integral approach of Morton, Fan and Brooks (1969) presented a general analytical formulation for both plane and round buoyant jets.

Integral methods are fairly successful in describing turbulent buoyant jets discharged in an infinite ambient under the influence of ambient current and stratification. A very general method which is capable of predicting buoyant jets with three dimensional trajectories discharge to flowing, stratified ambient through a single submerged round diffuser is presented by Hirst (1971a). He derived the integral equations from the basic equations by using so called " natural coordinates". Based on Morton's entrainment hypothesis, a new entrainment function was introduced which includes the effects of internal turbulence, buoyancy and cross flow. The coefficients of entrainment were determined by fitting the prediction to the experimental data. This method successfully predicts a very wide range of flows.

Hirst (1971b) also investigated the flow in the zone of flow establishment. The similar integral equations as in reference Hirst (1971a) were used to solve for starting length, and the values of the jet width, jet orientation, and centerline temperature and salinity at the end of this zone.

Hossain and Rodi (1982) reported a mathematical model for buoyant jets which is different from integral methods. The velocity component, the temperature and the concentration are determined by solving partial differential equations. The performance of this method depends entirely on the turbulence model employed.

Turbulent buoyant jets from multi-port discharges have been studied extensively. There are many informative papers concerning the mixing and merging processes of adjacent jets. Koh and Fan (1970) presented a mathematical model of multi-port discharges by interfacing single round jets and slot jet solutions at a transition point. Jirka and Harleman (1973) presented and "equivalent slot" method in which the same discharge per unit diffusion length and the same momentum flux per unit length as the multi-port discharge are required.

Davis (1975) proposed a mathematic model to calculate the plume trajectory and dilution from multiple cell mechanical draft cooling towers with the ambient wind. This was the first model which considered the details of the merging process. By assuming merging profiles, calculation can proceed smoothly from single plume to merged plume without a discontinuity in plume properties. This gradual merging approach was successfully used by Kannberg and Davis (1977) in predicting deep submerged multi-port buoyant jets. Based on this model, an integral model which includes the effects of moisture for merging plumes was also presented by Macduff (1980).

Kannberg (1977) performed an experimental investigation of deep submerged multiple buoyant discharges, which considered the effect of merging on dilution and trajectory. Experimental studies of buoyant discharges have also been performed by Davis et.al. (1978) (1982).

Buoyant discharges in shallow water are more complicated. As a buoyant jet discharges into shallow receiving water, the jet rises toward the water surface because of the effect of buoyancy. As it reaches the surface, the water available for jet entrainment is limited and therefore decreasing the dilution rate. For vertical discharge in shallow water, this decreased rate of dilution is more significant than horizontal and inclined discharges because the jet reaches the water surface sooner than horizontal and inclined jets.

A review is provided by Jirka (1982) for a buoyant jet discharged in shallow water. The influences of the free surface and buoyancy are discussed in this review. Several analytical studies of submerged buoyant jets in shallow water have been performed by Robideau (1972), Maxwell and Pazwash (1973), Trent (1973), Lee and Jirka (1981) , and Tai and Schetz (1984).

Maxwell and Pazwash (1973) developed a mathematic model of the discharge of a horizontal axisymmetric non-buoyant jet in shallow water. For momentum jets, the maximum velocity migrates toward the closer horizontal surface, the Coanda effect. Robideau (1972) proposed an integral model, based on the three conservation relations, for a plane and a round buoyant jet in quiescent shallow water. For the zone of surface impingement, the free surface interaction is represented as a momentum jet impinging on a rigid plate. With this approach, an assumption was made that there is no further dilution of the buoyant jet in the surface impingement zone. The equations for the conservation of mass, momentum and energy are solved using an assumed velocity distribution to give the maximum surface temperature. Trent (1973) presented a numerical solution of the differential equations for vertical buoyant jets in quiescent shallow water. The water surface was simulated by a free slip of the fluid along the flat plate. The differential equations were written in terms of vorticity and stream function and were solved by finite difference methods. Lee and Jirka (1981) presented an integral method analysis for a round buoyant jet discharged vertically into quiescent shallow water. An analytical investigation of the stability and mixing characteristics in the large horizontal extend was reported in this study. Tai and Schetz (1984) developed a finite difference treatment based on the steady, Navier-Stokes equation written in terms of primitive variables for buoyant jets in shallow water. The free surface is approximated by a flat plate. A case of a rectangular horizontal, buoyant jet in shallow co-flowing main stream in a waterway was tested and good agreement was obtained compared to measurements.

Experimental studies on submerged buoyant jets in shallow water are reported by Bain and Turner (1969), Ryskiewich and Hafetz (1975), Pryutniewicz and Bowley (1975), Balasubramanian and Jain (1978), Lee and Jirka (1981), and Sobey and Johnston (1988).

Sobey and Johnston (1988) in their recent study have investigated a buoyant jet in quiescent shallow water. The experiments were conducted in a non-overflowing tank. A round buoyant jet was discharged horizontally from a vertical side wall into a flat-bottomed body of water. The influences of bed and free surface on the near-field flow and mixing characteristics were investigated. Ryskiewich and Hafetz (1975) conducted an experiment principally to verify the Robideau's model. The experiments of Lee and Jirka (1981), and Pryutniewicz and Bowley (1975) were on vertical jets in quiescent shallow water. Balasubramanian and Jain (1978) presented an experiment of a horizontal buoyant jet discharged into quiescent shallow water. Temperature measurements in the vertical plane of the jet axis were obtained to determine the surface layer stability, maximum temperature rise in the zone of surface impingement and the distribution of surface temperature.

All of these studies involved discharges in shallow water that were either into quiescent ambient or from a diffuser with fixed discharge angle. Studies on turbulent buoyant jets in shallow water, which include the influences of ambient current and discharge angle on the flow behavior in the near field region where the flow behaves much like a surface jet, are limited.

1.3 Study Objectives

Buoyant jet outfalls from industrial and municipal plants are commonly situated in relatively shallow water. The presence of the free water surface is expected to influence the behavior of the buoyant jet. This thesis is concerned primarily with single-port buoyant discharges into flowing, shallow water and the effect of various parameters on dilution. The investigation is both experimental and analytical. Recent integral methods are fairly successful for a buoyant jet discharge into an unconfined environment. However, the extension of this approach to a shallow water environment is uncertain. The proximity of the free surface has a significant influence on the mixing processes. Details of these processes in the development of a predictive integral model are sought initially from laboratory experiments.

The results of this investigation are presented in two parts. The first part presents a series of laboratory experiments to investigate the flow behavior of a round buoyant jet in shallow water with ambient current. The effects of densimetric Froude number, ambient current, discharge angle and water depth on dilution and trajectory are of major concern. In second part details of the application of an integral method of analysis for multiple port discharges first proposed by Davis (1975) are presented. By using the method of images solution, the merging model for multiple port discharges was used to simulate the single port discharge in shallow water. The results of this application to the discharge conditions considered in the experiments are also presented. Finally the comparisons are made between numerical predictions and experimental observation.

2. APPARATUS AND EXPERIMENTS

This chapter introduces modeling parameters, experimental apparatus, experimental procedures, and data treatments.

2.1 Dimensional Analysis

In order to model the single round buoyant jet, the law of geometric and dynamic similarity must be followed. This can be obtained by dimensional analysis which defines the length, velocity and buoyancy scales with appropriate choice of the dominant parameters. The independent parameters chosen in the present study can be grouped into source and field parameters. The source parameters are: 1) The densimetric Froude Number, $Fr= U_0/(gD\Delta\rho/\rho)^{1/2}$, which is the ratio of inertial force to buoyant force; 2) The velocity ratio, $R=U_\infty/U_0$, which is the ratio of ambient current to discharge velocity; 3) The source Reynolds Number, $Re=U_0D/\nu$. The field parameters are : 1) The discharge angle, θ; 2) The position coordinates x,y and z and the source location, Z_0 above the bed and H below the water surface. The receiving water depth is $(H+Z_0)$ and the (x,y,z) cartesian system is located at the bed in the vertical plane of the buoyant jet ,the jet being located at $(0,0,Z_0)$.

Since the plume is usually turbulent, the effect of

Reynolds Number can be neglected. The densimetric Froude number is a major influential parameter of buoyant jets. The velocity ratio parameter represents the influence of the ambient current. The free surface and bed parameters are the influences of the shallow water.

The dependent parameters are : 1) The ratio of local concentration deficit, $(C-C_\infty)/(C_0-C_\infty)=\Delta C/\Delta C_0$; 2) Plume trajectory coordinate, X/D and Y/D, and 3) Dilution which is basically the inverse of concentration deficit.

The ranges of independent parameters investigated in the present experiment were:

a. Densimetric Froude Number, Fr=5.6, 13.5, 25

b. Discharge angle, θ= 0°, 45°, 90° from the horizontal

c. Submergence Depth, H/D=3, 10, 15

d. Velocity Ratio, R=0.11, 0.22, 0.44

and Z_0/D was held constant at nominally 2 for all combinations.

Uncertainties of the independent variables Fr, H/D, R and X/D are ∓0.036, ∓0.033, ∓0.046 and ∓0.02 respectively. Details of the uncertainty analysis of independent variables are given in Appendix A.

Figure 2-1 shows the schematic diagram of plume coordinates. Data were collected primarily in a vertical plane along the axis of the plume. Table 2-1 gives all combinations of experiments undertaken.

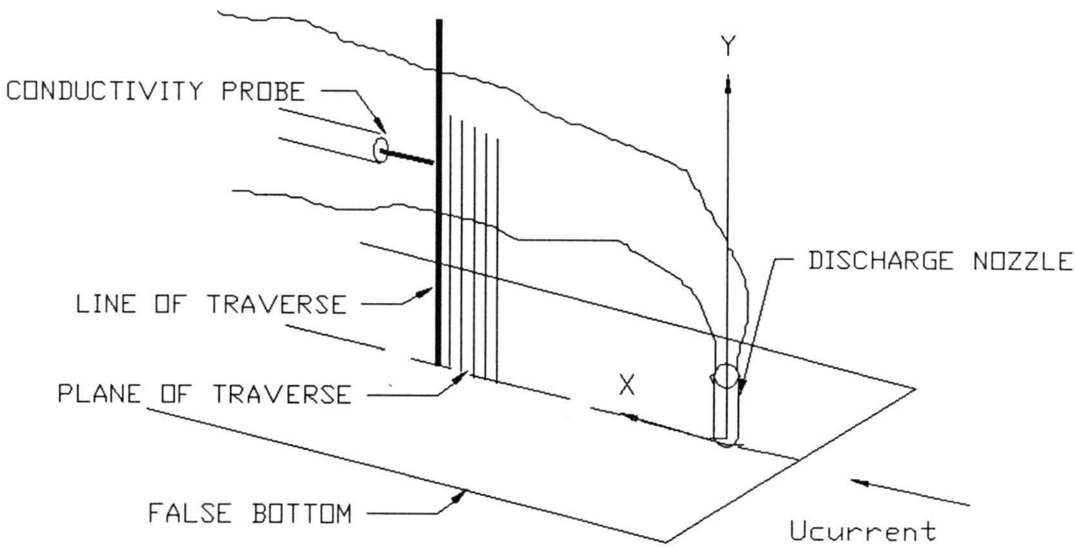

Figure 2-1. Schematic diagram of plume coordinate and sampling plane.

2.2 Apparatus and Data Acquisition

The experiments were conducted in a 12.1m long, 0.61m wide and 0.91m height towing channel containing salt water. The desired density (salinity) was obtained by mixing fresh water and coarse salt. A buoyant jet was achieved by discharging fresh water into the salt water. A false bottom was used to simulate the shallow water.

Two carriages containing discharge and sample collecting units were towed simultaneously along the rails above the towing channel by a motor as shown on Figure 2-2. This was done to simulate the ambient current.

The discharge unit shown on Figure 2-2 consisted of an acrylic fresh water reservoir, a water pump with speed control, a plenum chamber, and a discharge nozzle. The discharge system, which was connected to a fresh water reservoir by supply lines at both ends, consisted of a main discharge valve and a 0.0155m I.D. nozzle. This nozzle was located at the center width of the towing channel and could be replaced for a different discharge angle. For some cases, a 0.01129m I.D. nozzle was chosen in order to have high discharge velocities.

In order to hydraulically simulate the shallow water, a false bottom was placed at the distance 0.46m above the channel bottom as shown on Figure 2-2. The false bottom

Fr=5.6			Fr=13.5			Fr=25		
H/D	Θ	R	H/D	Θ	R	H/D	Θ	R
3	0°	0.11 0.22 0.44	3	0°	0.11 0.22 0.44	3	0°	0.11 0.22
	45°	0.11 0.22 0.44		45°	0.11 0.22 0.44		45°	0.11 0.22
	90°	0.11 0.22 0.44		90°	0.11 0.22 0.44		90°	0.11 0.22
10	0°	0.11 0.22 0.44	10	0°	0.11 0.22 0.44	10	0°	0.11 0.22
	45°	0.11 0.22 0.44		45°	0.11 0.22 0.44		45°	0.11 0.22
	90°	0.11 0.22 0.44		90°	0.11 0.22 0.44		90°	0.11 0.22
15	0°	0.11 0.22 0.44	15	0°	0.11 0.22 0.44	15	0°	0.11 0.22
	45°	0.11 0.22 0.44		45°	0.11 0.22 0.44		45°	0.11 0.22
	90°	0.11 0.22 0.44		90°	0.11 0.22 0.44		90°	0.11 0.22

Table 2-1. Table of experimental parameters.

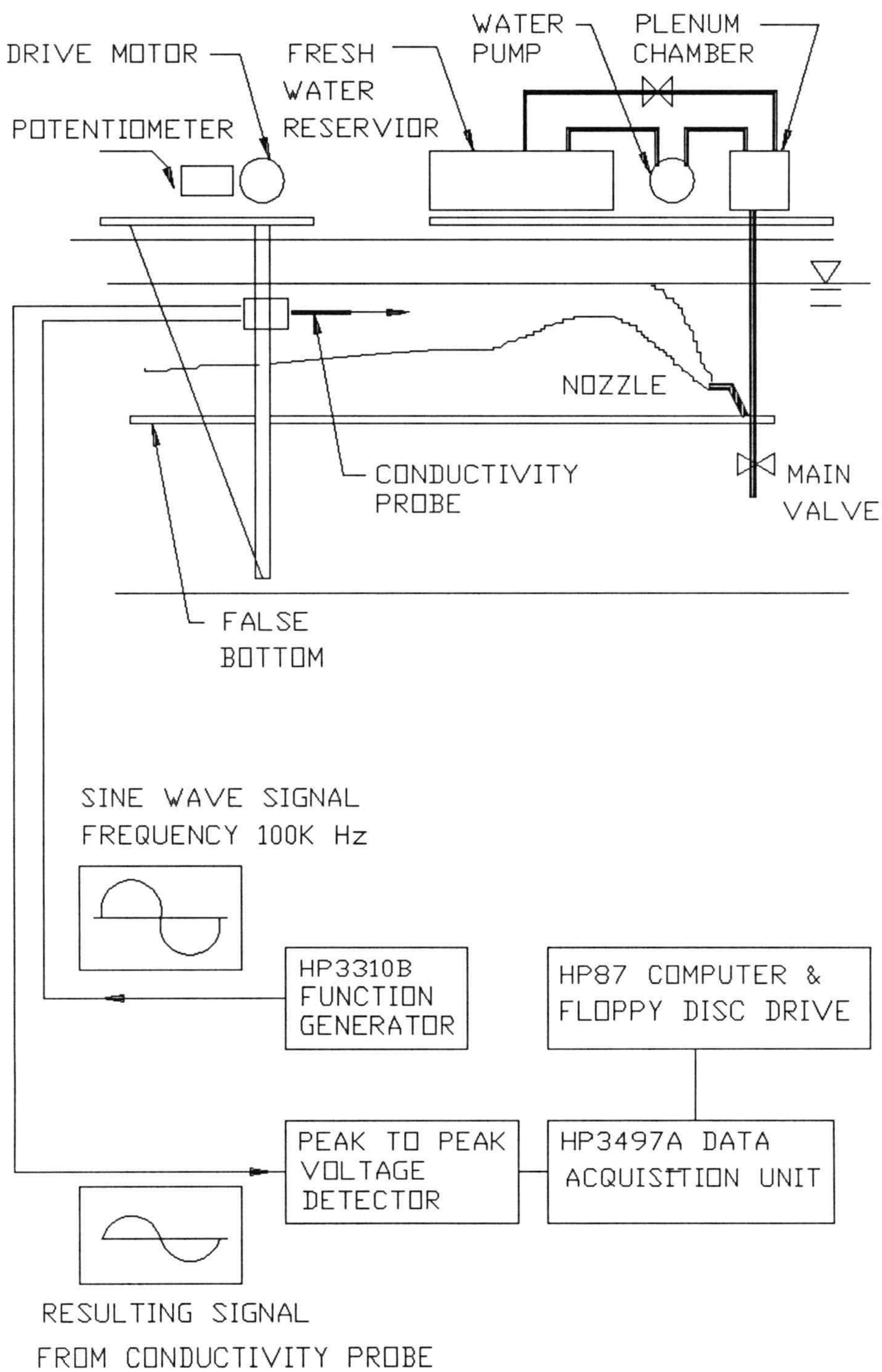

Figure 2-2. Arrangement of experiment apparatus.

started from the line of discharge and extended 1.5m behind it. The maximum boundary layer thickness developed on the false bottom was calculated 0.01456m from flat plate boundary layer theory. The effect of the false bottom on the dilution was considered to be negligible since the maximum boundary layer thickness was smaller than Z_0/D. Fresh water was discharged into the salt water by a Masterflex water pump. An injection of dye was introduced in some cases to facilite flow visualization. The pump was calibrated by a graduated cylinder and a stop watch. The desired discharge velocity was obtained by adjusting the speed of the pump. Before entering the discharge tube, the fresh water passed through a plenum chamber which dampen pump pulsation. There was an additional pipe equipped with an on-off valve between plenum chamber and reservoir. This valve was opened when the main valve was closed. After the plenum chamber was filled with water, the on-off valve was closed and the main valve was opened at the same time. This procedure ensured no air was in the supply line when fresh water was discharged.

The sample collecting unit consisted of a conductivity probe, and signal generator and data collecting systems. The conductivity probe, shown in Figure 2-3, was used to measure salinity in the field of the plume. The conductivity probe was calibrated using known salt water

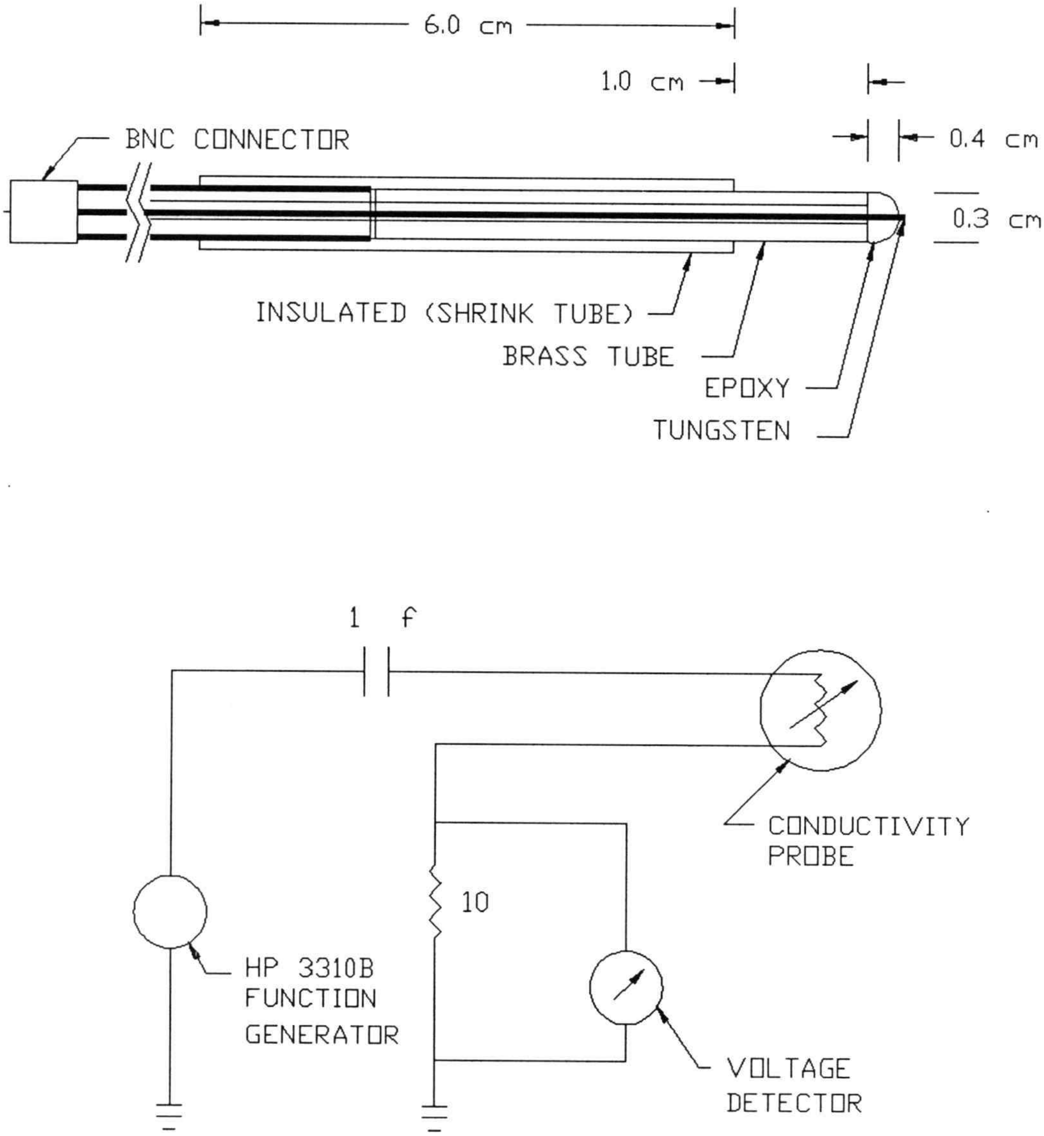

Figure 2-3. Conductivity probe and conductivity probe circuit.

solutions. These solutions were standardized by a Guildline model 8400 salinometer. The probe was mounted on a vertical moving sting at the plume centerplane. The vertical motion was motorized and its direction and speed were controlled remotely. The probe was fixed at a desired downstream positions, X/D, relative to the line of discharge for each run. During each run the probe was positioned several times across the plume. In this manner the vertical concentration profile could be obtained at a single downstream distance. The conductivity probe was connected to a function generator which provided 5000 kHz sine wave signal. The output sine wave signals from the conductivity probe were transferred to a peak-to-peak voltage detector for conversion to peak-to-peak voltage. The values then were recorded on a HP3497A data acquisition unit and stored in floppy disks. The complete arrangement of the apparatus is shown in Figure 2-2.

The sampling was started a short time after initiating discharge in order to avoid fluid transients. The control unit for the conductivity probe was connected to a HP87 computer. Sampling by the conductivity probe was "on demand" by pressing a "read" key on the computer. Once activated, the system took 10 different readings in a 3 second period and then waited for the next "read" command. Near the region of maximum concentration deficit, more than one set of samples was taken (usually 3-5). These residence times were sufficient to have a reasonable approach to the true mean value of the signal. Shorter periods were not sufficient to provide a consistent statistic data base from the turbulent time histories. Therefore, more than one run was performed for one downstream position X/D for most cases. This provided a better average of concentration.

The signals were carefully examined at a later time and a value of the maximum concentration deficit in the vertical profile and its position were recorded.

The sequence of events, called a run, which formed the basic experimental test was as follows:

1) The tank was filled with salt water to the desired depth and salinity. The water was well mixed to ensure uniformity of ambient salinity(density) through the tank.
2) The conductivity probe was adjusted for the desired downstream distance, X/D.
3) The pump speed was adjusted to have desired discharge velocity.
4) The towing speed was adjusted to have desired velocity ratio, R.
5) Initial probe height was measured. Main valve was closed and on-off valve between reservoir and plenum chamber was opened.
6) Water pump was turned on. The main valve was

opened and on-off valve was closed when fresh water filled up plenum chamber.

7) Towing was initiated.
8) The probe was moved down to a particular depth Y/D and the signals were recorded.
9) Step 8 was repeated until the probe traversed the plume. Particular emphasis was placed on the region of maximum concentration deficit during traverse.
10) After the traverse of the probe, towing was stopped.
11) The final probe height was recorded.

2.3 Data Treatment

At each combination of water depth, H/D, discharge angle, θ, densimetric Froude number, Fr, and velocity ratio, R, several measurements were obtained for various downstream distance X/D. The reading of potentiometer indicated the vertical location of the probe. As mentioned earlier, a time interval of about 3 second was used for the conductivity probe to scan 10 samples. The mean average value of the 10 readings was taken and converted to salinity using the calibration curve of that probe. The local concentrations were then obtained from measured salinity and reduced by normalizing them relative to ambient concentration. The normalizing equation is

$$(C-C_\infty)/(C_0-C_\infty)=\Delta C/\Delta C_0$$

For each downstream distance X/D, the concentrations were averaged at each Y/D position for several similar run. The maximum value of concentration deficit was defined as $\Delta C_m/\Delta C_0$. Dilution is defined as the total volume divided by the volume of effluent within it. In an unstratified ambient it is equivalent to the inverse of the concentration.

The trajectory was determined from the locus of maximum concentration deficit and normalized to the jet diameter.

An example of the plot and data points for the maximum concentration deficit is shown on Figure 2-4. Some of the data points were shifted off the true X/D value in order clarify the plot. The curve drawn through the data indicates the mean average values of maximum concentration deficit. Appendix B contains all the curves of maximum concentration deficit and trajectory obtained in this study. A catalog of all data points contributing to the plots of the maximum concentration deficit and trajectory in this study is given in Appendix C.

An error analysis for the ratio of concentration deficit due to the finite size of the probe and calibration of conductivity probe is given in Appendix A. Figure 2-5 shows the uncertainty of the maximum concentration deficit for the case Fr=25, H/D=15, $\theta=0°$ and

R=0.11. This case has the maximum uncertainty in the experiments. The high uncertainty near the source is due to the finite size of the probe and high concentration gradients. Beyond X/D of 25 there is very little uncertainty in the reading.

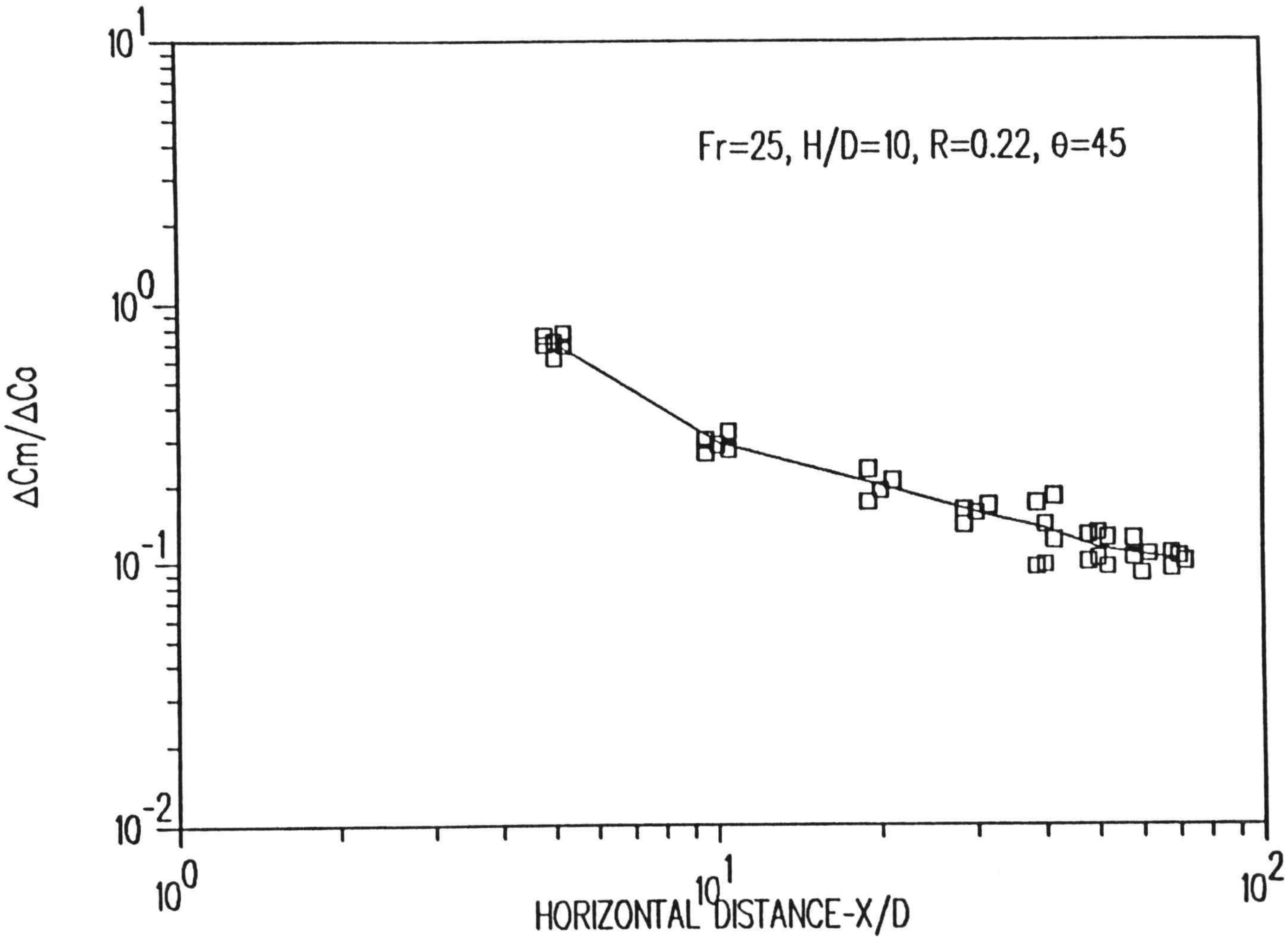

Figure 2-4. Example of typical maximum concentration deficit data and representative curve.

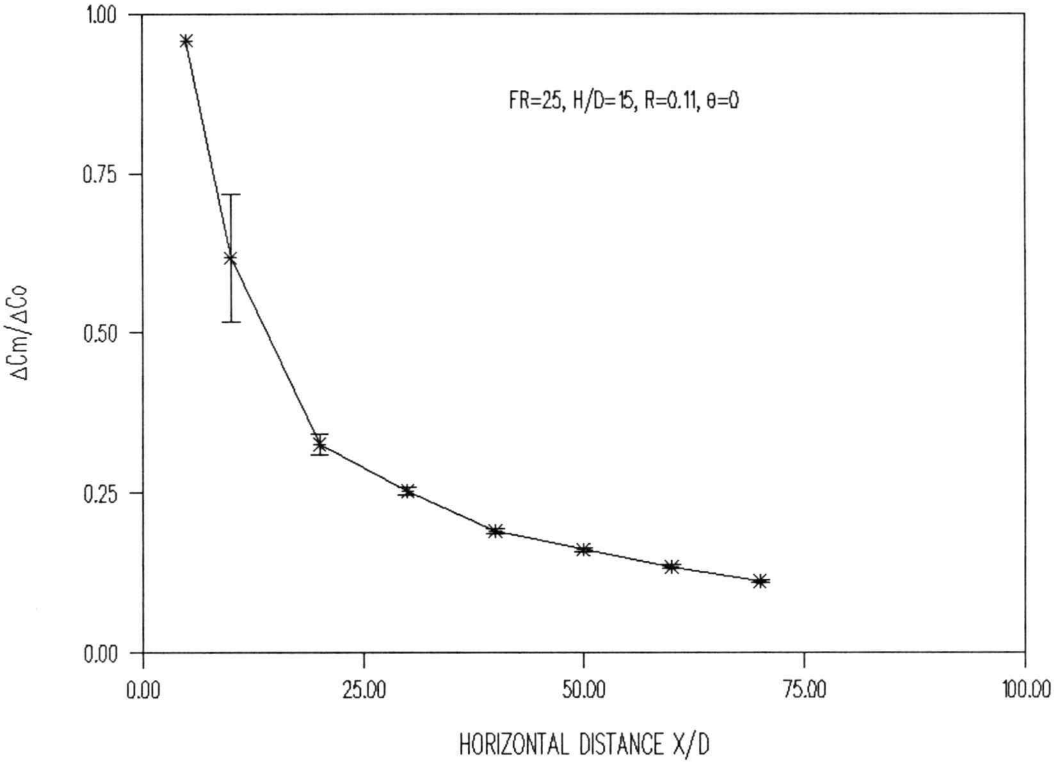

Figure 2-5. Uncertainty of maximum concentration deficit for Fr=25, H/D=15, R=0.11 and $\theta=0°$.

3. RESULTS AND DISCUSSION

Major concerns in this study were the effect of densimetric Froude number, Fr, water depth, H/D, velocity ratio, R, and discharge angle, θ, on dilution and trajectories. The results are best illustrated by showing the maximum concentration deficit $\Delta C_m/\Delta C_0$ and trajectory Y/D plotted as a function of horizontal distance X/D for various combinations of Fr, H/D, R and θ. The horizontal distances, X_s/D, where the submerged buoyant jets reach the surface for various parameters combination are presented as well.

3.1 Experiment Results

Robideau (1972) and Ryskiewich and Hafetz (1975) suggested a reduction in the entrainment rate when the plume reaches the surface. Assuming such an effect does exist, a plot of the maximum concentration deficit versus horizontal distance X/D should show a "bending tail" emerging from the curve of the submerged buoyant jet as the jet reaches the surface. This tailing condition would be as shown on Figure 3-1. The maximum concentration deficit of the free submerged buoyant jet would decrease monotonically with horizontal distance while the curve of the surface jet would flatten out at X_s/D. The horizontal distance X_s/D where the surface effect emerged was found

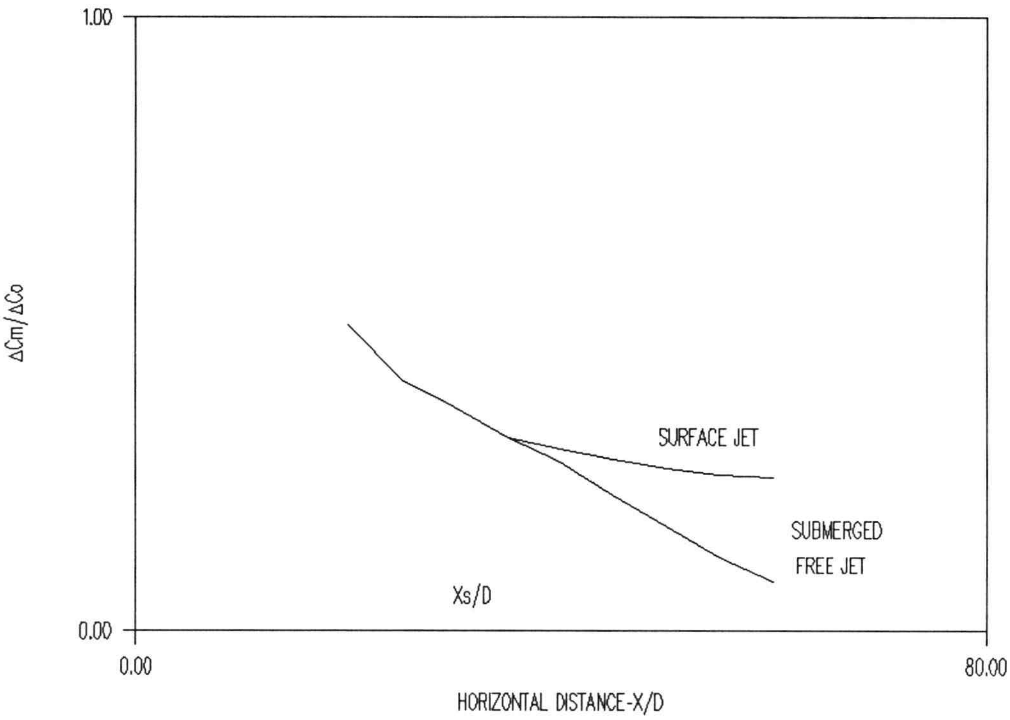

Figure 3-1. Maximum concentration deficit curve of surface jet emerges from the curve of submerged free jet at $X/D=X_s/D$.

in this study to be a function of densimetric Froude number, velocity ratio, water depth and discharge angle. For the convenience of study, the buoyant jet was termed submerged jet for the regime before X_s/D and surface jet for the regime beyond X_s/D. In this study, the mixing length is defined as the distance along the submerged jet axis and the initial dilution is defined as the dilution rate of submerged jet.

Table 3-1 gives the values of X_s/D for various discharge angles over various combinations of Fr, R and H/D. In general, the results shown in Table 3-1 indicate that X_s/D increases for increasing Fr, R and decreasing θ.

Figures 3-2 and 3-3 show the effect of current ratio, R, on maximum concentration deficit for various combinations of Fr, θ and H/D. Normally the dilution was greater for higher velocity ratio. This is because high velocity ratios provide not only a higher entrainment velocity but also a later occurrence of the surface effect. This observation is supported by the trajectory plots shown on Figures 3-4 and 3-5. However, in the cases of vertical discharges, the trend is different. Figures 3-6 and 3-7 illustrate cases with $\theta=90°$. In these runs, the dilution rate for the submerged portion was greater for decreasing velocity ratio at a particular downstream distance, X/D. It is noted that the plots were made versus horizontal downstream distance, X/D, not jet axis,

			X_s/D		
Fr	H/D	R	Θ=0°	Θ=45°	Θ=90°
5.6	3	0.11	20	10	5
		0.22	20	10	5
		0.44	20	20	5
	10	0.11	20	10	5
		0.22	30	30	10
		0.44	40	30	30
	15	0.11	30	20	10
		0.22	40	20	20
		0.44	70	70	60
13.5	3	0.11	20	5	5
		0.22	20	5	5
		0.44	30	10	5
	10	0.11	30	20	5
		0.22	30	20	20
		0.44	**	40	40
	15	0.11	50	30	20
		0.22	50	50	40
		0.44	**	70	70
25	3	0.11	20	5	5
		0.22	30	10	5
	10	0.11	70	10	5
		0.22	**	10	10
	15	0.11	**	20	5
		0.22	**	70	50

** $X_s/D > 70$

Table 3-1. Table of the horizontal distances X_s/D.

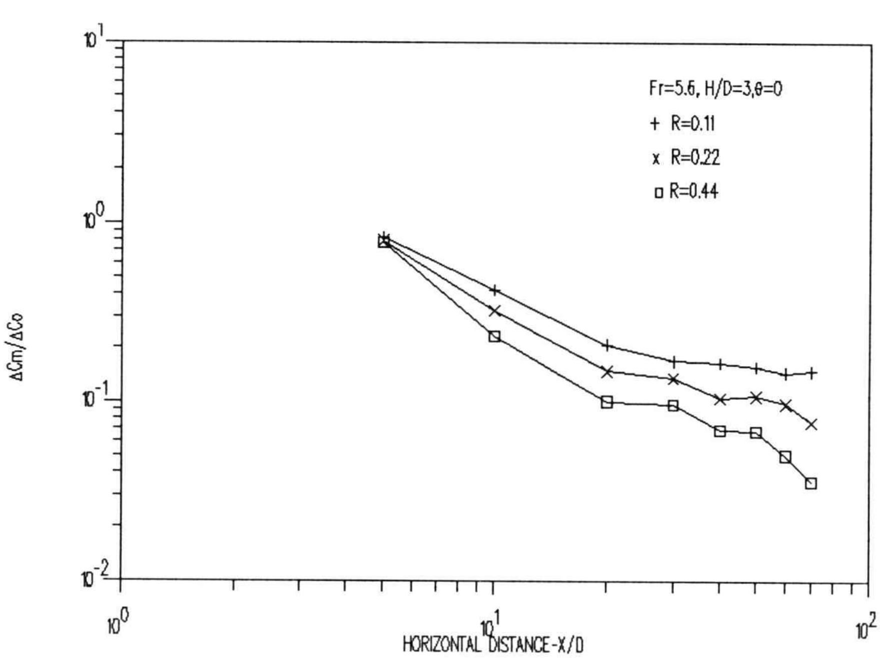

Figure 3-2. Effect of varying R on maximum concentration deficit for Fr=5.6, H/D=3 and θ=0°.

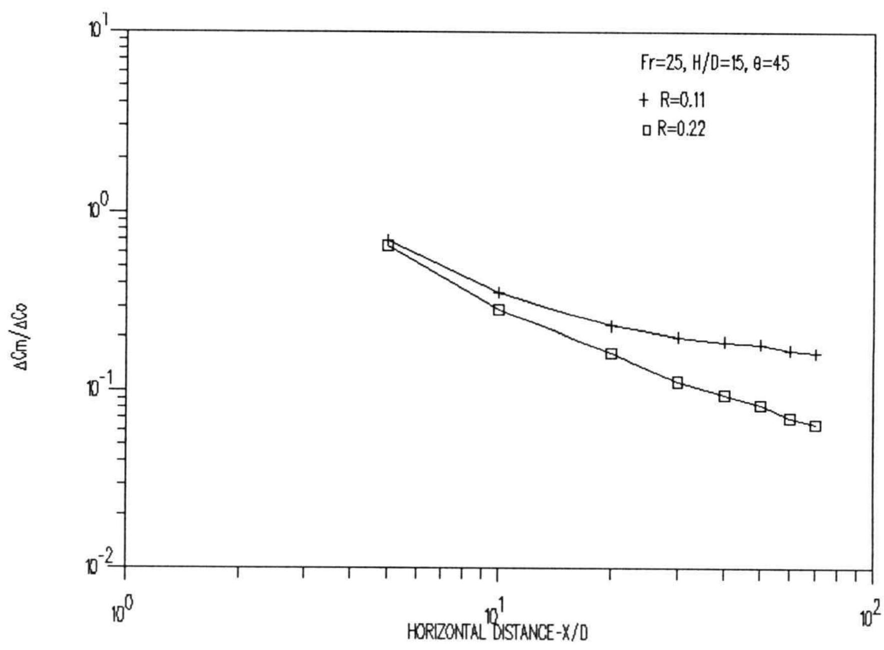

Figure 3-3. Effect of varying R on maximum concentration deficit for Fr=25, H/D=15 and θ=45°.

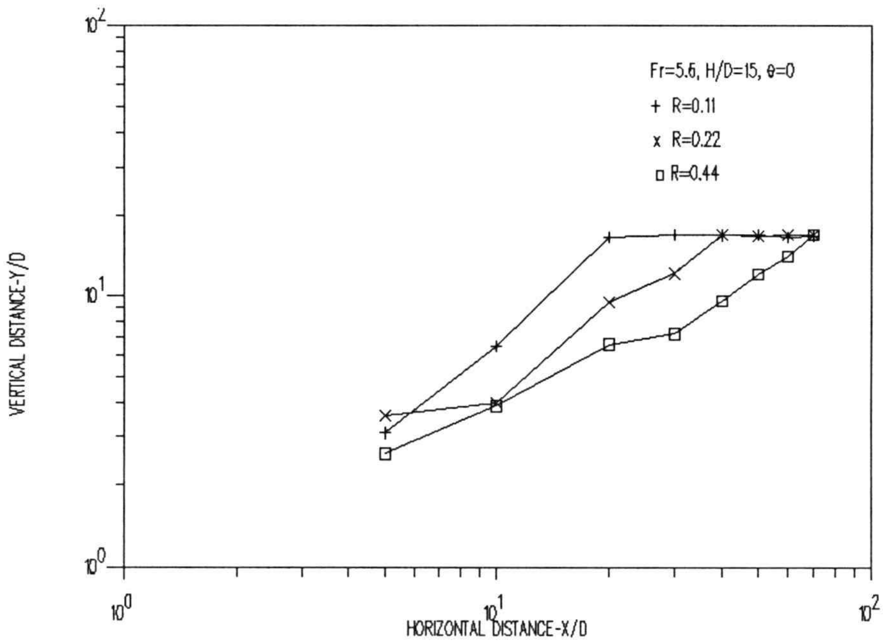

Figure 3-4. Effect of varying R on trajectory for Fr=5.6, H/D=15 and θ=0°.

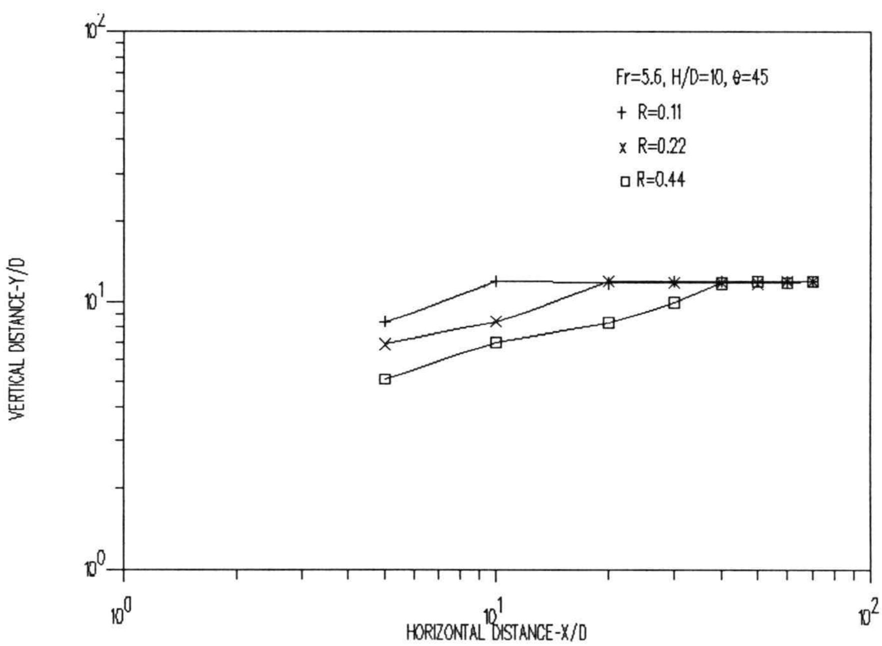

Figure 3-5. Effect of varying R on trajectory for Fr=5.6, H/D=10 and θ=45°.

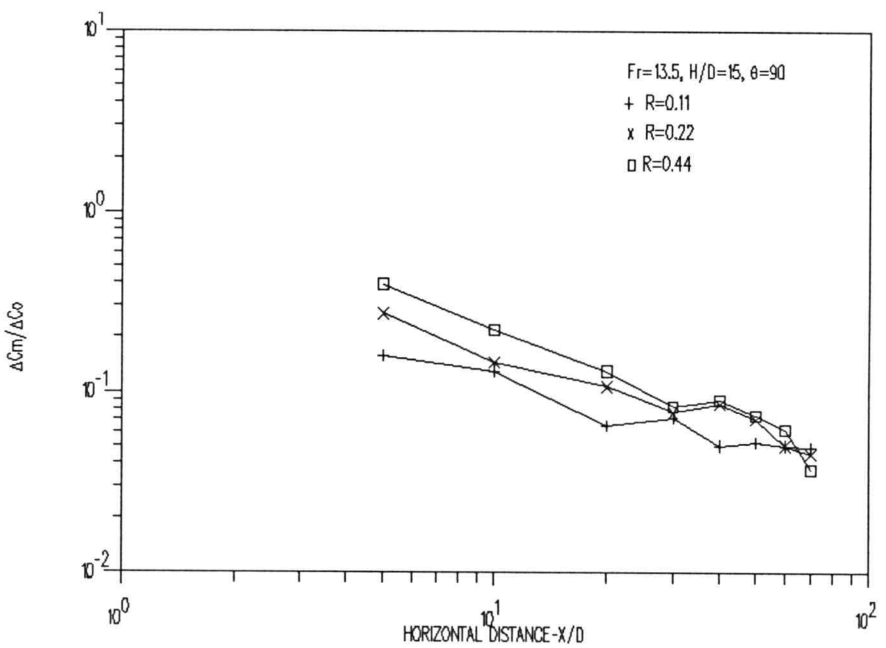

Figure 3-6. Effect of varying R on maximum concentration deficit for Fr=13.5, H/D=15 and θ=90°.

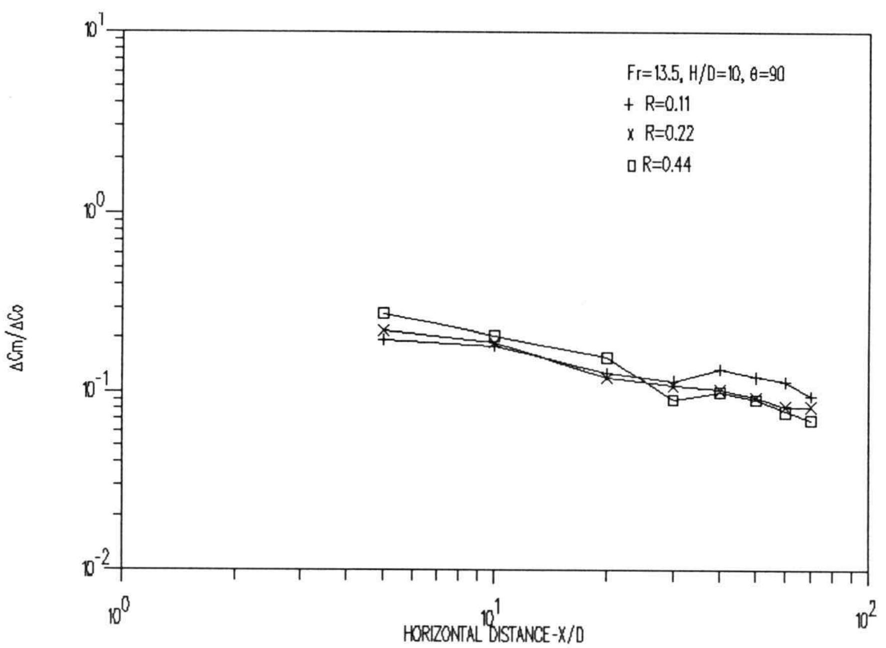

Figure 3-7. Effect of varying R on maximum concentration deficit for Fr=13.5, H/D=10 and θ=90°.

S/D. The normal component of the current increases dilution until the component of the current in the direction of plume motion stretches the plume out.

The trajectories were dramatically affected by velocity ratio. Figures 3-4 and 3-5 show the effect of R on trajectory for $\theta=0°$ and $\theta=45°$. After the submerged jets reach the water surface, the trajectories stay close to the water surface and are independent of R.

Figures 3-8 and 3-9 show the influence of Froude number on maximum concentration deficit for R=0.11 and R=0.22. Some examples of the effect of Froude number on trajectory are given in Figures 3-10 and 3-11. The information offered in these plots indicates that the dilution increased with decreasing Froude number for both submerged and surface jets. Thus, a jet with high buoyancy dilutes faster than one without.

Figures 3-12 and 3-13 show the influence of discharge angle on maximum concentration deficit. It can be seen that increasing the angle of discharge increases the dilution. This is appropriate due to the greater initial dilution from the normal component of the velocity in vertical discharge as compared to horizontal discharge.

The effect of discharge angle on trajectories for several combinations of Fr, R and H/D is illustrated on Figures 3-14 and 3-15.

It is noted that the surface effect should be

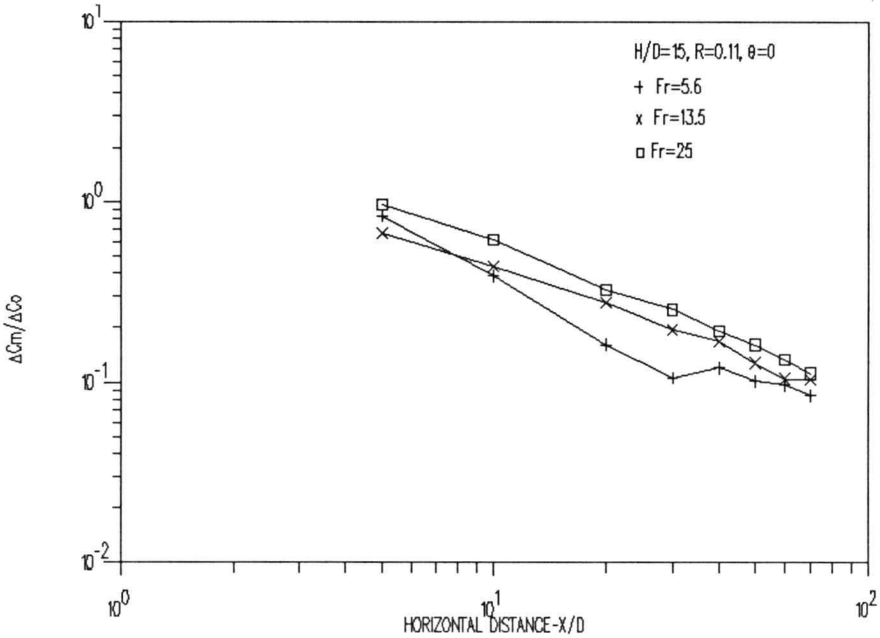

Figure 3-8. Effect of varying Fr on maximum concentration deficit for H/D=15, R=0.11 and θ=0°.

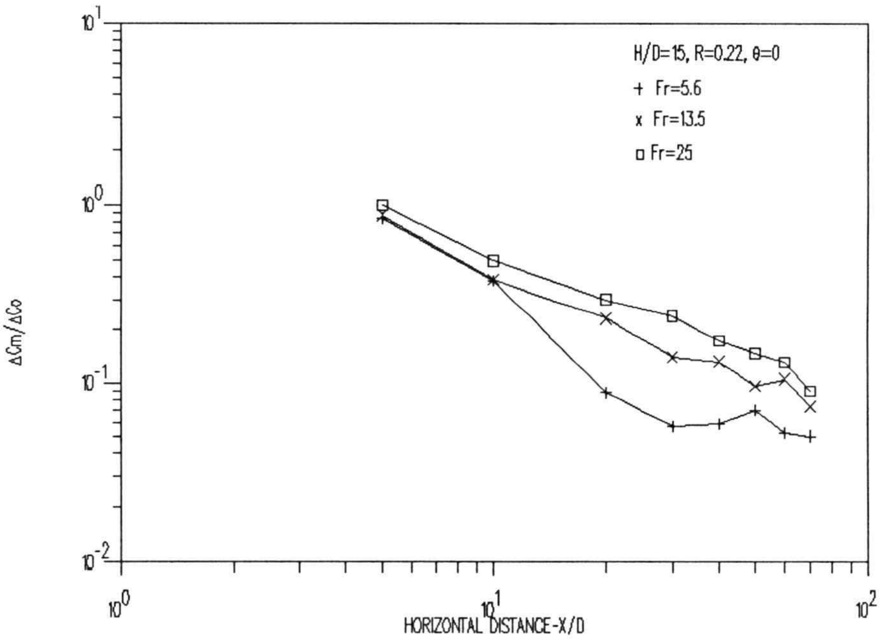

Figure 3-9. Effect of varying Fr on maximum concentration deficit for H/D=15, R=0.22 and θ=0°.

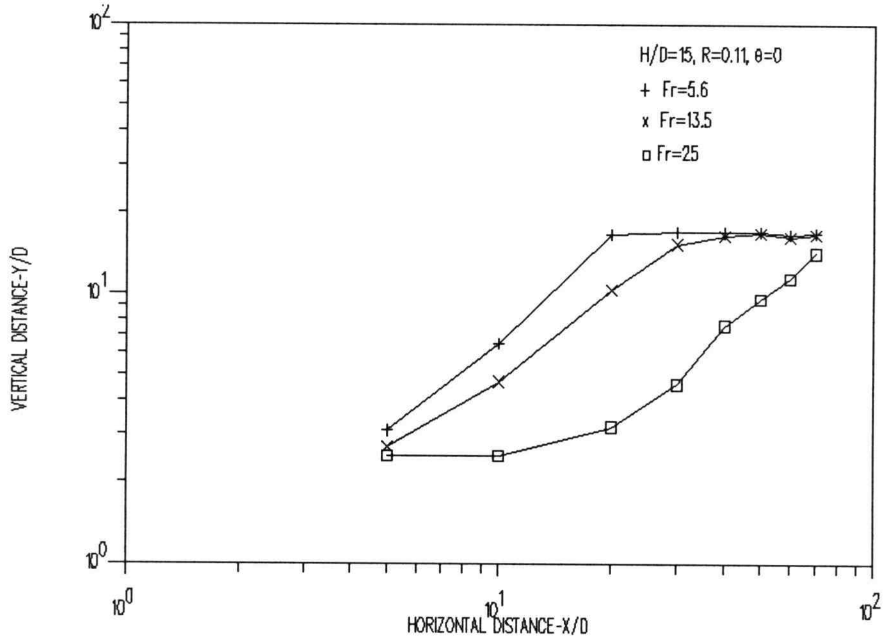

Figure 3-10. Effect of varying Fr on trajectory for H/D=15, R=0.11 and θ=0°.

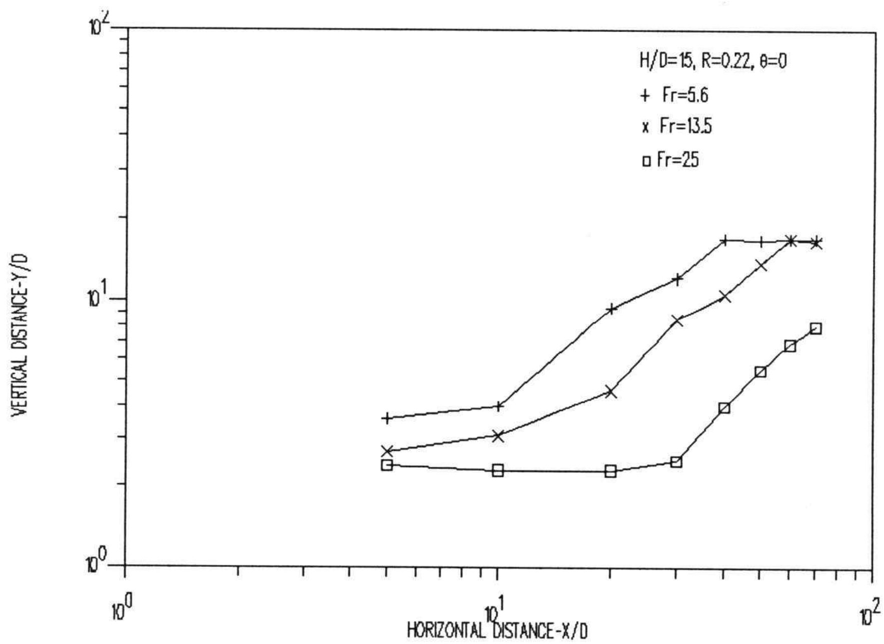

Figure 3-11. Effect of varying Fr on trajectory for H/D=15, R=0.22 and θ=0°.

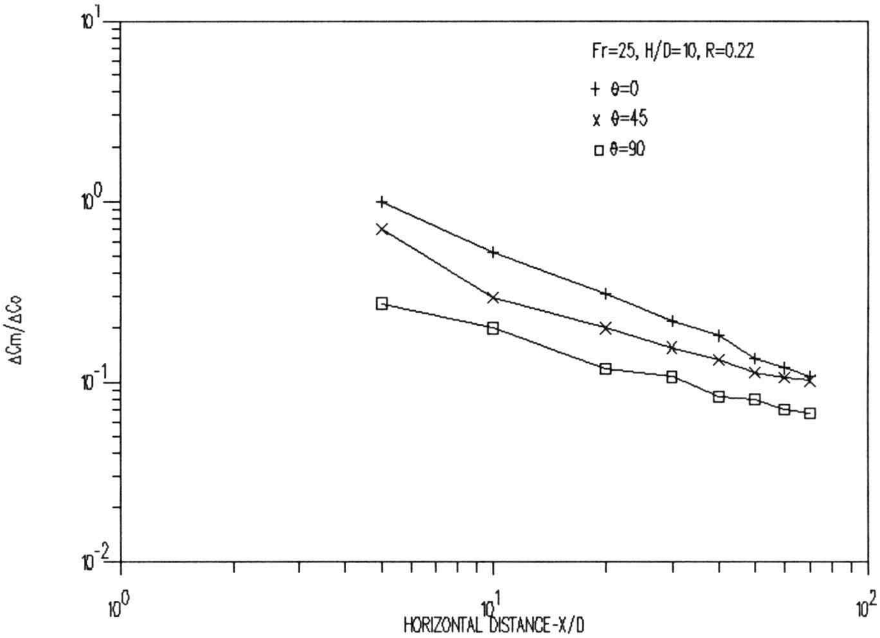

Figure 3-12. Effect of varying θ on maximum concentration deficit for Fr=25, H/D=10 and R=0.22.

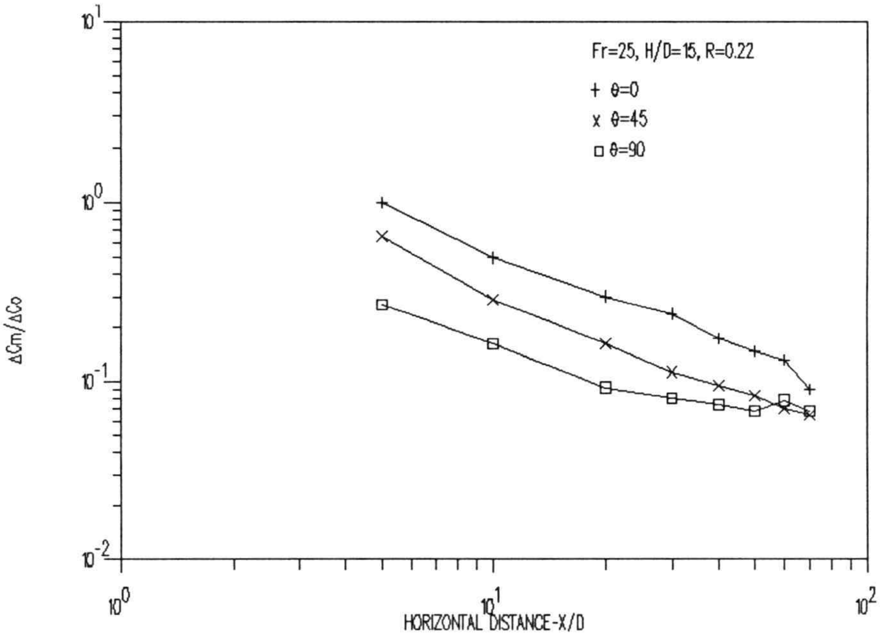

Figure 3-13. Effect of varying θ on maximum concentration deficit for Fr=25, H/D=15 and R=0.22.

included in the discussion of the influences of Fr, R and θ on the dilution for buoyant jet in shallow water. From the previous discussion, jets with small Fr or large θ should have the greater initial dilution. However, small Froude number and large discharge angle also provide an earlier occurrence of the surface effect which limits the entrainment and decreases the dilution rate. An example for H/D=10, R=0.22 and $\theta=0°$ is shown in Figure 3-16. The curves of maximum concentration show the bending at X/D=20 and X/D=40 for cases Fr=5.6 and Fr=13.5 respectively. As the curves flatten out which indicates the plume has reached water surface, dilution is reduced dramatically. For Fr=25, the jet stays submerged because of small buoyancy. Thus, the curve of maximum concentration continues to decline. A similar result is shown in Figure 3-17 for H/D=10, R=0.22 and $\theta=0°$.

Another interesting example showing the effect of different discharge angles is shown on Figure 3-18 for Fr=5.6, R=0.11 and H/D=15. As with the previous discussion, the vertical jet had the greatest initial dilution but the shortest distance to reach the surface. As a result, the curves of maximum concentration deficit of the vertical jet flattens out soon after discharge due to the surface effect. On the other hand, the curves of inclined and horizontal jets stay submerged and continue to dilute. As a result, at X/D =40 where the inclined and horizontal jets both reach the water surface, the dilution of all three are nearly the same. Figure 3-19 illustrates a similar result for Fr=5.6, R=0.22 and H/D=15.

Of all the parameters of interest the submerged depth H/D seems to be the most critical. Figures 3-20 through 3-27 offer the comparison of H/D effects for various combinations of Fr, R and θ. These figures show that the dilution is markedly dependent on H/D. The trend is a decreasing dilution with decreasing water depth as one would expect, especially for low velocity ratio cases. The free buoyant jet performance is shown by the monotonically decreasing curve. The surface effect which decreases dilution is exposed by a "bending tail" flattening out from the free jet curve. For shallow water, the surface effect usually occurs in a very close proximity to the jet discharge. An example given in Figure 3-20 for Fr=5.6, R=0.44 and θ=45° shows a monotonical decreasing curve for H/D=15 while the bending occurs at X/D=20 for H/D=3 and X/D=30 for H/D=10. Figures 3-21, 3-22 and 3-23 show more dramatic effects of submerged depth on dilution. For vertical discharged buoyant jets, Figures 3-24, 3-25, 3-26 and 3-27 also show the same dramatic effects of H/D on dilution. As one notices, the initial dilution for H/D=3 is much less than the initial dilution for H/D=10 and H/D=15. For H/D=3, it is obvious that the jets reach the surface immediately

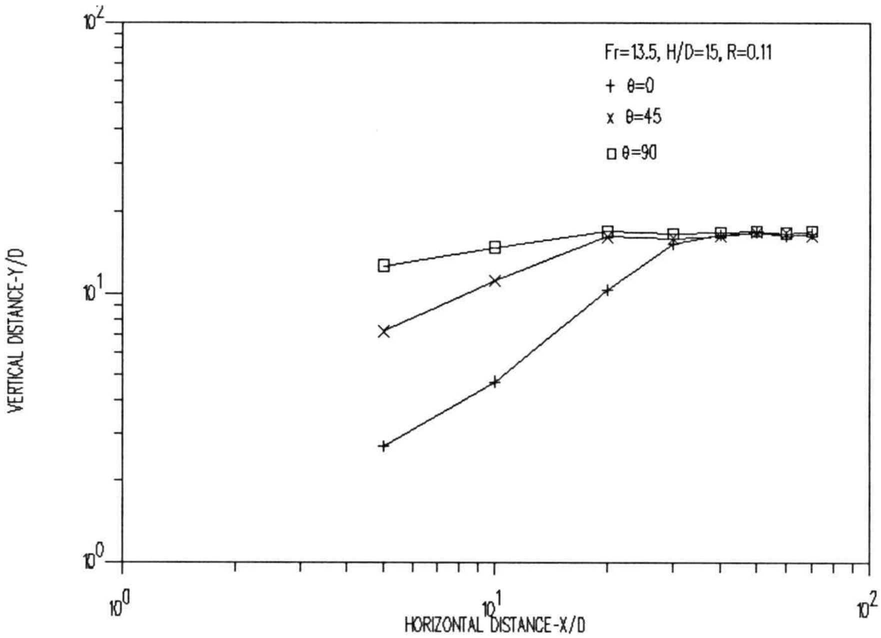

Figure 3-14. Effect of varying θ on trajectory for Fr=13.5, H/D=15 and R=0.11.

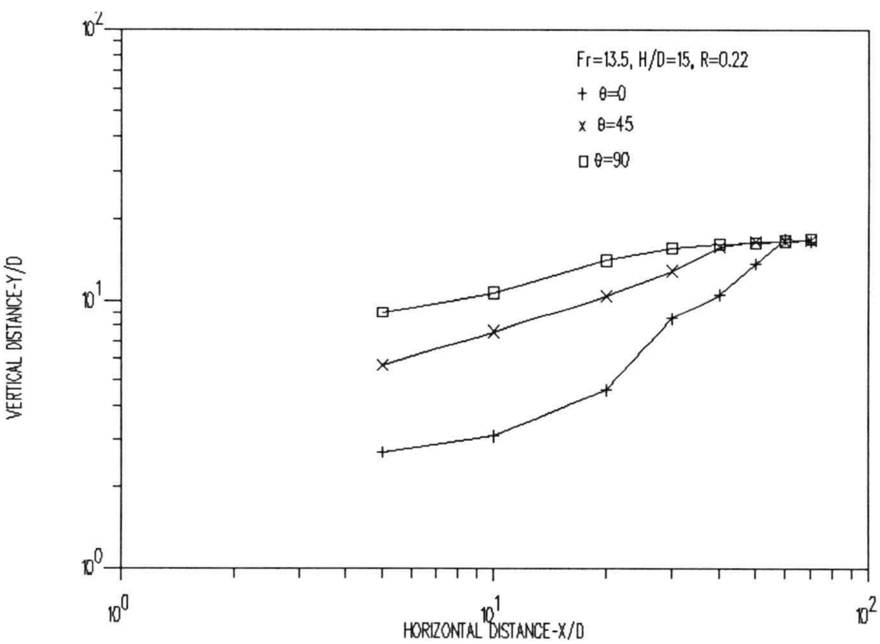

Figure 3-15. Effect of varying θ on trajectory for Fr=13.5, H/D=15 and R=0.22.

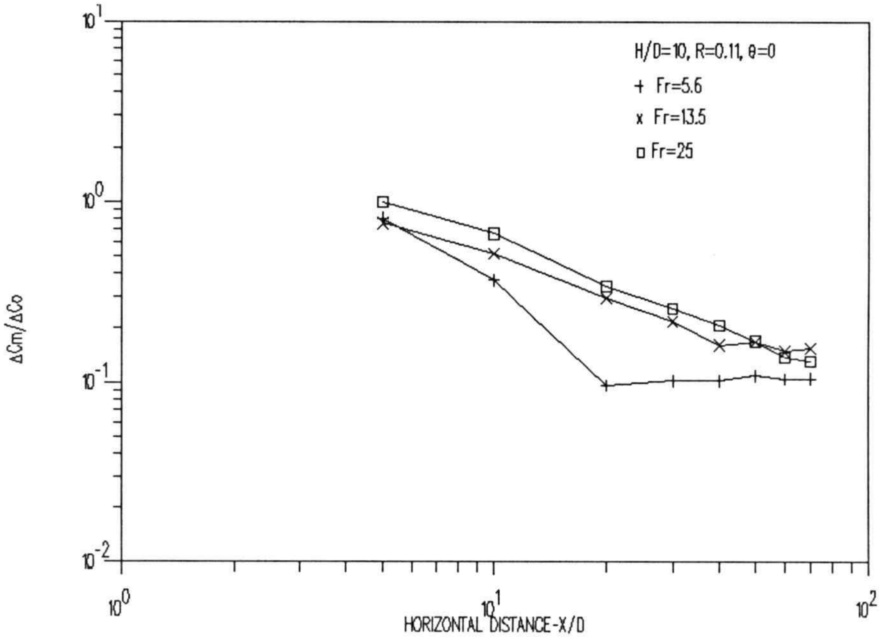

Figure 3-16. Effect of varying Fr on maximum concentration deficit for H/D=10, R=0.11 and θ=0°.

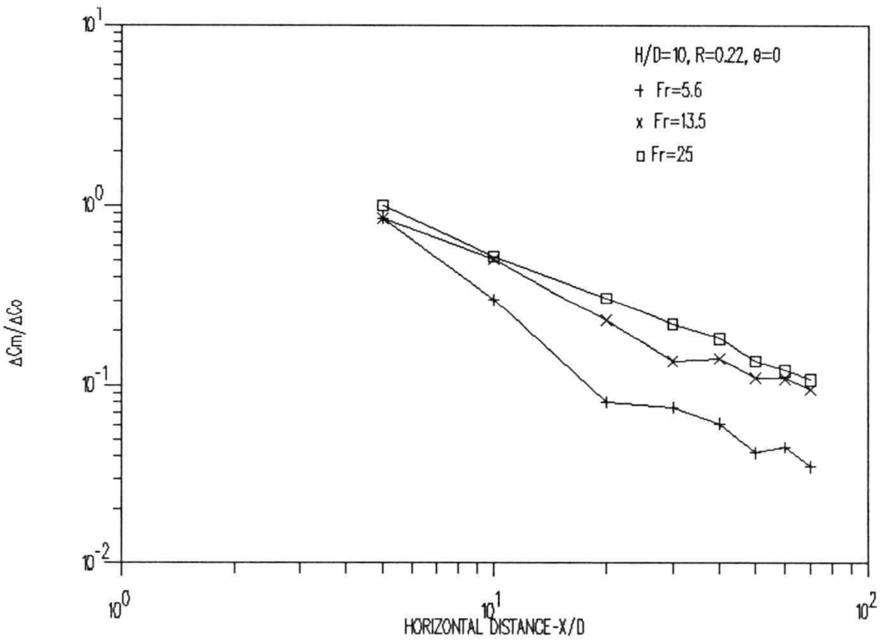

Figure 3-17. Effect of varying Fr on maximum concentration deficit for H/D=10, R=0.22 and θ=0°.

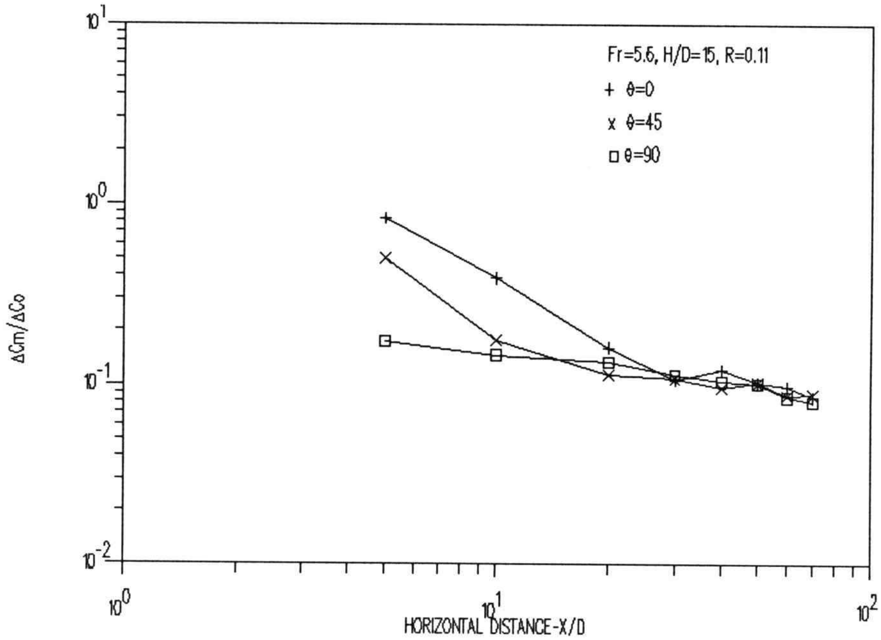

Figure 3-18. Effect of varying θ on maximum concentration deficit for Fr=5.6, H/D=15 and R=0.11.

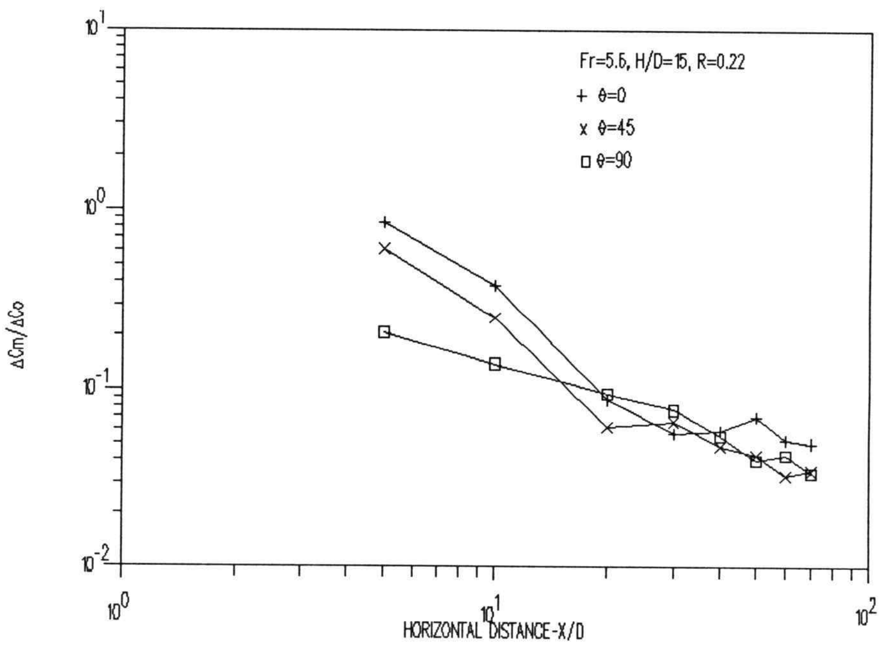

Figure 3-19. Effect of varying θ on maximum concentration deficit for Fr=5.6, H/D=15 and R=0.22.

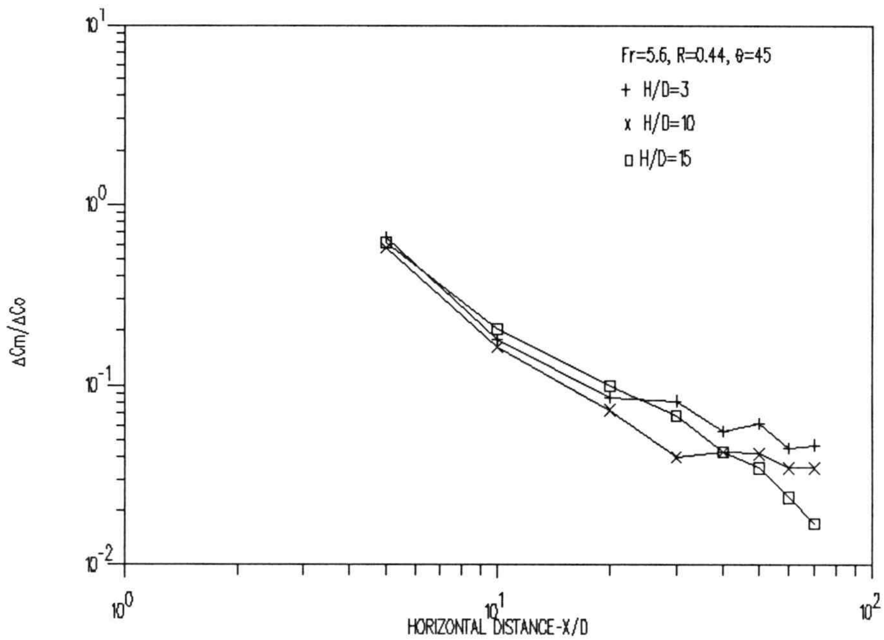

Figure 3-20. Effect of varying H/D on maximum concentration deficit for Fr=5.6, R=0.44 and θ=45°.

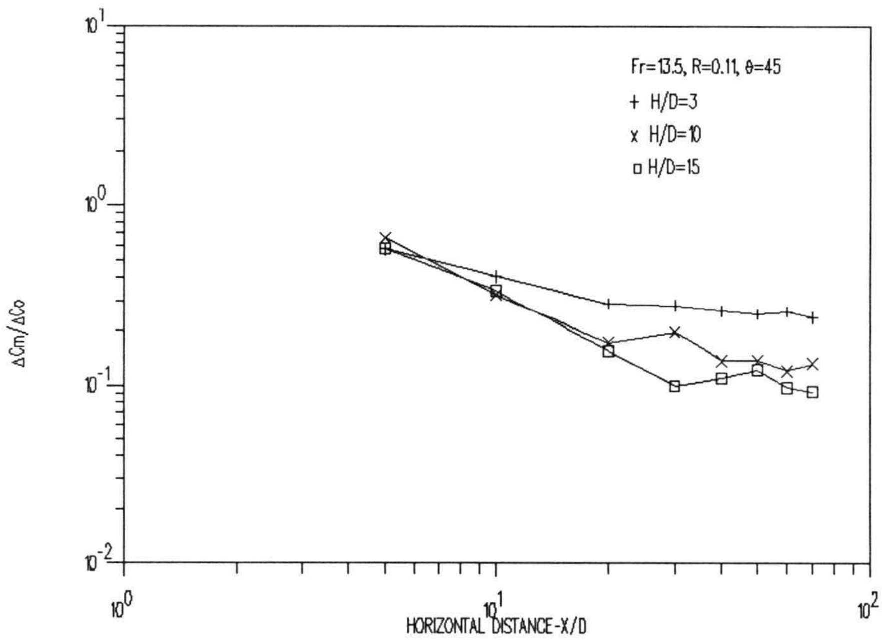

Figure 3-21. Effect of varying H/D on maximum concentration deficit for Fr=13.5, R=0.11 and θ=45°.

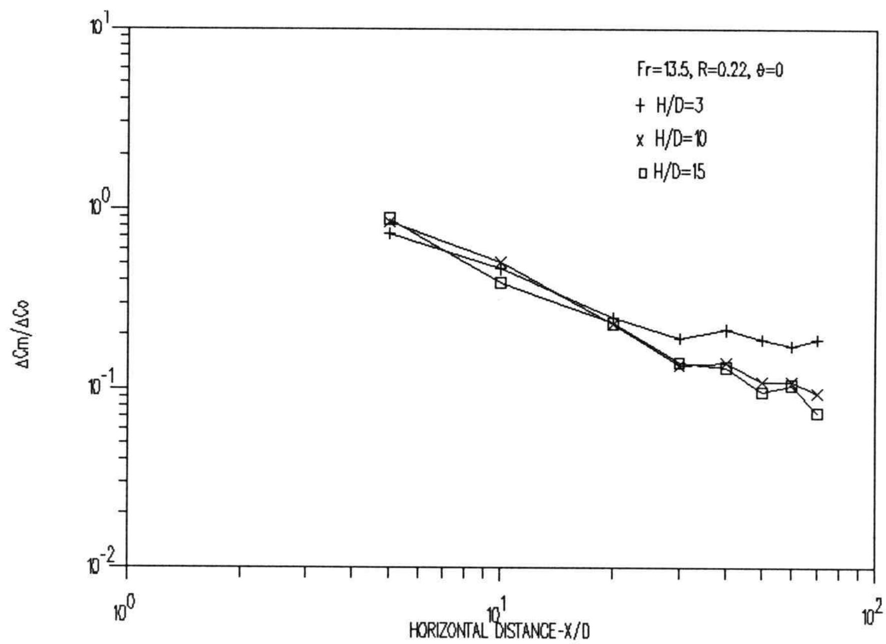

Figure 3-22. Effect of varying H/D on maximum concentration deficit for Fr=13.5, R=0.22 and θ=0°.

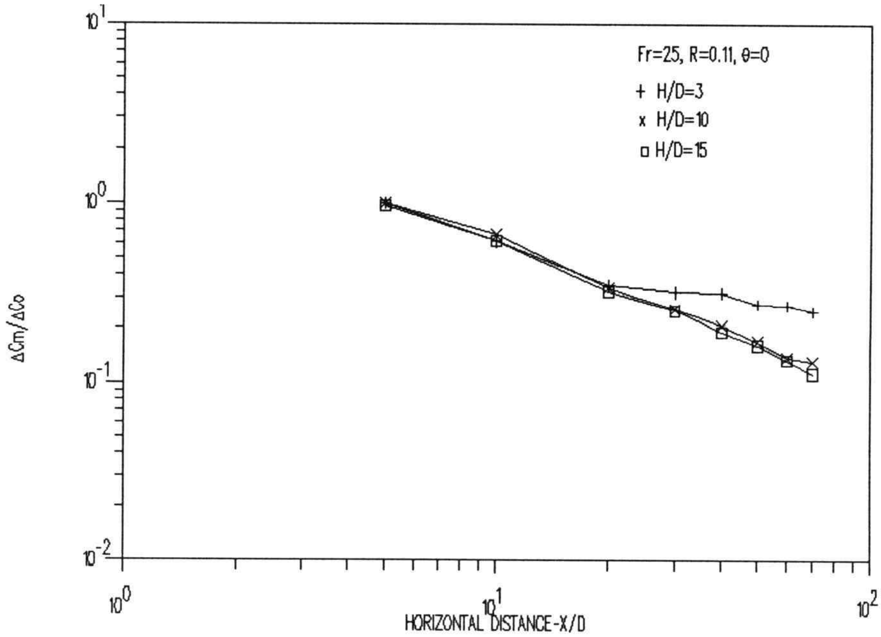

Figure 3-23. Effect of varying H/D on maximum concentration deficit for Fr=25, R=0.11 and θ=0°.

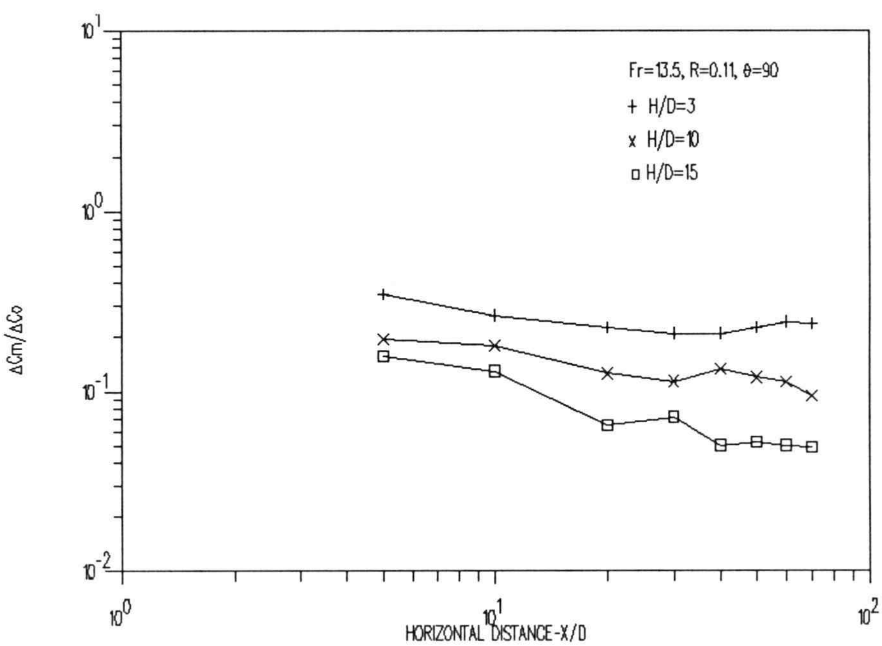

Figure 3-24. Effect of varying H/D on maximum concentration deficit for Fr=13.5, R=0.11 and θ=90°.

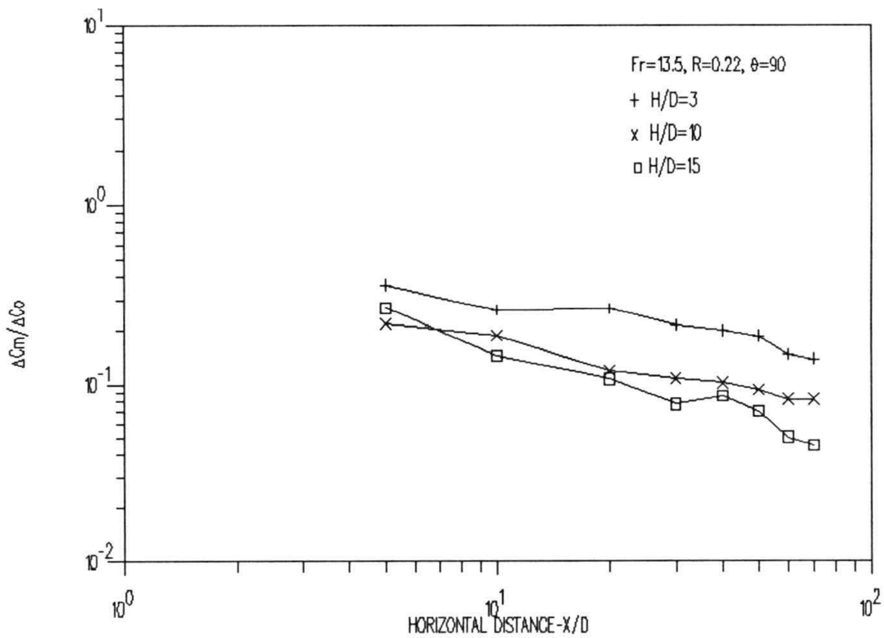

Figure 3-25. Effect of varying H/D on maximum concentration deficit for Fr=13.5, R=0.22 and θ=90°.

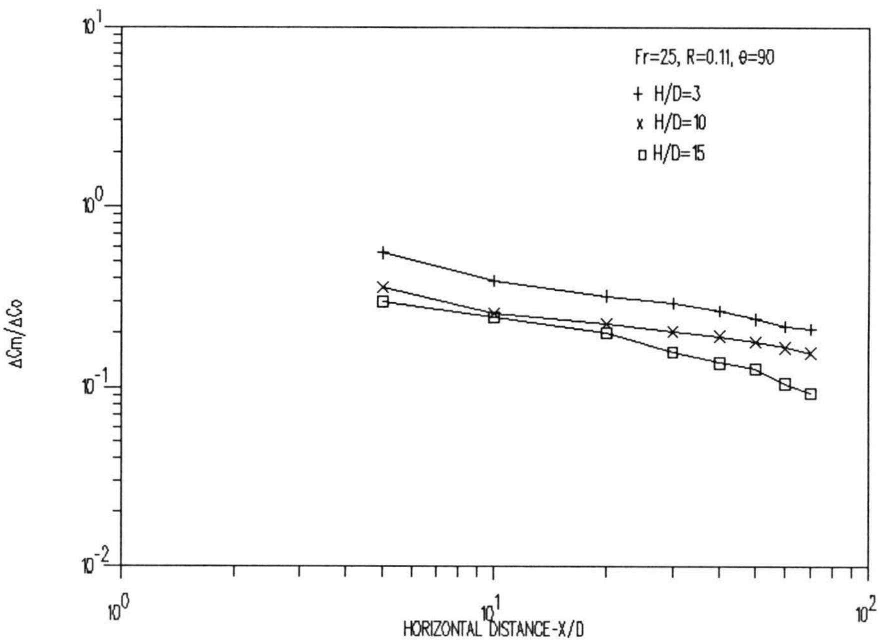

Figure 3-26. Effect of varying H/D on maximum concentration deficit for Fr=25, R=0.11 and θ=90°.

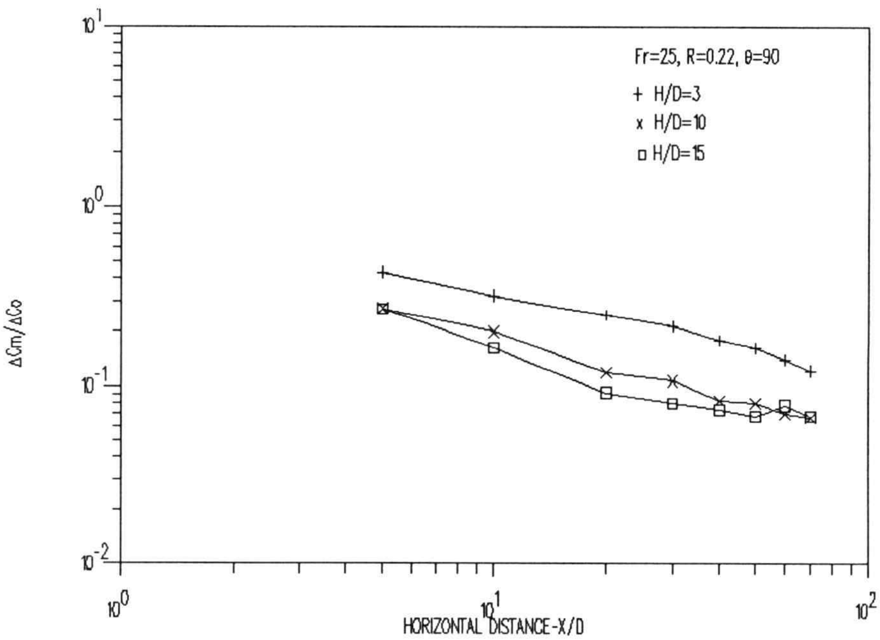

Figure 3-27. Effect of varying H/D on maximum concentration deficit for Fr=25, R=0.22 and θ=90°.

after discharge which decreases the dilution due to insufficient mixing length.

3.2 Regression Analysis

It is a basic premise of the science of weights and measures that all measurements have same error. Therefore, in order to prevent misleading conclusion and to offer an unbiased examination of the data collected, a further analysis was made. A functional relationship may be reduced from the two or more measurements involving one or more independent variables by the methods of linear regression. A statistic analysis program StatGraphics was used to perform a multiple regression analysis where the least-squares regression curve fit provided was in algebraic form. The algebraic equation is of the form

$$Y=a_0+\Sigma a_i X_i$$

where Y is the dependent variable and X_i (i=1,2,3....m) are the independent variables. The correlation coefficients a_i (i=0,1,2....m) which give the best least-squares fit are obtained from regression analysis.

By letting Y be the logarithm of a measured dependent variable $\Delta C_m/\Delta C_0$ or X_s/D and X_i be the logarithm of the independent variables Fr, H/D, θ, R and X/D the algebraic equation becomes

$$\ln(Y)=a_0+\sum_{i-1}^{m} a_i \ln(X_i)$$

This equation may be rewritten as a more suitable form

$$Y=e^{a0}(X_1)^{a1}(X_2)^{a2}(X_3)^{a3}(X_4)^{a4}(X_5)^{a5}$$

where $Y=\Delta Cm/\Delta C_0$ or X_s/D and $X_1=Fr$, $X_2=H/D$, $X_3=(\pi-\theta)$, $X_4=R$ and $X_5=X/D$.

It is noted that the discharge angle is taken as an independent variable in regression analysis in the form of $(\pi-\theta)$ because the logarithm of θ is undefined for horizontal discharge.

Referring to previous figures for maximum concentration deficit as a function of X/D, the curves have "bending tails" for most cases. The buoyant jet was divided into submerged jet and surface jet at the bend. The regression analysis was carried out for submerged and surface jets separately resulting in two least-squares fit curves. It is likely that the two curves fit provide a better fit than a single curve for both submerged and surface jets regimes.

The results of the regression analysis for various discharge angle are shown in Table 3-2. In a multiple regression analysis, the value of adjusted multiple coefficient of determination, R^2, can be used as a measure of how useful the linear model is when the sample contains more data points than the number of a_i parameters in the model. The values of R^2 for every curve fit is also given in Table 3-2. In general, the closer the value of R^2 is to 1, the better the model fits the data. The lowest value of R^2 is 0.708 for curve fit of X_s/D is acceptable. For $\Delta C_m/\Delta C_0$ cases, all the values of R^2 are greater than 0.88 which means the models provide a good fit to all data points in the population.

The coefficients of the curve fit for $\Delta C_m/\Delta C_0$ and X_s/D, a_i (i=0-5), as well as the number of observations for each curve fit are given for each discharge angle. One is reminded that the regression coefficients is for log-log curve fit. The regression analysis results for X_s/D and dilution of submerged and surface jets are shown graphically in Figures 3-28, 3-29 and 3-30.

The effects of Fr, R, θ and H/D on X_s/D and dilution are best demonstrated by the regression coefficients a_i shown in Table 3-2. The regression coefficients of Fr, H/D, $(\pi-\theta)$ and R for X_s/D are all positive which indicates that X_s/D increased with increasing Fr, R, H/D and decreasing θ. The magnitudes of the coefficients show that the major effects on X_s/D are H/D, θ and R. For inclined and vertical discharges, small Froude number provides large buoyancy while large Froude number provides great vertical velocity component and both conditions reduce X_s/D. Therefore, the influences of Fr on X_s/D are minor.

For the submerged jet regime ($X/D < X_s/D$), the regression coefficients offer an interesting result. The

$$(X_s/D) = e^{a0} (Fr)^{a1} (H/D)^{a2} (\pi - \theta)^{a3} (R)^{a4}$$

a_0	a_1	a_2	a_3	a_4	a_5	N^*	R^2
+0.894	+0.104	+0.772	+1.607	+0.669		67	0.708

SUBMERGED PORTION $(X/D < X_s/D)$

$$(\Delta C_m / \Delta C_0) = e^{a0} (Fr)^{a1} (H/D)^{a2} (\pi - \theta)^{a3} (R)^{a4} (X/D)^{a5}$$

a_0	a_1	a_2	a_3	a_4	a_5	N^*	R^2
-1.067	+0.416	-0.072	+1.043	-0.100	-0.901	250	0.897

SURFACE PORTION $(X/D > X_s/D)$

$$(\Delta C_m / \Delta C_0) = e^{a0} (Fr)^{a1} (H/D)^{a2} (\pi - \theta)^{a3} (R)^{a4} (X/D)^{a5}$$

a_0	a_1	a_2	a_3	a_4	a_5	N^*	R^2
-1.889	+0.401	-0.415	+0.218	-0.563	-0.425	378	0.880

* N : Number of Observation
** θ is in radians

Table 3-2. Coefficient matrix for multiple regression analysis.

very small values of a_2 suggest that there is a negligible effect of H/D on dilution on the submerged portion of the jet. The coefficients a_1, as expected, are moderate and positive values which show that the dilution is greater with decreasing Fr. The values a_3 indicates that the major effect on the dilution rate for the submerged portion of the jet is θ. It shows that the dilution increases with increasing θ.

The effect of Fr, θ, R and H/D on a surface jet regime ($X/D > X_s/D$) can also be demonstrated from the regression coefficients shown in Table 3-2. Increasing H/D, θ or R increases dilution while dilution is greater for decreasing Fr. This is due to the favor of the plume to the surface by high buoyancy. Also notice, from the magnitudes of a_1, a_2, a_3 and a_4 indicate that there is no dominant factor on dilution for surface jets. One has to be reminded that the surface jets discussed here are the portions remaining after the submerged buoyant jets reach the surface. The characteristics of regression curves for surface jets are highly influenced by initial dilution. For instance, the greater H/D provides the late occurrence of surface effects and the major portion of dilution occurs before the jet reaches the water surface. Therefore the values of $\Delta C_m/\Delta C_0$ shown in the regression analysis for surface jets are greater for small H/D. This provides the major contribution to the trend that increasing H/D increases dilution for surface jets. In fact, the influence of H/D on surface discharge jets are negligible except for very shallow discharge. The effects of R and Fr on initial dilution should also be considered in a manner similar to the effect of H/D on the dilution when the regression results for the surface jets are employed. The regression results for surface jets shown in Table 3-2 cannot be separated from the dependence of submerged jets.

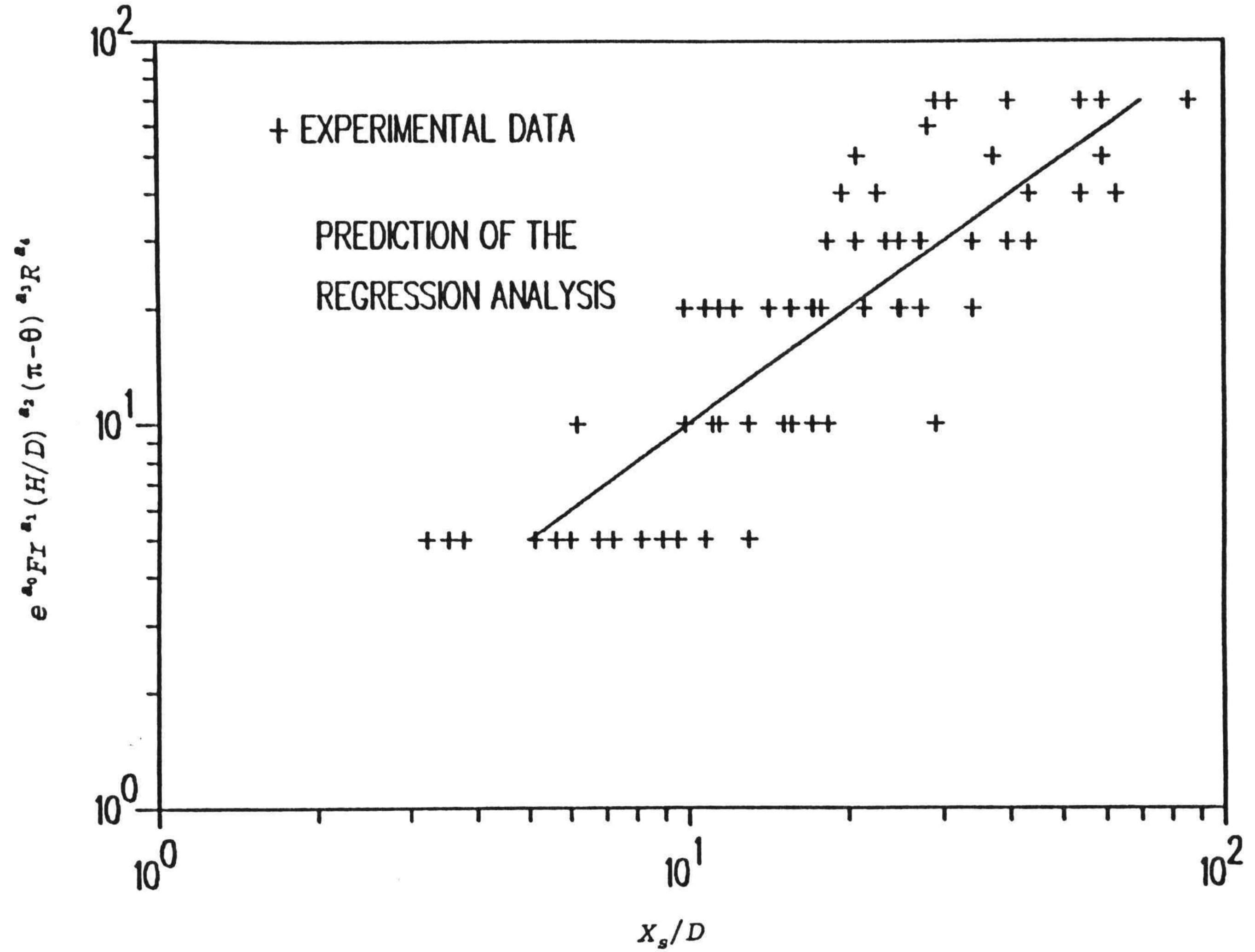

Figure 3-28. Horizontal distance, X_s/D, where the submerged buoyant jets reach the water surface.

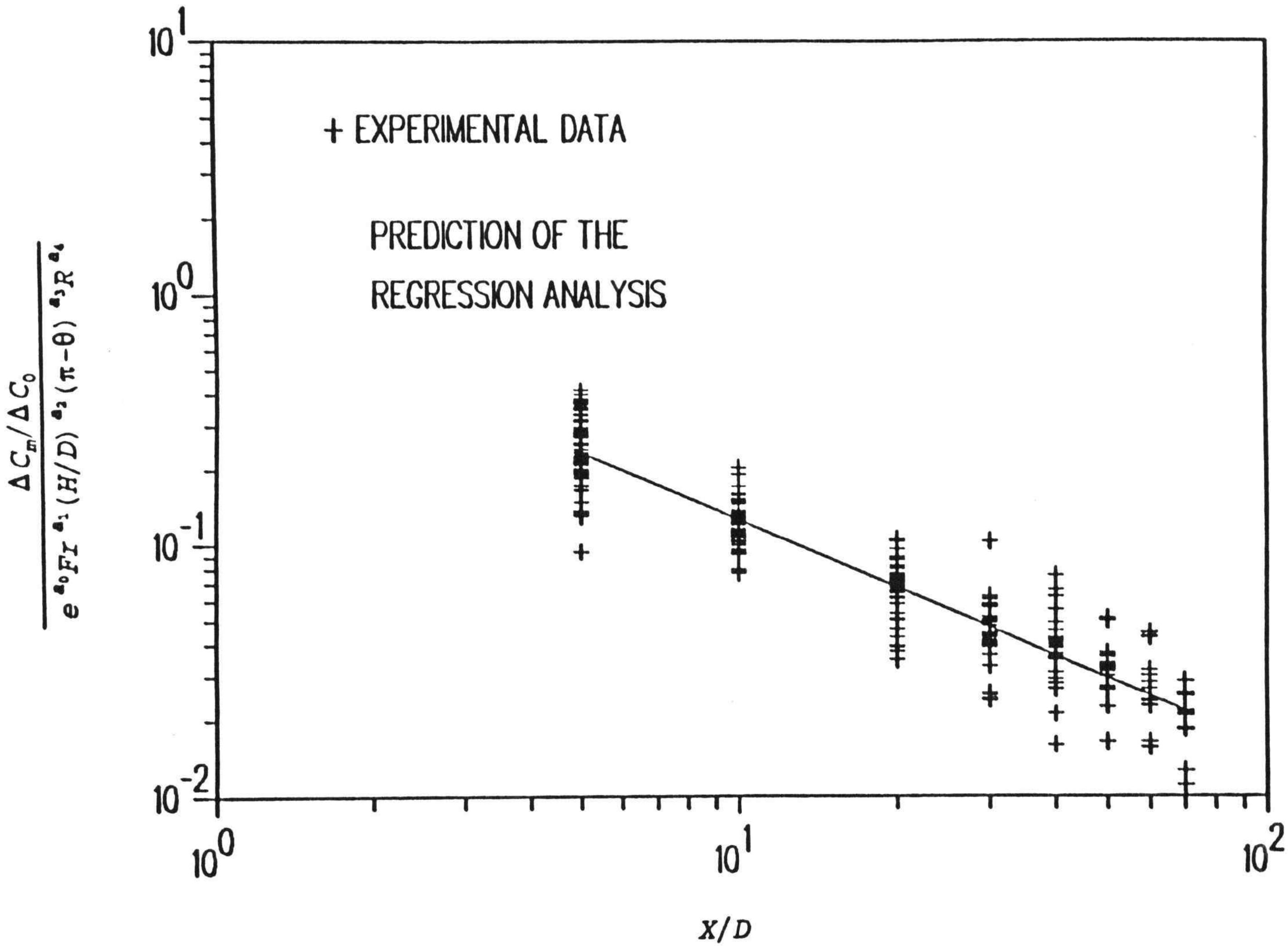

Figure 3-29. Maximum concentration deficit of submerged portion jets.

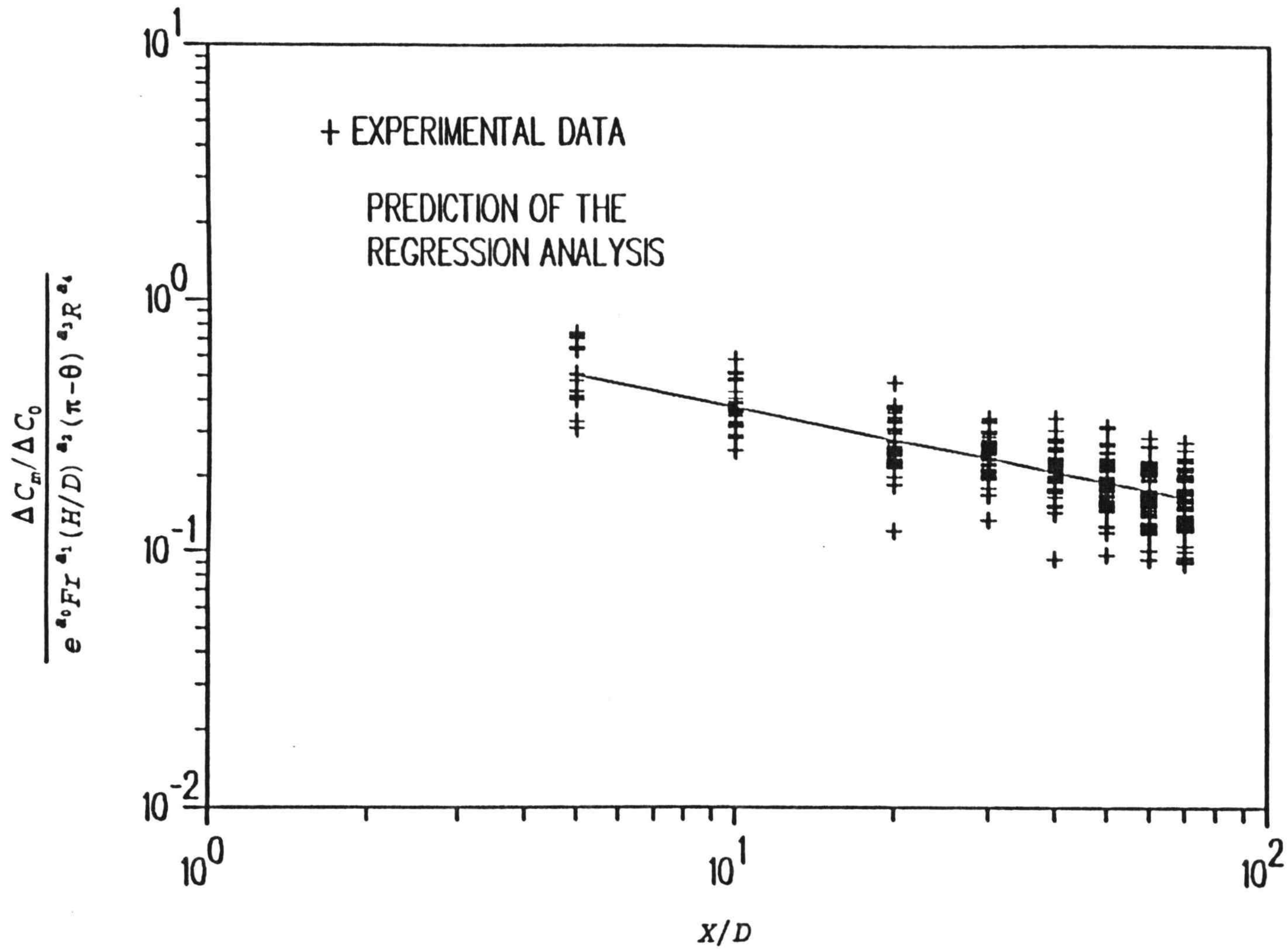

Figure 3-30. Maximum concentration deficit of surface portion jets.

4. ANALYTICAL WORK

In the previous chapter, a discussion of experimental data describing dilution and trajectory of a shallow submerged buoyant jet has been presented. In this chapter, a computer program UDKHDEN, which is based on the integral method proposed by Davis (1975) and Kannberg and Davis (1978), is used to predict the dilution of a shallow submerged buoyant discharge. The mathematical concept of the computer model will be introduced as well. The model will be extended to simulate shallow discharge using the method of images within the model. Finally, a comparison between the calculated results and experimental results will be made.

4.1 The Analytical Problem

Integral methods recently are successful in describing turbulence jets in unconfined medium under the influence of buoyancy, ambient stratification and cross-flow. Integral methods reduce the partial differential equations to ordinary equations by introducing empirical similarity profiles for velocity, temperature, or concentration across the jet. The resulting ordinary differential equation describe the variation of the velocity, temperature, or concentration scales and the jet width along the jet axis. Further relations which relate the entrainment of ambient fluid at the jet boundary are necessary. The entrainment coefficients in the entrainment function are determined empirically.

Computer Model

The computer model UDKHDEN developed to predict dilution in submerged buoyant jets is one of the many models that the EPA selected to include in their guidelines to predict the behavior of ocean discharge (Soldate et.al. (1983)). The model based on the technical developments of Davis (1975) and Kannberg and Davis (1978) will determine the plume characteristic of the turbulent buoyant jet discharge either from a single or multiple ports into moving, stratified ambient. The detailed development through the zone of flow establishment, zone of established flow and the detail dynamics of the gradual merging of the multiple buoyant jets are considered in this model. UDKHDEN has been proven to give a good prediction for submerged multiple port discharge buoyant jets.

The merging approximation proposed by Davis (1989) (1990) used in UDKHDEN can be used to simulate the discharge of a single port jet in shallow water investigated in present study. This can be done by employing the method of images as shown in Figure 4-1 where the depth of the water is simulated by the spacing between images.

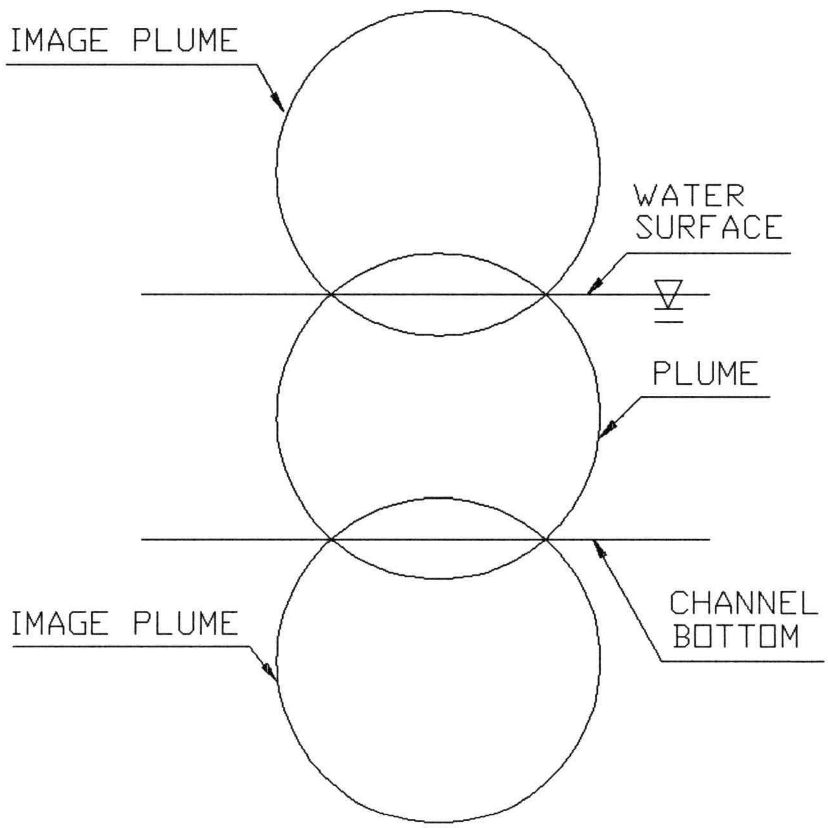

Figure 4-1. Image method of simulating buoyant jet in shallow water for UDKHDEN model.

The entrainment function employed in this study was based on the one proposed by Hirst (1971a). It has been modified to include merging effects. Further modifications were found necessary in this study to account for the physical boundary at the water surface.

4.2 Mathematic Model

Integral Method

The model to be presented in this section is for a submerged multiple buoyant plume. This model uses the Hirst (1971a)(1971b) submerged single port model as a starting point. In these references, Hirst presented an excellent analysis of the single port discharge. He considered the dynamics of a buoyant jet discharged from a round diffuser. The jet density may be different from the ambient density due to temperature or salinity difference. The characteristic of the turbulent jet were determined by the initial considerations at the diffuser exit (discharge velocity and outlet orientation), the buoyant force, ambient velocity and turbulence levels.

The equations governing the dynamics of the jet as it moves through the ambient are, conservation of mass,

$$\frac{\partial \rho}{\partial t}+\nabla\cdot(\rho\overline{V})=0 \qquad (4-1)$$

conservation of momentum,

$$\frac{\partial \overline{V}}{\partial t}+\frac{1}{2}\nabla\overline{V}^2-\overline{V}\times(\nabla\times\overline{V})=\frac{-\nabla P+\rho\overline{F}}{\rho}+\nu\nabla^2\overline{V} \qquad (4\text{-}2)$$

conservation of energy,

$$\frac{\partial T}{\partial t}+\overline{V}\cdot(\nabla T)=\frac{1}{\rho C_v}\nabla\cdot(k\nabla T)+\frac{\nu}{C_v}\phi-T\left(\frac{\partial P}{\partial T}\right)_\rho(\nabla\cdot\overline{V}) \qquad (4\text{-}3)$$

and conservation of species,

$$\frac{\partial C}{\partial t}+\overline{V}\bullet(\nabla C)=\nabla\bullet(D_c\nabla C) \qquad (4\text{-}4)$$

In addition to these equations, there is the equation of state relating density to temperature,

$$\rho=\rho(T,C)$$

The equations (4-1)-(4-4) are three dimensional, nonlinear and couple, therefore, they are very difficult to solve. In order to simplify the problem, the following assumptions were introduced (c.f. Hirst (1971a)):

(1) steady flow

(2) fully turbulent flow (ie. Reynolds Number $\geq$ 2500); molecular diffusion is neglected

(3) incompressible flow; the density variations appear only in the buoyancy terms (Boussinesq Approximation) of the momentum equation

(4) constant fluid properties

(5) pressure are purely hydrostatic

(6) fluid velocity are low enough to neglect

frictional heating

(7) the jet is axisymmetric

(8) boundary layer approximations are valid for the flow within the jet

The maximum discharge velocity in the experiments was 0.495m/sec. The kinetic energy associated with this discharge velocity is 0.112 j/kg. By assuming that all the kinetic energy is dissipated after discharge and only effects the effluent, the temperature increase due to dissipation would be $\Delta T=2.68\times10^{-5}$°C/kg. Thus, the dissipation term can be neglected due to the low discharge velocity.

With these assumptions, the governing equations can be rewritten as :

continuity

$$\nabla\cdot\overline{V}=0 \tag{4-5}$$

energy

$$\overline{V}\cdot(\nabla T)=0 \tag{4-6}$$

species

$$\overline{V}\cdot(\nabla C)=0 \tag{4-7}$$

momentum

$$\frac{1}{2}\nabla\overline{V}^2-\overline{V}\times(\nabla\times\overline{V})=\frac{\rho-\rho_\infty}{\rho_0}g \tag{4-8}$$

In order to solve equations (4-5)-(4-8), Hirst defined a so call "natural" coordinate system in which to express these equations. Figure 4-2 shows the coordinate system used in this analysis.

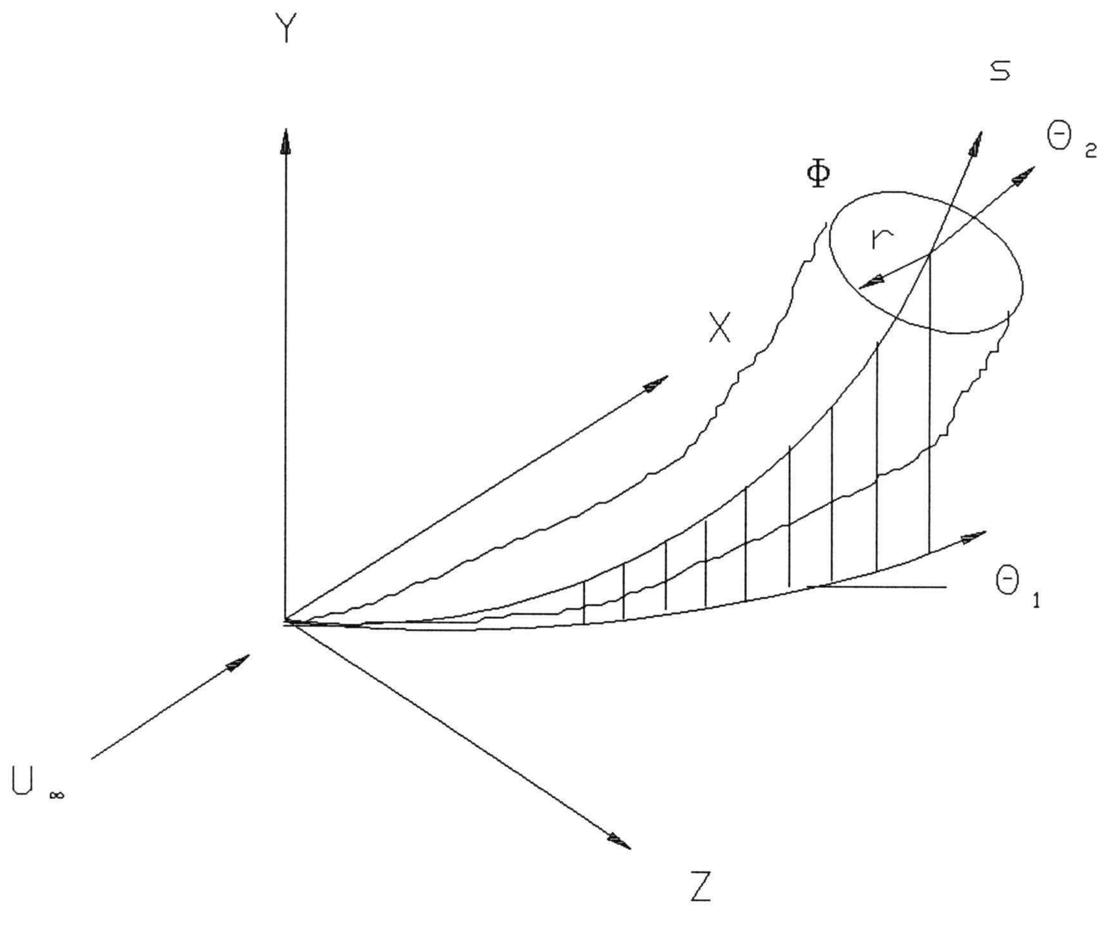

Figure 4-2. Natural coordinate system used by Hirst (1971a, 1971b).

Employing the axisymmetric assumption, that w (velocity in ϕ direction) is zero and boundary layer assumptions (u > v and $\partial/\partial r > \partial/\partial s$), the governing equations (4-5)-(4-8) can be simplified considerably. They become:

continuity

$$\frac{\partial \bar{u}}{\partial s}+\frac{1}{r}\frac{\partial r\bar{v}}{\partial r}=0 \qquad (4\text{-}9)$$

energy

$$\bar{u}\frac{\partial \bar{T}}{\partial s}+\bar{v}\frac{\partial \bar{T}}{\partial r}=-\frac{1}{r}\frac{\partial (r\overline{v'T'})}{\partial r} \qquad (4\text{-}10)$$

species

$$\bar{u}\frac{\partial \bar{C}}{\partial s}+\bar{v}\frac{\partial \bar{C}}{\partial r}=-\frac{1}{r}\frac{\partial (r\overline{v'C'})}{\partial r} \qquad (4\text{-}11)$$

s-momentum

$$\bar{u}\frac{\partial \bar{u}}{\partial s}+\bar{v}\frac{\partial \bar{u}}{\partial r}=\frac{\rho_\infty-\bar{\rho}}{\rho_0}g\sin\theta_2-\frac{1}{r}\frac{\partial (r\overline{u'v'})}{\partial r} \qquad (4\text{-}12)$$

y-momentum

$$(\bar{u}\frac{\partial \bar{u}}{\partial s}+\bar{v}\frac{\partial \bar{u}}{\partial r})\sin\theta_2=\frac{\rho_\infty-\bar{\rho}}{\rho_0}g-q\kappa_2\cos\theta_2$$

$$-\frac{1}{r}\frac{\partial (r\overline{u'v'})}{\partial r}\sin\theta_2 \qquad (4\text{-}13)$$

and x-momentum

$$(\bar{u}\frac{\partial \bar{u}}{\partial s}+\bar{v}\frac{\partial \bar{u}}{\partial r})\cos\theta_1\cos\theta_2=q(\kappa_1\sin\theta_1\cos\theta_2+\kappa\cos\theta_1\sin\theta_2)+$$

$$\frac{1}{r}\frac{\partial (r\overline{u'v'})}{\partial r}\cos\theta_1\cos\theta_2 \qquad (4\text{-}14)$$

κ_1= curvature of s with respect to θ_1

κ_2= curvature of s with respect to θ_2

and

$$q=\overline{u}^2-\frac{r}{4}\left(\frac{\partial\overline{v}^2}{\partial r}+\frac{\partial\overline{v}'^2}{\partial r}\right)$$

It is noted that equations (4-9)-(4-14) are rewritten in terms of average and fluctuating components to include the turbulent effects. In general, buoyant jets may not be axisymmetric in a cross flow because the fluid tends to roll up into twin parallel vortices at the edges of the jets due to the shearing action of the current and causes the jets to have horseshoe shaped profile. But the asymmetry can be neglected by taking the integral over the jet's cross section which averages out the asymmetry. Although the equations (4-9)-(4-14) have been simplified considerably, they are still very difficult to solve. At this point Hirst reduced the complexity of these equations by one more order with integration in the radial direction from the jet axis to infinity. The resulting equations of (4-9)-(4-14), which become the set of ordinary differential equations containing s as the only independent variable, are shown as:

continuity

$$\frac{d}{ds}\int_0^\infty \overline{u}r\,dr=-\lim_{r\to\infty}(r\overline{v})=E \qquad (4\text{-}15)$$

conservation of energy

$$\frac{d}{ds}\int_0^\infty \overline{u}(\overline{T}-\overline{T}_\infty)rdr=-\frac{d\overline{T}_\infty}{ds}\int_0^\infty \overline{u}rdr-\lim_{r\to\infty}(r\overline{v'T'}) \tag{4-16}$$

conservation of species

$$\frac{d}{ds}\int_0^\infty \overline{u}(\overline{C}-\overline{C}_\infty)rdr=-\frac{d\overline{C}_\infty}{ds}\int_0^\infty \overline{u}rdr-\lim_{r\to\infty}(r\overline{C'v'}) \tag{4-17}$$

and conservation of s-momentum

$$\frac{d}{ds}\int_0^\infty \overline{u}^2rdr=\int_0^\infty g\frac{\overline{\rho}_\infty-\overline{\rho}}{\rho_0}rdr\sin\theta_2+$$

$$EU_\infty\sin\theta_1\cos\theta_2-\lim_{r\to\infty}(r\overline{u'v'}) \tag{4-18}$$

The x-momentum and y-momentum equations can be simplified by using equation (4-18). The reduced equations are

$$\frac{d\theta_1}{ds}=\frac{EU_\infty\cos\theta_1}{\overline{q}\cos\theta_2}=\kappa_1 \tag{4-19}$$

$$\frac{d\theta_2}{ds}=\frac{\int_0^\infty g[\frac{\rho_\infty-\rho}{\rho_0}]rdr\cos\theta_2-EU_\infty\sin\theta_1\sin\theta_2}{\overline{q}}=\kappa_2 \tag{4-20}$$

where

$$\overline{q}=\int_0^\infty \overline{u}^2rdr-\frac{1}{4}E^2-\frac{1}{4}\lim_{r\to\infty}(r^2\overline{v'^2})$$

Hirst stated that the process of integration, which implies an average, obscures some of the information contented in the differential equations. This missing information can be reintroduced implicitly by the entrainment function E and velocity, temperature and concentration profiles. After using integration, equations (4-15)-(4-20) become a set of ordinary differential equations instead of boundary value type equations.

In order to solve this simultaneous ordinary differential equation, the profiles of velocity, temperature, concentration and density in the r direction need to be specified. The assumption may be made that these profiles are invariant in shape with streamwise coordinate s. The only difference between profiles are the changing of the centerline values of velocity, temperature, species, density and width of the jet. With these profiles and entrainment function properly specified, u, T, C, θ_1, θ_2 and width of the jet b can be obtained.

It is noted that the free stream turbulence terms in equations (4-15)-(4-20) can be neglected because of insignificant influence of ambient turbulence on jet development in the near field.

Similar Profiles

In general, submerged buoyant jets pass through several regions as they move from the discharger through the ambient. The most commonly considered regions shown in Figure 4-3 are:

(1) The zone of flow establishment (ZFE) - The ZFE is usually a few discharge diameters long in which the velocity, temperature and density profiles change from top-hat shapes at the point of discharge to bell-shaped profiles at the end of this zone. The length of ZFE is termed starting length, Se. In this zone the properties along the central core are constants.

(2) The zone of established flow (ZEF) - This zone is characterized by continuous similar bell-shaped profiles. The jet characteristics are influenced by the jet's momentum and buoyancy and ambient conditions rather than by the initial discharge condition. In this region there is no central core.

(3) The zone of surface impingement - This is the zone of transition at the free water surface or the maximum height of the rise in stratified environments.

(4) The drift zone - This is the zone beyond the zone of surface impingement. In this zone the jet momentum is depleted and jet fluid is convected by ambient currents.

(5) The merging zone - This zone occurs only for multiport discharges in which the neighboring plumes merge due to entrainment and plume growth. Plume merging can occur anywhere along the plume depending on the distance between discharge ports, Froude number, and velocity

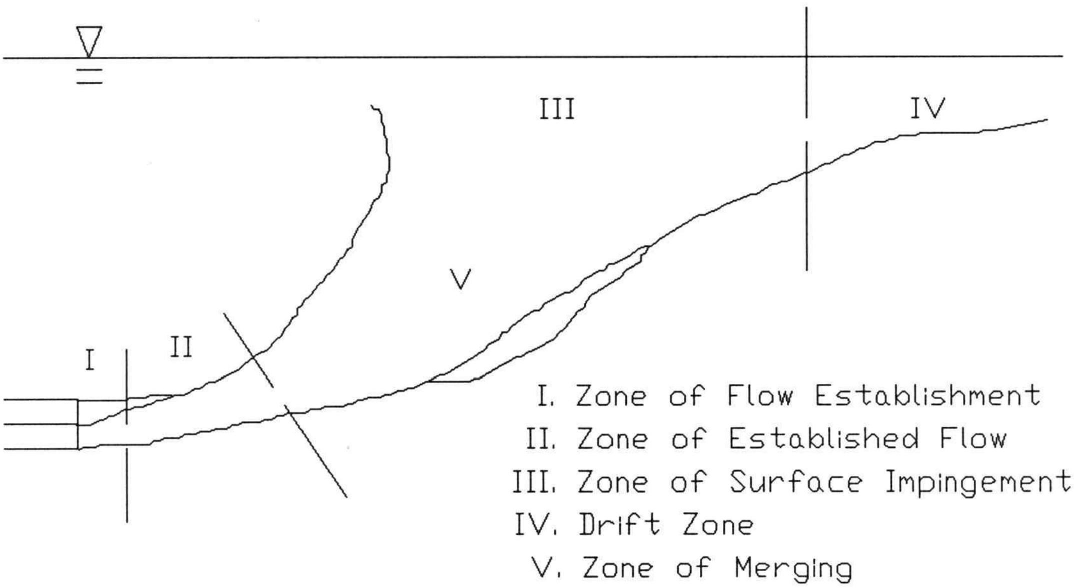

Figure 4-3. Flow regimes for multi-port buoyant jets.

ratio.

In order to solve equation (4-15)-(4-20) the velocity, temperature and concentration profiles must be specified. For the different zones, different profiles are employed according to the characteristics of that zone. With the appropriate profiles specified for the ZFE, the equations can be solved numerically by using outfall conditions as initial conditions. The solution advances until the central core disappears. The end conditions of ZFE are used as initial conditions for ZEF. Then the equations for ZEF are solved successively with modified profiles as the solution continues on in s direction. In this manner the equations (4-15)-(4-20) are solved for each zone.

For most integral methods, the profiles are assumed to be similar which means that the shape of the profile is invariant with s. The most popular profile shape is Gaussian profile shown as:

$$\bar{u} \propto e^{-\left(\frac{r}{b_1}\right)^2}, \bar{T} \propto e^{-\left(\frac{r}{b_1 \lambda}\right)^2}, \bar{C} \propto e^{-\left(\frac{r}{b_1 \lambda}\right)^2}$$

where λ is a measure of the relative spreading of temperature, species and velocity profiles, and b_1 is the value of r at which u reduces to some specified fraction of U_c. (usually chosen to be either 0.5 or 0.37).

Davis (1975) suggested a more suitable profile shape for a merging plume, the 3/2 power profile. The profiles then can be written as

$$\bar{u} \propto [1-(\frac{r}{b})^{3/2}]^2, \bar{T} \propto [1-(\frac{r}{b})^{3/2}]^2, \bar{C} \propto [1-(\frac{r}{b})^{3/2}]^2$$

where $b_1=0.53b$.

With these profiles, the integral can now be taken and equations (4-15)-(4-20) become the nonlinear ordinary differential equations which can be solved by Runge-Kutta or Hamming Predictor - Corrector method for each zone.

<u>Zone of Flow Establishment</u>

For jets discharged to an ambient flow, the longitudinal velocity far from the jet axis is $U_\infty \sin\theta_1 \cos\theta_2$. Therefore, the similar profiles for the zone of the flow establishment are

$$u=U_0, r \leq r_u$$

$$u=(U_0-U_\infty \sin\theta_1 \cos\theta_2)[1-(\frac{r-r_u}{b})^{\frac{3}{2}}]^2 +$$

$$U_\infty + \sin\theta_1 \cos\theta_2, r \geq r_u \qquad (4\text{-}22)$$

$$T-T_\infty=T_0-T_\infty, r \leq r_t$$

$$T-T_\infty=(T_0-T_\infty)[1-(\frac{r-r_t}{b})^{\frac{3}{2}}]^2, r \geq r_t \qquad (4\text{-}23)$$

and

$$C-C_\infty=C_0-C_\infty, r \leq r_c$$

$$C-C_\infty=(C_0-C_\infty)[1-(\frac{r-r_c}{b})^{\frac{3}{2}}]^2, r \geq r_c \qquad (4\text{-}24)$$

where b is the half width of the free turbulent jets, and r_u, r_t and r_c are the potential core widths for velocity, temperature and concentration. For most cases, temperature and concentration grow at the same rate which indicates that equations (4-23) and (4-24) are identical and $r_t = r_c$.

By substituting these profiles into the integral appearing in differential equations (4-15)-(4-20), a new set of six non-linear coupled ordinary differential equations with six unknowns is obtained. With initial conditions set as the conditions of jet discharge, the unknowns r_u, r_t, r_c, b, θ_1 and θ_2 are solved as functions of the streamwise coordinates by using a Hamming Predictor-Corrector method. The calculation continues until r_u and r_t are zero.

Zone of Established Flow

The zone of established flow starts where r_u and r_t are zero. In general the jet is fully developed by this time s/D reaches 10 [Fischer et.al. (1979)]. At this point the plume width will be about 2.6 port diameters [Kannberg (1977)]. In this region the profiles of the plume remain axisymmetric and similar until merging occurs. The similar profiles of velocity and temperature then are assumed to be

$$u = \Delta u + U_\infty \sin\theta_1 \cos\theta_2$$

where

$$\Delta u = \Delta u_c [1 - (\frac{r}{b})^{\frac{3}{2}}]^2$$

$$\Delta T = \Delta T_c[1-(\frac{r}{b})^{\frac{3}{2}}]^2$$

$$\Delta C = \Delta C_c[1-(\frac{r}{b})^{\frac{3}{2}}]^2$$

and b is the full half width of the plume.

Employing these 3/2 power profiles, equations (4-15)-(4-20) become a set of ordinary first order differential equations. Using the final conditions of the zone of flow establishment as initial conditions, these equations then can be solved by stepwise integration using a Runge-Kutta or Hamming Predictor-Corrector method. The solution to these six equations yields values of Δu_c, ΔT_c, ΔC_c, b, θ_1 and θ_2 as functions of s.

<u>Zone of Merging Plumes</u>

As the plume continues growing, the width of the plume reaches to the spacing between the jets and the plumes begin to merge. At this point, the profiles are no longer axisymmetric and become dependent on the angle with respect to the neighboring plume. In order to have smooth transition and a continuous solution of the differential equations between the zone of established flow and the zone of merging, some certain adjustments of the profiles must be made.

A new coordinate system shown in Figure 4-4 is used as the merging occurs. The new coordinate system ζ lies

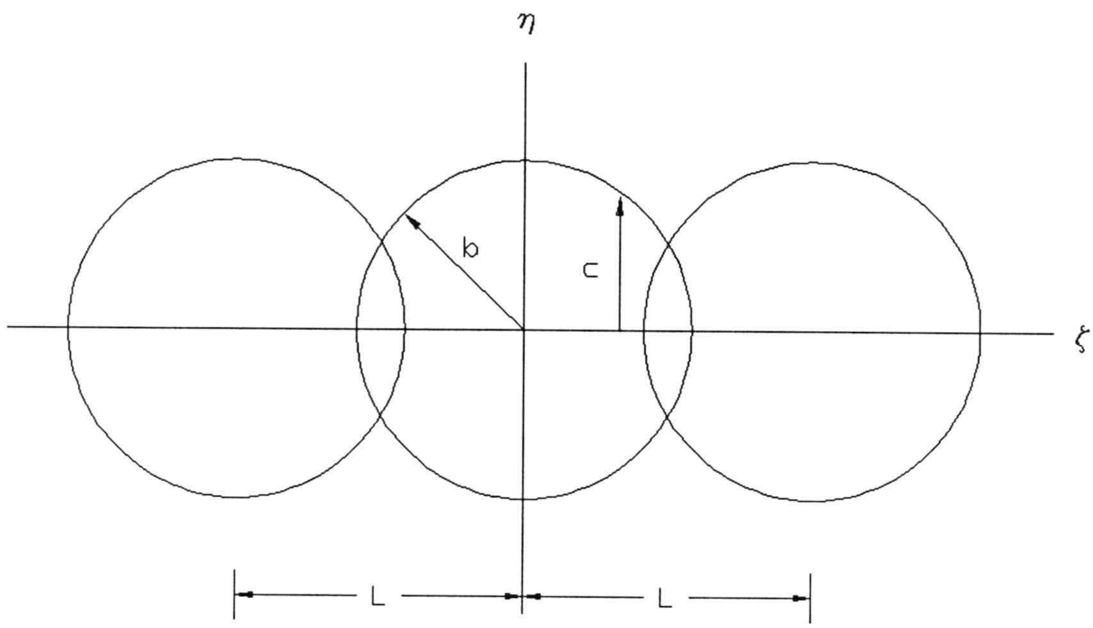

Figure 4-4. The coordinate system used by Davis (1975) for merging plume analysis.

through the axis of a line of adjacent jets and η is perpendicular to the line of the jets. As the merging begins, the merging profiles should satisfy the following conditions [Davis (1975)] :

(1) The profiles should be smooth in all directions.

(2) The slopes should be zero at $\zeta=0$, $\eta=0$ and $\zeta=L/2$, $\eta=0$.

(3) When the plumes just begin to merge, they should retain their single plume profiles.

(4) The profiles should be the superposition of the single plume profiles with no point allowed to exceed center-line properties.

(5) The profiles should maintain the characteristics of similar profiles in the streamwise coordinate, s.

With these considerations, the similar profiles of the zone of merging are written as

$$u=\Delta u+U_\infty \sin\theta_1 \cos\theta_2$$

$$\Delta u=\Delta u_\eta=\Delta u_\zeta[1-(\frac{\eta}{c})^{\frac{3}{2}}]^2$$

$$\Delta u_\zeta=\Delta u_c[1-(\frac{\zeta}{b})^{\frac{3}{2}}]^2 \ ,0\leq\zeta\leq L-b$$

$$\Delta u_\zeta=\Delta u_c[(1-(\frac{\zeta}{b})^{\frac{3}{2}})^2+(1-(\frac{L-\zeta}{b})^{\frac{3}{2}})^2],L-b\leq\zeta\leq L/2$$

$$\Delta T = \Delta T_{\eta}[1-(\frac{\eta}{c})^{\frac{3}{2}}]^2$$

$$\Delta T_{\zeta} = \Delta T_c[1-(\frac{\zeta}{b})^{\frac{3}{2}}]^2 \quad ,0 \leq \zeta \leq L-b$$

$$\Delta T_{\zeta} = \Delta T_c[(1-(\frac{\zeta}{b})^{\frac{3}{2}})^2 + (1-(\frac{L-\zeta}{b})^{\frac{3}{2}})^2], L-b \leq \zeta \leq L/2$$

where $c^2=b^2-\zeta^2$ and the species has the same profile as the temperature.

It is assumed that $\Delta u_{\zeta}=\Delta u_c$ for all ζ after $\Delta u_{\zeta}=\Delta u_c$ at $\zeta=L/2$ and $\Delta T_{\zeta}=\Delta T_c$ for all ζ after $\Delta T_{\zeta}=\Delta T_c$ at $\zeta=L/2$.

With these similar profiles the integral in equations (4-15)-(4-20) can be evaluated and a system of ordinary equations similar to the equations for the zone of established flow can also be obtained. By using the final plume conditions of the zone of established flow as initial conditions, the quantities Δu_c, ΔT_c, b, θ_1 and θ_2 can be obtained by solving the system equation for the zone of merging.

<u>Entrainment Function</u>

In order to solve equations (4-15)-(4-20), the entrainment function E in the righthand side of equation (4-15) must be specified. The entrainment physically is the rate of ambient fluid brought into the jet by turbulent action or shear flow near the edge of the jet and basically is determined empirically. It determines the growth and development of buoyant jets. The accuracy of solutions of equations (4-15)-(4-20) depends on how accurately the entrainment function is calculated.

The basis of the entrainment method is to relate the rate of inflow of ambient fluid to the local properties of the jet, and the ambient current. Morton (1956) probably was the first to hypothesize that the entrainment into any jet would be proportional to the mean velocity in the jet at the level of inflow. Numerous other researchers have employed this concept to develop other entrainment equations which better agree with the widely varying discharge and ambient conditions that affect the plume. In general, the entrainment function should depend on the following factors (c.f. Hirst (1971a)):

(1) local mean flow conditions within the jet, u_c and b,

(2) local buoyancy within the jet, Fr,

(3) velocity ratio, R,

(4) ambient turbulence,

(5) discharge orientation.

For the merging plume Davis (1975) also proposed that the entrainment function should contain a term to include the effect of competition and reduction of the entrainment surface.

Davis (1975) suggested that for the zone of flow establishment before merging, the entrainment is expressed as

$$\frac{E}{r_0 U_0} = c_1(0.0204 + 0.0144\frac{b}{r_0})[|(1 - R\sin\theta_2)|(1 - \frac{c_4 r_0}{L}) +$$

$$c_3 R\sqrt{1 - (\sin\theta_2 \cos\theta_2)^2}\,(1 + \frac{c_2}{Fr}) \qquad (4\text{-}25)$$

For the zone of established flow before merging, the entrainment function is expressed as

$$E = (a_1 + \frac{a_2}{Fr})[b|u_c - U_\infty \sin\theta_1 \cos\theta_2|(1 - \frac{a_4 b}{L}) +$$

$$a_3 U_\infty \sqrt{1 - (\sin\theta_1 \cos\theta_2)^2} \qquad (4\text{-}26)$$

and for the zone of merging, the entrainment function is expressed as

$$E = (a_1 + \frac{a_2}{Fr})[b|u_c - U_\infty \cos\theta_2|(1 - \frac{a_4}{2})(1 - \frac{2}{\pi}\cos^{-1}\frac{L}{2b}) +$$

$$a_3 U_\infty \frac{L}{2}\sqrt{1 - (\sin\theta_1 \cos\theta_2)^2} \qquad (4\text{-}27)$$

where a_1, c_1 are coefficients for jet induced entrainment, a_2, c_2 are coefficients for buoyancy effect, a_3, c_3 are coefficients for free stream effect and a_4, c_4 are coefficients for plume merging effect. These coefficients must be determined empirically. The values of these coefficients recommended by Kannberg (1977) are :

c_1=1.06, c_2=34, c_3=6.0, c_4=0.20,

a_1=0.05, a_2=0.0, a_3=11.5, a_4=0.16.

The entrainment functions as presented need to be modified for a single-port discharge in shallow water to account the free surface effect. As a buoyant jet reaches the water surface, it is deflected and flows horizontally. Therefore, as image solution is used, the angle θ_2 in equation (4-27) then is assumed to be zero and the entrainment function for merged plumes (ie. L/D < 0.95) is expressed as

$$E=(a_1+\frac{a_2}{Fr})\,[b|u_c-u_\infty \sin\theta_1 \cos\theta_2|(1-\frac{a_4}{2})(1-\frac{2}{\pi}\cos^{-1}\frac{L}{2b})+ a_3 U_\infty \frac{L}{2}\cos\theta_1] \qquad (4\text{-}28)$$

4.3 Model Performance

The purpose of this analytical development of the model was to obtain a predictive tool to handle single-port discharge in shallow water. In the previous section, the governing differential equations and entrainment function were determined. A computer code based on these analysis was assigned the name UDKHDEN. The program was applied to simulate the discharge in shallow water with various combinations of Fr, H/D, θ and R. Several test cases were used and comparisons of maximum concentration deficit were made with experimental data.

An example of comparison between results of UDKHDEN and experimental data for co-flow discharge is illustrated in Figure 4-5. The controlled conditions considered for Figure 4-5 were velocity ratio, R=0.22; densimetric Froude number, Fr=25 and submergence depth, H/D=10. Under these conditions, high discharge momentum and high ambient velocity move the zone of impingement far downstream. therefore, the character of the jet approaches that of a submerged buoyant jet. Figure 4-5 shows that variations on the dilution were observed. This is believed attributed to the disparity of the starting length between prediction and experiment. An effort was made to improve the prediction of starting length by employing the empirical formulation of starting length suggested by Soldate et.al. (1983) for submerged buoyant jets. The starting length is expressed as

$$Se/D = 2.8*Fr^{2/3} \qquad Fr < 2$$
$$Se/D = 0.113*Fr^2 + 4 \qquad 2 \leq Fr \leq 3.2 \qquad (4-29)$$
$$Se/D = (5.6*Fr^2)/(Fr^4 + 18)^{1/2} \qquad Fr \geq 3.2$$

where Se is the starting length and D is the discharge diameter.

The computer code in which the starting length was calculated by equation (4-29) was assigned a name UDKHSE. It is in all aspects the same as UDKHDEN except in starting length. The results of UDKHSE are also shown on Figure 4-5 for comparison. The results of UDKHSE compared well with the measured data within the range of X/D values of 5 and 70. It is noted that the maximum concentration deficit curves for UDKHDEN and UDKHSE do not have flattening out "tails" which indicates no surface effect occurs within that range.

In Figures 4-6 to 4-10 experimental data for co-flow discharge were shown. Comparison was made between prediction and experiment. Cases were run for velocity ratio R of 0.11 and 0.22 with densimetric Froude number ranging from 5.6 to 25. The receiving water depth H/D is 3 for all combinations. And again predictions of UDKHDEN and UDKHSE are shown. As given in Figures 4-6 through 4-9, the locations of the bend of maximum concentration deficit curve are matched quite well. The model slightly overpredict the dilution for the low current case and slightly underpredict the dilution for high current case. This is probably due to the deviation of the trajectory of maximum concentration deficit. In general, the agreement between theory and experiment is quite good.

For low Froude number discharge shown in Figure 4-10, UDKHSE and UDKHDEN both underpredict the dilution. This is believed due to the presence of strong buoyancy influence. As the buoyancy force dominate the mixing process, the surface effect indicated in model prediction takes place faster than the surface effect in experiment. Thus, the underpredictions of the dilution of UDKHDEN and UDKHSE are shown for low Froude number discharge. The presence of the strong buoyancy also causes the deviation of the trajectory between prediction and experiment. When the image solution is used for buoyant jet in shallow water, the plume is assumed to be compressed in a shallow regime between two images boundaries and the trajectory is at the center of this regime. Actually, because of the influence of buoyancy, the jet favors to the water surface and the trajectory of maximum concentration deficit stays close to the free surface instead of at the center of the shallow layer. In general, the merging routine which UDKHDEN and UDKHSE are based on predicts the dilution accurately for the discharge of a single-port in shallow water only when buoyancy effects are minor.

The dilution comparisons of crossflow discharge (ie. θ=90°) for Froude numbers Fr of 13.5 and 25 are given in Figures 4-11 and 4-12. An experimental dye test showed that the plumes reach the water surface right after discharge with H/D=3 for vertical discharge. Therefore, equation 4-29 which estimates the starting length for submerged buoyant jets could not be used since the values of Se/D computed by equation 4-29 are greater than submergence depth. In Figure 4-11 and 4-12, comparisons are made only between the prediction of UDKHDEN and experimental data for various velocity ratio R. The trend for different velocity ratio is opposite but the agreements between model prediction and experimental data are quite well. This is probably attributed to the modification of the entrainment function. As the merging routine produces the merged plumes, θ_2 in equation (4-27) is forced to be zero in order to simulate the deflected jet when it reaches the water surface.

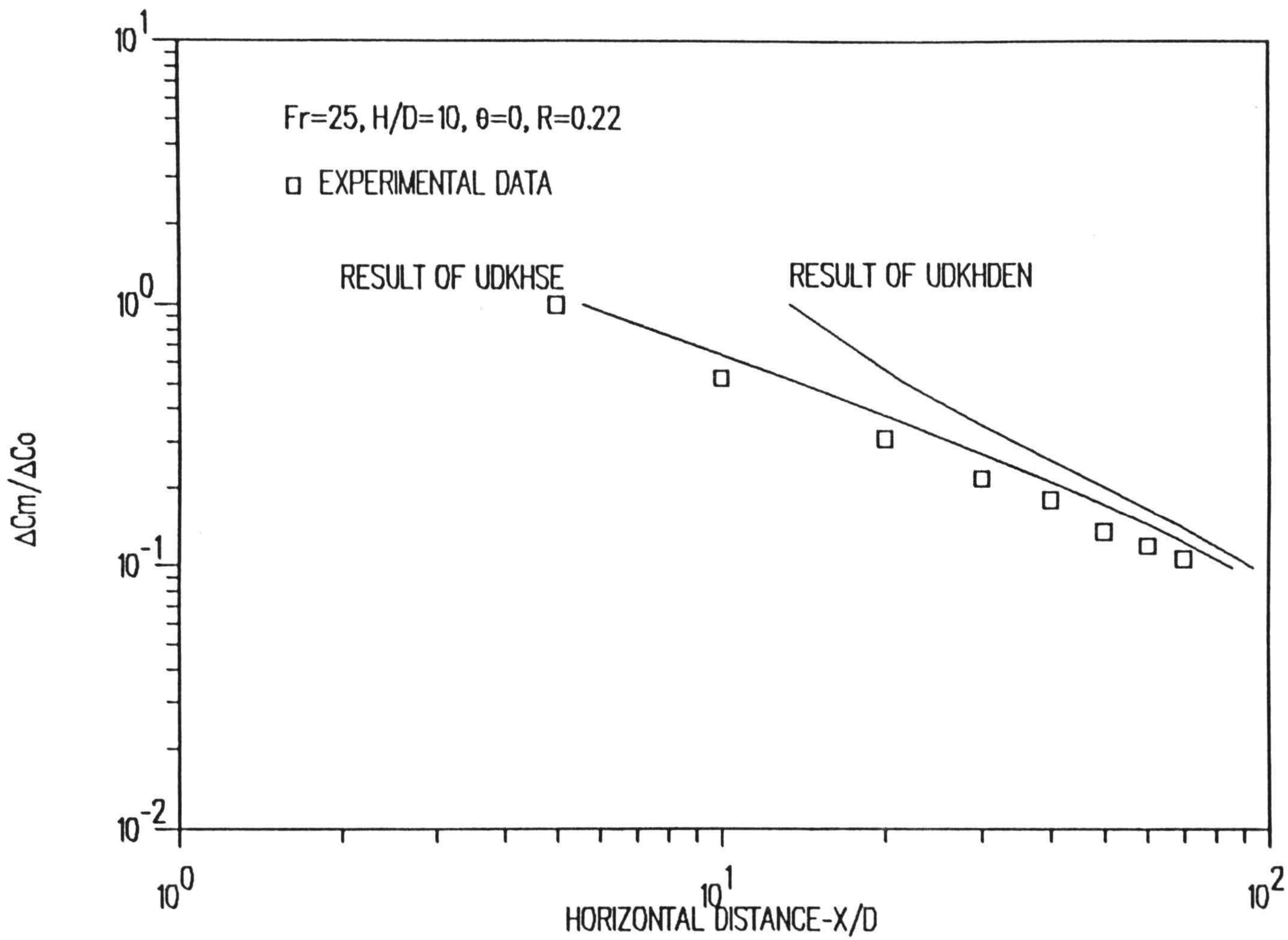

Figure 4-5. Comparison of experimental and model predicted maximum concentration deficit for Fr=25, R=0.22, H/D=10, co-flow discharge.

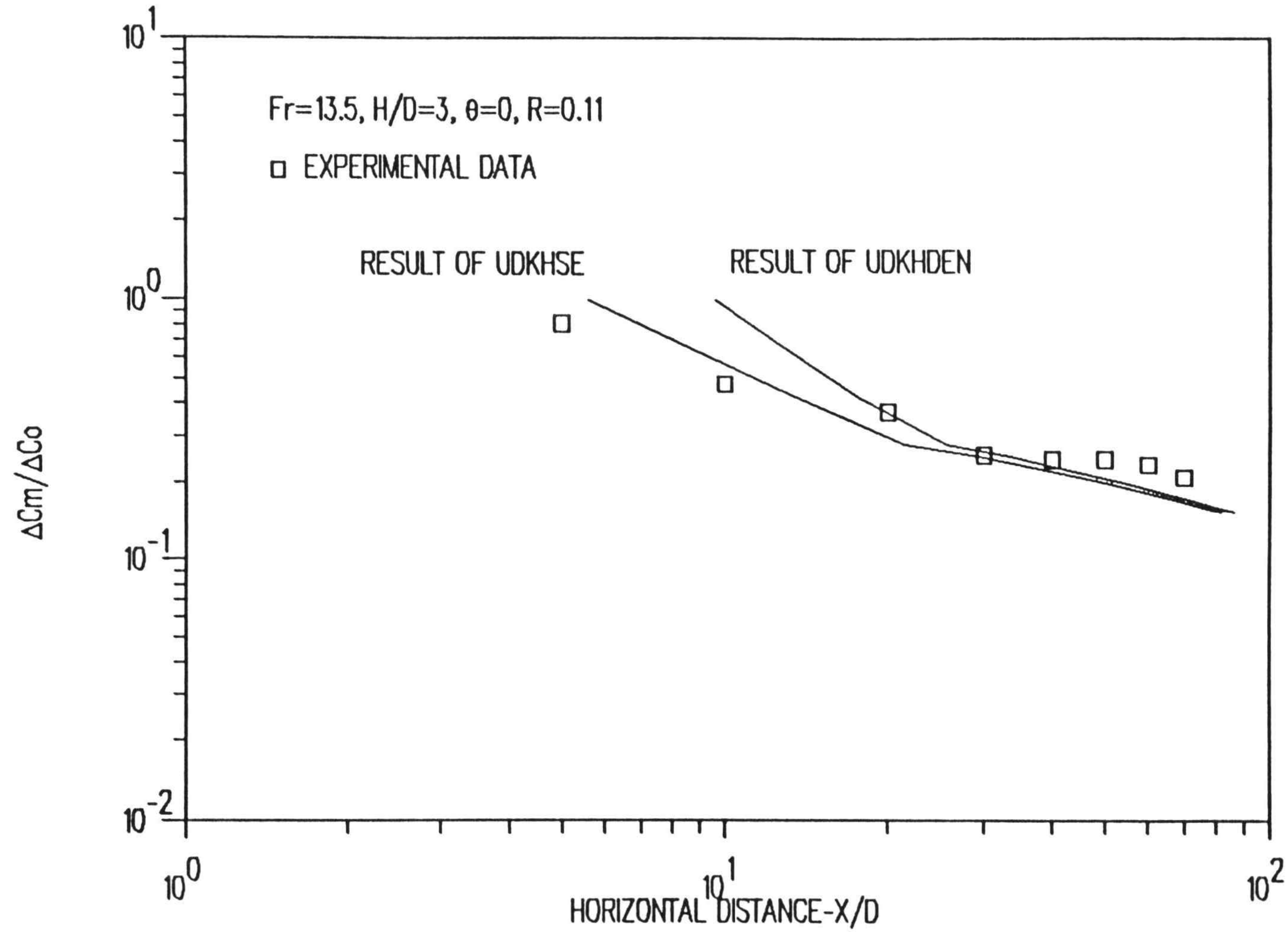

Figure 4-6. Comparison of experimental and model predicted maximum concentration deficit for Fr=13.5, R=0.11, H/D=3, co-flow discharge.

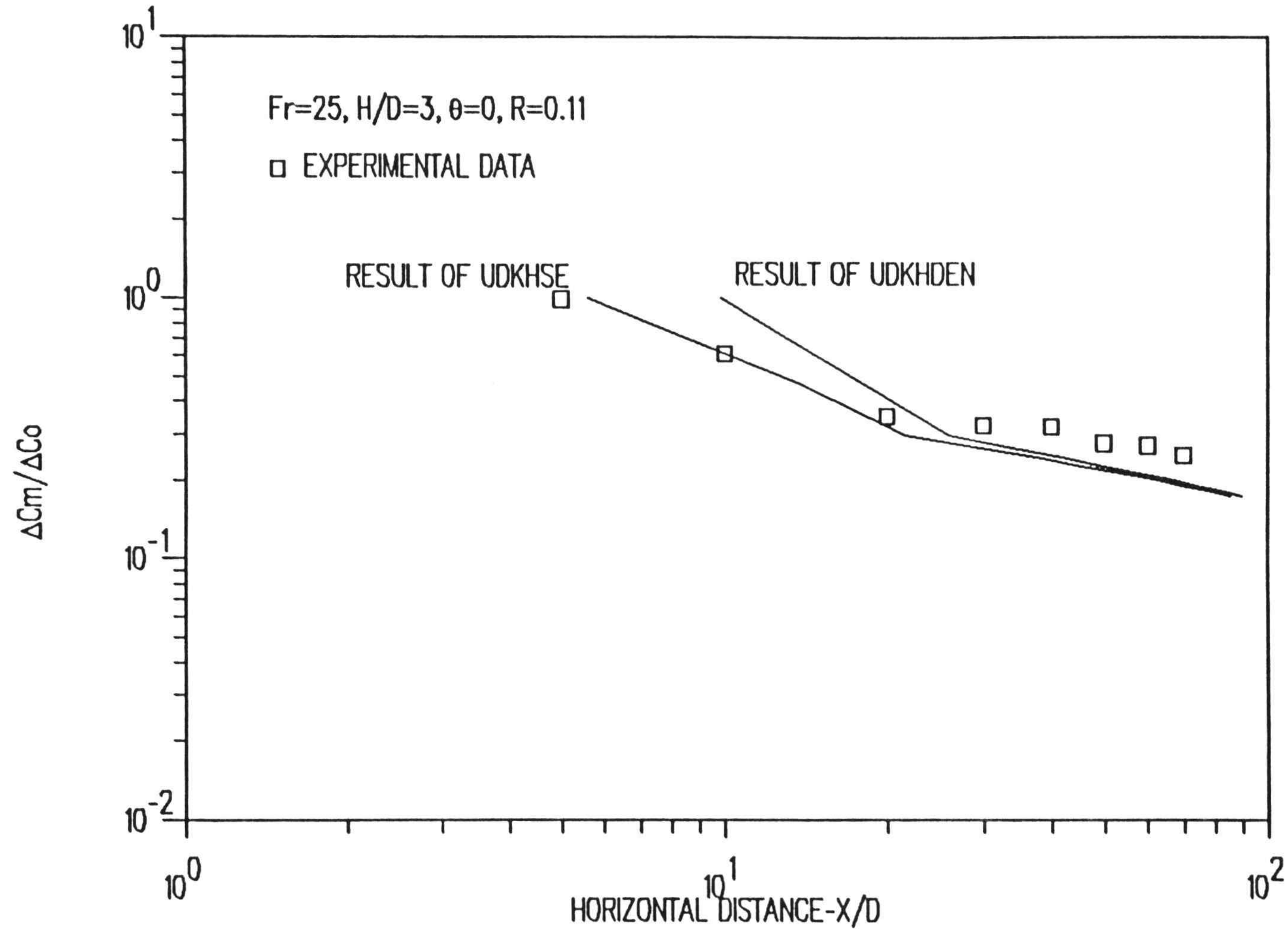

Figure 4-7. Comparison of experimental and model predicted maximum concentration deficit for Fr=25, R=0.11, H/D=3, co-flow discharge.

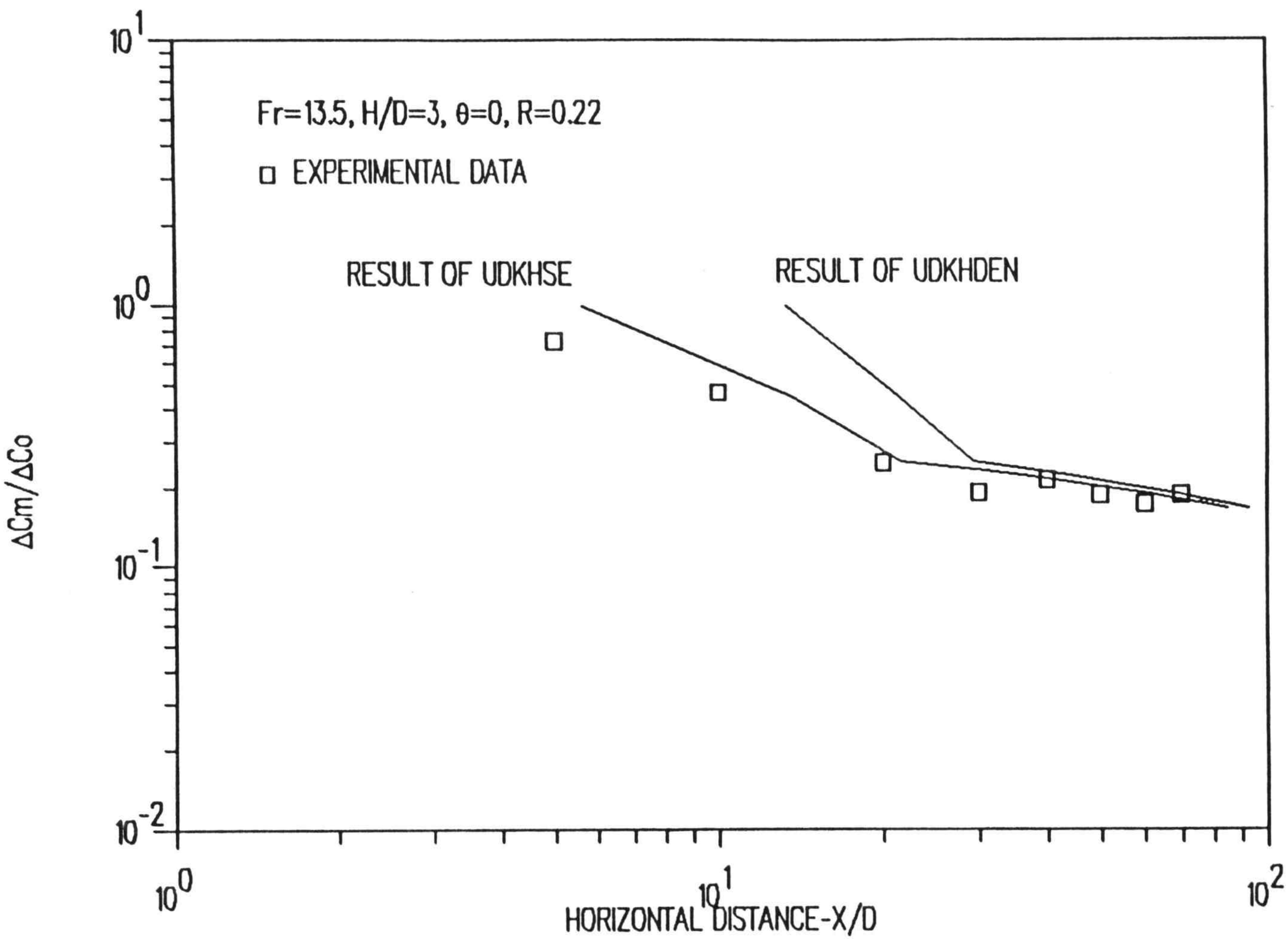

Figure 4-8. Comparison of experimental and model predicted maximum concentration deficit for Fr=13.5, R=0.22, H/D=3, co-flow discharge.

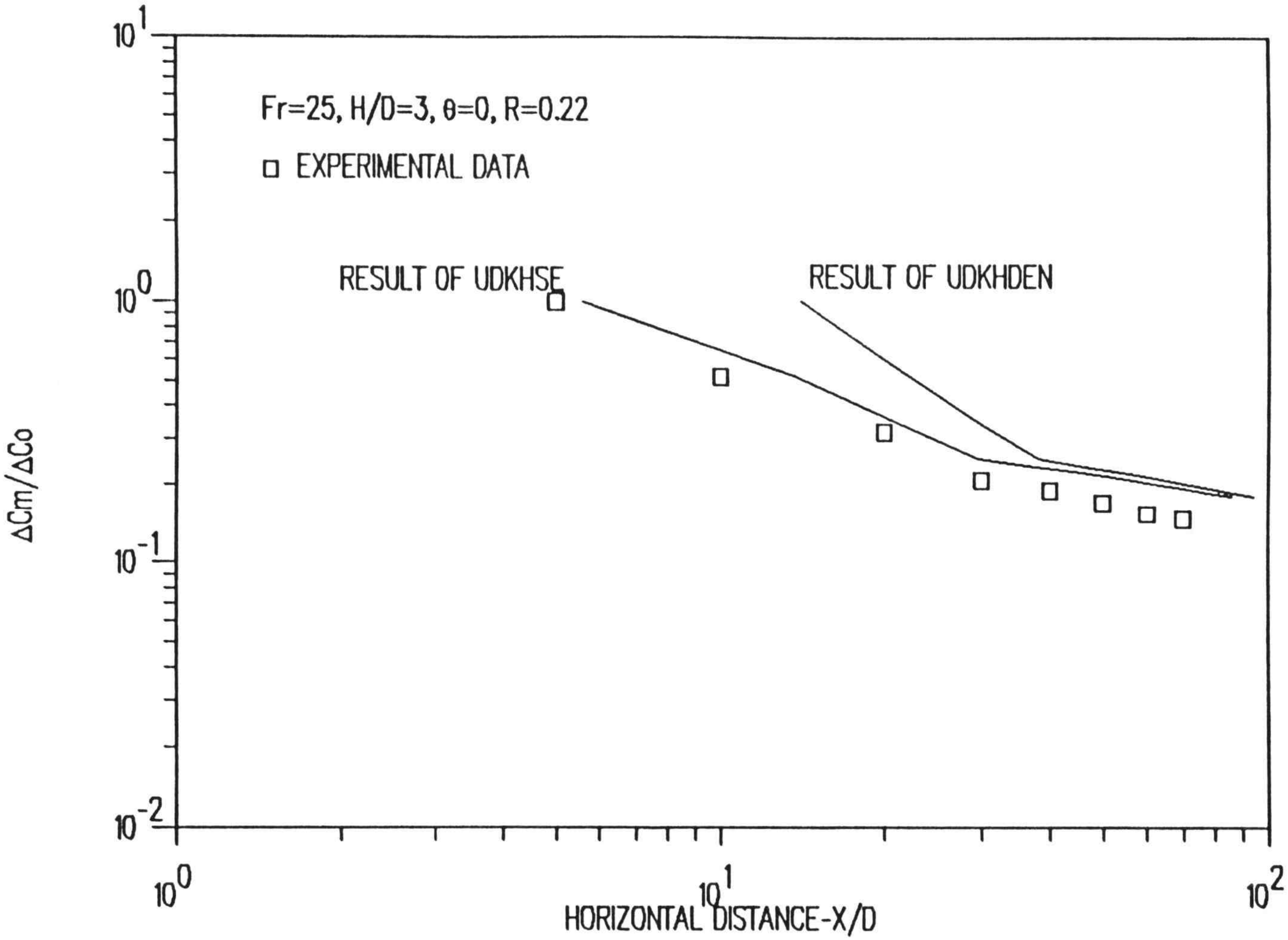

Figure 4-9. Comparison of experimental and model predicted maximum concentration deficit for Fr=25, R=0.22, H/D=3, co-flow discharge.

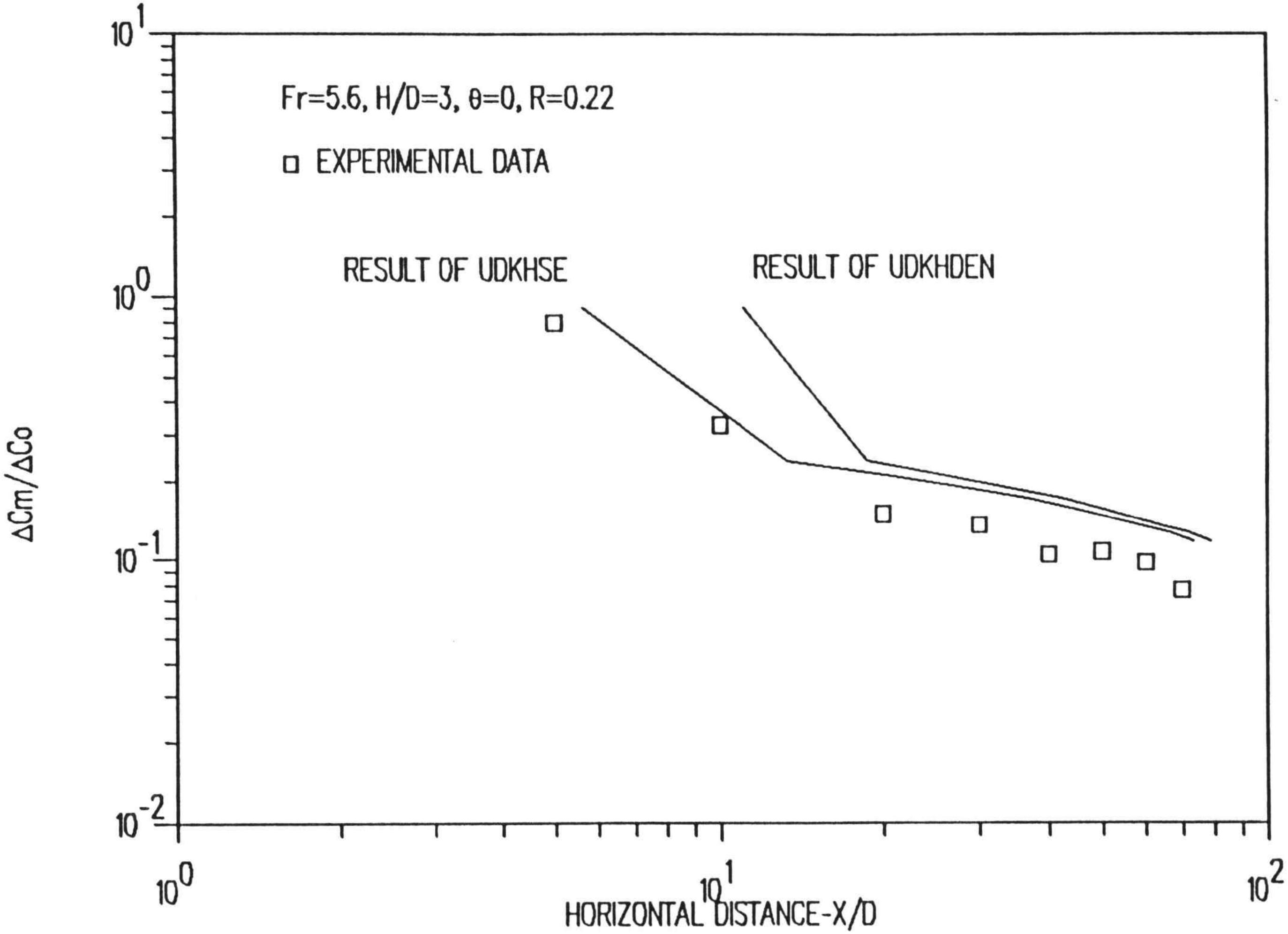

Figure 4-10. Comparison of experimental and model predicted maximum concentration deficit for Fr=5.6, R=0.22, H/D=3, co-flow discharge.

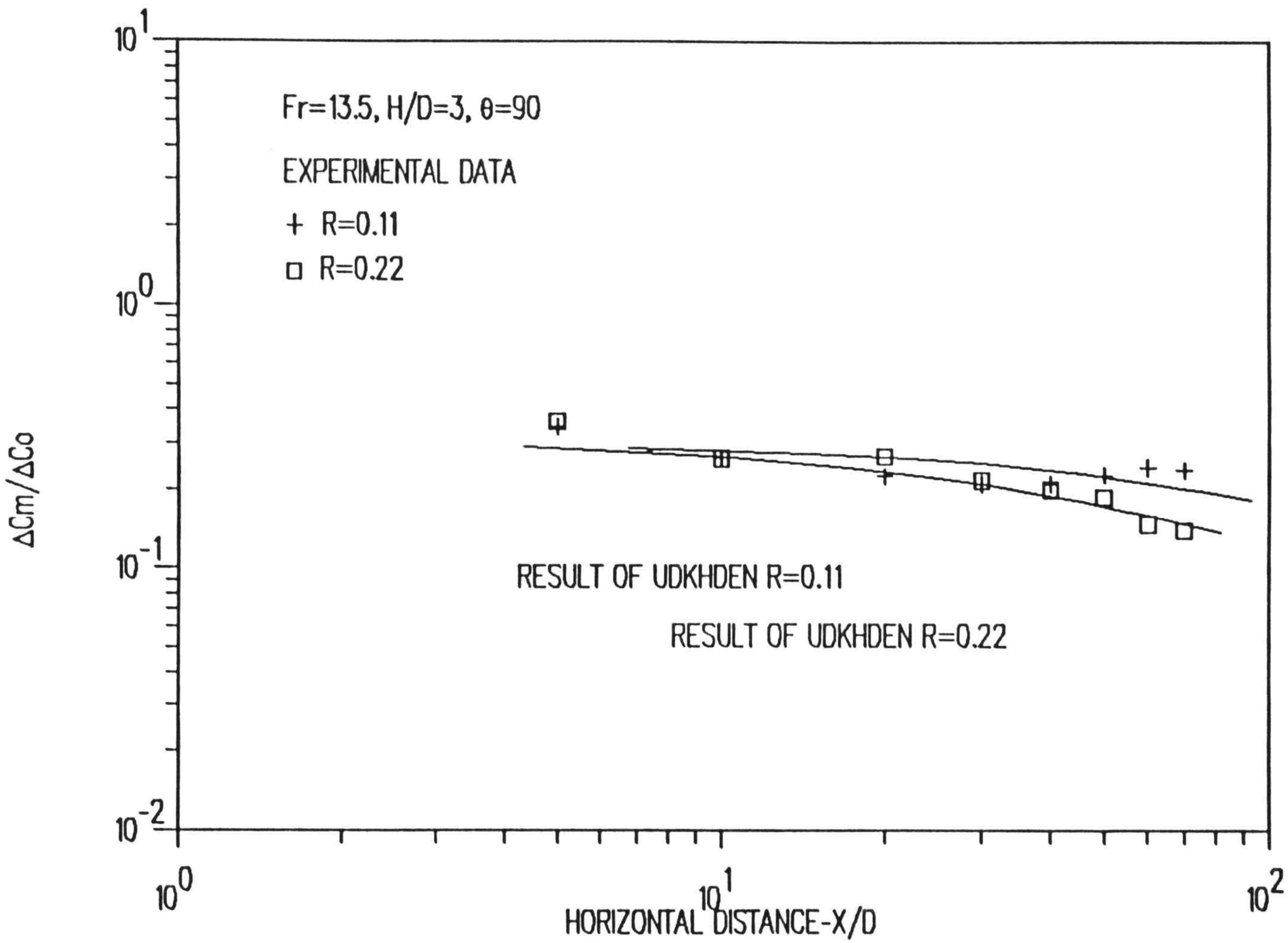

Figure 4-11. Comparison of experimental and model predicted maximum concentration deficit for Fr=13.5, H/D=3, cross-flow discharge.

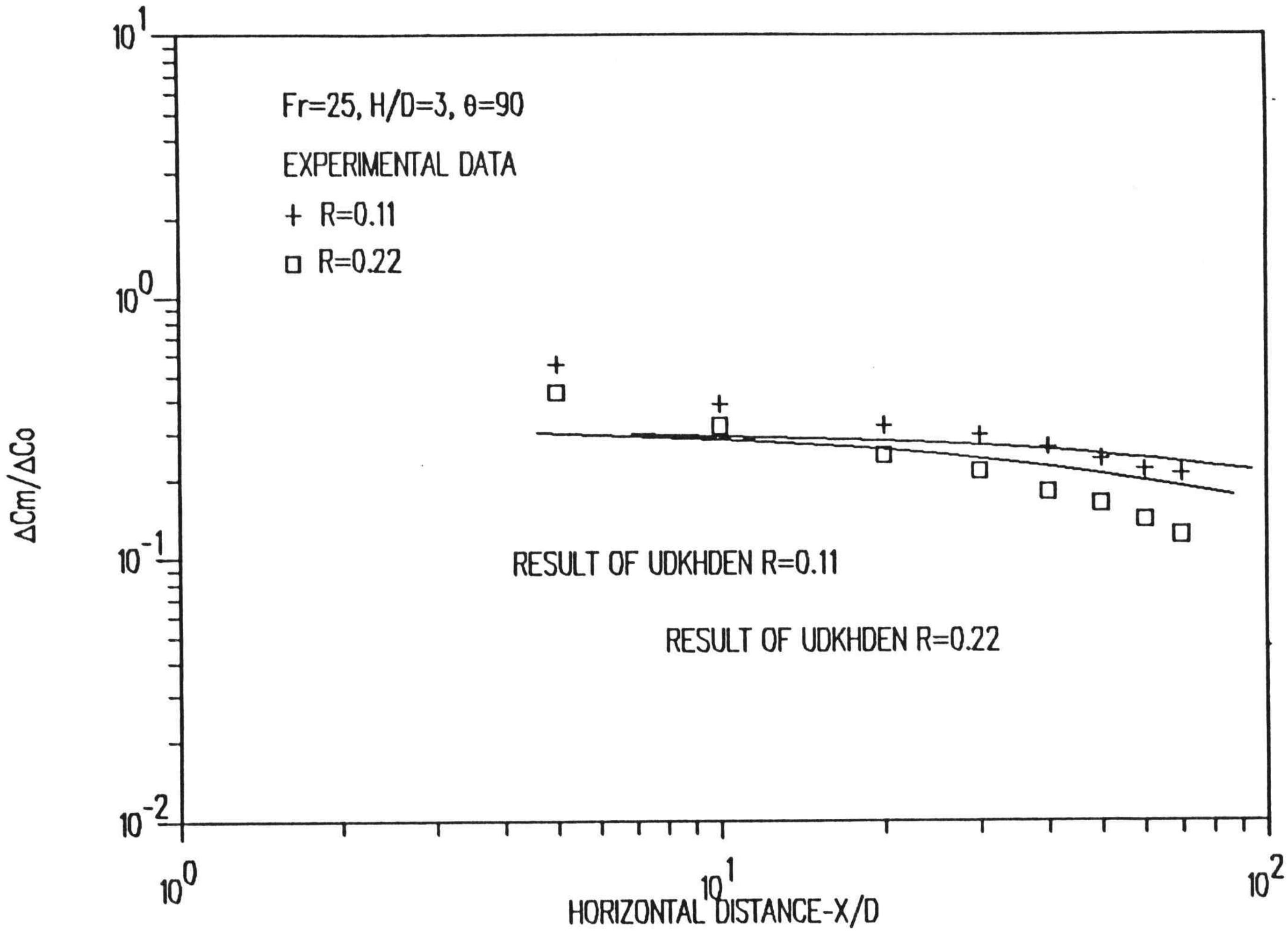

Figure 4-12. Comparison of experimental and model predicted maximum concentration deficit for Fr=25, H/D=3, cross-flow discharge.

5. CONCLUSION

The proximity of the free surface has a great influence on the near field flow characteristic for turbulent buoyant jets discharged into shallow water. A series of experiments were conducted to investigate the flow field induced by a submerged buoyant jet in shallow water for various combinations of densimetric Froude number Fr, velocity ratio R, discharge angle θ and submerged depth H/D. These experiments provided results that offer important information on the dilution and trajectory of turbulent buoyant discharge in shallow water. The conclusions drawn from the experimental study may be summarized as follows:

1. Decreasing the submerged depth decreased the dilution dramatically. As the buoyant plume reached the free surface, it was converted to a surface plume with further progress in the horizontal direction. Entrainment was reduced and the centerline dilution grew less rapidly.
2. For co-flow discharge, increasing the velocity ratio, R, increased dilution with downstream distance. For cross-flow discharge, the initial dilution decreased with increasing velocity ratio at the particular X/D. The trajectories were also affected by velocity ratio. The occurrence of the

surface effect was delayed by increasing velocity ratio.

3. For moderate and large values of submerged depth, $H/D \geq 10$, the dilution decreased for increasing densimetric Froude number. Increasing discharge angle from the horizontal increased initial dilution.
4. For small values of submerged depth, $H/D=3$, decreasing the densimetric Froude number and increasing discharge angle provided not only an increased initial dilution but also accelerate the occurrence of the surface effect. This limited the entrainment and reduced the dilution.

The integral model presented by Davis (1975) for multi-port buoyant jets was used to simulate single-port submerged buoyant jet in shallow water by employing an image method (Davis (1989)(1990)). Dilution was predicted for a round buoyant jet in shallow water for various combinations of Froude number, velocity ratio, discharge angle and submerged depth. Dilution for discharge into a cross-flow were predicted reasonably well by the model. For co-flow discharge, it was found that employing of empirical starting length proposed by Soldate et.al (1983) allowed for better agreement between the model prediction and experiment. Dilution was predicted reasonably well for single-port buoyant jets in shallow water of moderate and high Froude number by model. While the prediction results deviated from experiments as Froude number is 5.6. This variation of dilution between model prediction and experiment increases with decreasing Froude number. This research has shown that even though discharge into shallow is a very complicated process, reasonable predictions can be obtained for many single port discharges using an integral model if entrainment is modified using an image method and an empirical development length is used. The limits of application depend on the discharge angle and densimetric Froude number. In particular it is recommended that the image method be used for Froude numbers greater than 10 and discharge angles of 45° or less.

For lower Froude numbers, buoyancy causes the plume to violate the assumptions in the image method. For 90° discharge into shallow water, the plume rapidly reaches the surface where the transfer of momentum from vertical to lateral is not correctly modeled in the image solution.

REFERENCES

Abraham, G., 1960, " Jet Diffusion in Liquid of Greater Density," Transactions ASCE Journal Hydraulics Div. Vol. 86, HY6, pp. 1-13.

Albertson, M.L., Dai, Y.B., Jensen, R.A., and Rouse, H., 1950, " Diffusion of Submerged Jets," Transactions ASCE, Vol. 115, pp.639-697.

Bains, W.B., and Turner, J.S., 1969, "Turbulent Buoyant Convection From a Source in a Confined Region," Journal of Fluid Mechanics, ASME, pp.51-80.

Balasubramanian, V., and Jain, S.C., 1978, " Horizontal Buoyant Jets in Quiescent Shallow Water," Journal of Environment Engineering, ASCE, 104(4), pp. 717-730.

Baumgartner, D.J., and Trent, D.S., 1970, " Ocean Outfall Design Part 1 : Literature Review and Theoretical Development," U.S. Dept. of Int., Federal Water Quality Adm.

Benedict, R.P., 1969, " Engineering Analysis of Experimental Data," Transaction of ASME, Journal of Engineering for Power, pp. 21-30.

Chen, C.J., and Rodi, W., 1980, " Vertical Turbulent Buoyant Jets - A review of Experimental Data," HMT, The Science and Applications of Heat and Mass Transfer, 4.

Dally, J.W., Riley, W.F., and McConnell, K.G., 1984 " Instrumentation for Engineering Measurements," John Wiley & Sons, Inc., New York.

Davis, L.R., and Shirazi M.A., 1978, " A Review of Thermal Plume Modeling, Keynote Address," Proceeding of 6th International Heat Transfer Conference, Toronto, Canada, 109-126.

Davis, L.R., Shirazi, M.A., and Slegel, D.L., 1978, " Measurement of Buoyant Jet Entrainment from Single and Multiple Sources," Transaction of ASME Journal of Heat Transfer, Vol. 100, pp. 442-447.

Davis, L.R., Gregoric, M., and Bushnell, D.J., 1982, " An Experimental Investigation of Merging Buoyant Jets in a Crossflow," ASME Journal of Heat Transfer, Vol 104, No. 2, pp. 236-240.

Davis, L.R., 1975, " Analysis of Multiple Cell Mechanical Draft Cooling Tower Plumes," USEPA, Corvallis Environmental Research Lab., EPA-660/3-75-039.

Davis, L.R., 1989, " Heat Transfer in Convective Flows," Proceeding at The 1989 National Heat Transfer Conference, 1989, Philadelphia, Pennsylvania.

Davis, L.R., 1990, " Heat and Mass Transfer in Frost and Ice, Packed Beds, and Environmental Discharges," Proceeding at AIAA/ASME Thermophysics and Heat Transfer Conference, 1990, Seattle, Washington.

Fan, L.N., and Brooks, N.H., 1969, " Numerical Solutions of Turbulent Buoyant Jet Problems," Report No. KH-R-18, W.M. Keck Laboratory of Hydraulics and Water Resources, California Institute of Technology, Pasadena, California.

Fischer, H.B., List, J.E., Koh, R.C.Y., Imberger, J., and Brooks, N.H., 1979, "Mixing in Inland and Coastal Waters," Academic Press, Inc., New York.

Hirst, E.A., 1971a, " Analysis of Round Turbulent, Buoyant Jets Discharged to Flowing Stratified Ambients," Oak Ridge National Laboratory, Report ORNL 4685.

Hirst, E.A., 1971b, " Analysis of Buoyant Jets within the Zone of Flow Establishment," Oak Ridge National Laboratory, Report ORNL-TM-3470.

Hossain, M.S., and Rodi, W., 1982, " Turbulence Model for Buoyant Flows and its Application to Vertical Buoyant Jets," HMT, The Science and Applications of Heat and Mass Transfer, 6, pp. 121-170.

Jirka, G.H., 1982, " Turbulent Buoyant Jets in Shallow Fluid Layers," HMT, The Science and Applications of Heat and Mass Transfer, 6, pp. 69-117.

Jirka, G., and Harleman, D.R.F., 1973, "The Mechanics of Submerged Multiport Diffusers for Buoyant Discharges in Shallow Water," Massachusetts Institute of Technology, R.M. Parsons Lab., Report 169.

Kannberg, L.D., 1976, " An Experimental and Analytical Investigation of Deep Submerged Multiple Buoyant Jets," PhD thesis, Oregon State University.

Kannberg, L.D., and Davis, L.R., 1977, " An Analysis of Deep Submerged Multiple-Port Buoyant Discharges,: ASME Journal of Heat Transfer, Vol 99, pp.648-655.

Koh., R.C., and Fan, L.N., 1970, " Mathematical Models for the Prediction of Temperature Distribution Resulting from the Discharge of Heat Water in Large Bodies of Water," USEPA Water Pollution Control Research Series Report, 16130DW0/70.

Lee, J.H., and Jirka, G.H., 1981, " A Vertical Round Buoyant Jet in Shallow Water," ASCE Journal of Hydraulic Engineering, 107(12), pp. 1,651-1,675.

List, E.J., 1982, " Mechanics of Turbulent Buoyant Jets and Plumes," W. Rodi, ed. HMT, The Science and Applications of Heat and Mass Transfer, 6, 1-66.

Macduff, R.B., 1980, "Multiple Cooling Tower Plumes, a Field Study and Analytical Model," PhD thesis, Oregon State University.

Maxwell, W.H.C., and Pazwash, H., 1973, " Axisymmetric Shallow Submerged Jets," Journal of Hydraulic Engineering, ASCE, 99(4), pp. 637-652.

Morton, B.R. 1959, " Force Plumes," Journal of Fluid Mechanics, 5, pp. 151-163.

Morton, B.R., Taylor, G.I., and Turner, J.S., 1956, " Turbulent Gravitational Convection from Maintained and Instantaneous Sources," Proceedings of the Royal Soc. of London, Vol. A234, pp.2-23.

Pryputniewicz, R.J., and Bowley, W.W., 1975, " An Experimental Study of Vertical Buoyant Jets Discharged into Water of Finite Depth," ASME Journal of Heat Transfer, Vol. 97, pp. 274-281.

Robideau, R.F., 1972, "The Discharge of Submerged Buoyant Jets into Water of Finite Depth," General Dynamics Corporation, Electric Boat Division, Report No. U440-72-121.

Ryskiewich, B.C., and Hafetz, L., 1975, " An Experimental Study of the Free Surface Effect on a Buoyant Jet," General Dynamics Corporation, Electric Boat Division, Report No. U440-74-103.

Sobey, R.J., Johnston, A.J., and Keane, R.D., 1988, " Horizontal Round Buoyant Jet in Shallow Water," Journal of Hydraulic Engineering, Vol. 114, No. 8.

Soldate, A.M., Davis, L.R., Schuldt, M.D. Baumgartner, W.E. Frick, W.E. , and Muellenhoff, W.P., 1983, " Initial Mixing Characteristics of Municipal Ocean Discharges," USEPA, Marine Division, Corvallis Environmental Research Laboratory.

Tai, C., and Schetz, J.A., 1984, " Numerical Calculation of Buoyant Jets in a Shallow Waterway," ASME paper 84-WA/HT-36.

Trent, D.S., 1973, " A Numerical Model for Predicting Energy Dispersion in Thermal Plumes Issuing from Large Vertical Outfalls in Shallow Coastal Water," PhD thesis, Oregon State University.

APPENDICES

APPENDIX A.

Error Analysis

A.1 Concentration Measurement

The conductivity probe used to measure salinity in the field of the plume, was calibrated using known salt water solution. These solutions were standardized by a Guildline model 8400 salinometer with a uncertainty error of ∓0.003 ppt. The calibration curve of the conductivity probe is shown on Figure A-1.

Two sources of error occurred in the calibration of the conductivity probe:

(a) error of the salinometer which was used to standardize the salt water solution.

(b) error due to the voltage measurement.

The combined uncertainty due to (a) and (b) as given by Dally et.al. (1984) is:

$$\frac{\omega_{cc}}{C} = \frac{(\omega_s^2 + m\omega_v^2)^{1/2}}{C} \qquad \text{(A-1)}$$

where ω_{cc}= combined uncertainty of probe calibration

ω_s= uncertainty of salinometer

ω_v= uncertainty of voltage measurement

m = local slope of calibration curve

C = local concentration (salinity)

The value of ω_{cc}/C then can be calculated using the

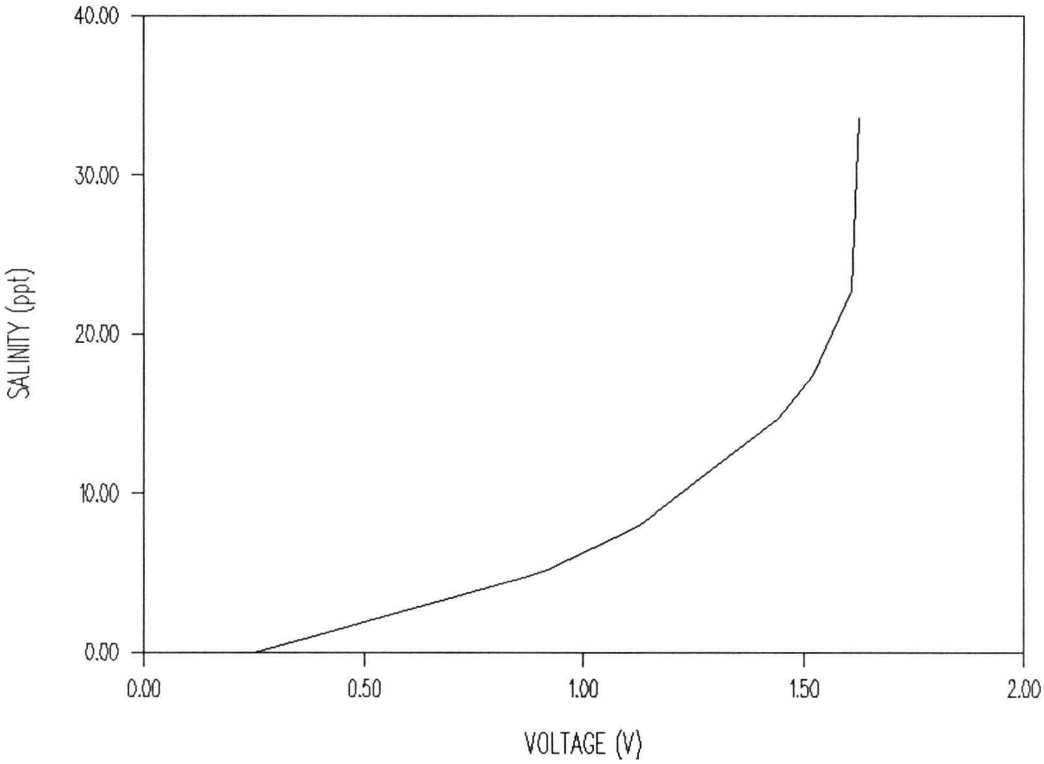

Figure A-1. Calibration curve of the conductivity probe.

uncertainty in each quantity based on the manufacture's specifications and experiments. The error in the voltage measurements was ∓0.01V. The maximum possible combined uncertainty is calculated employing the uncertainties in each terms as

$$\left(\frac{\omega_{cc}}{C}\right)_{max} = \pm[(0.003)^2+(0.02)^2]^{1/2} \approx \pm 0.02 \qquad \text{(A-2)}$$

Since the concentration was measured along the centerline of the plume, there is one more error due to the concentration gradient and the finite size of the probe. Figure A-2 shows the cross section of the conductivity probe and the electrical circuit which is an analog to the conductivity measured by the probe. It is assumed that the conductance measured by the probe in the average of the conductance in the four quadrants of the probe. Thus the total resistance measured by the conductivity probe is

$$R_T = \frac{1}{\frac{1}{R_1}+\frac{1}{R_2}+\frac{1}{R_3}+\frac{1}{R_4}} \qquad \text{(A-3)}$$

By assuming the relation between resistance and concentration (salinity) is R=K/C, where K is constant, equation A-3 can be rewritten as

$$R_T = \frac{K}{(C_1+C_2+C_3+C_4)} \qquad \text{(A-4)}$$

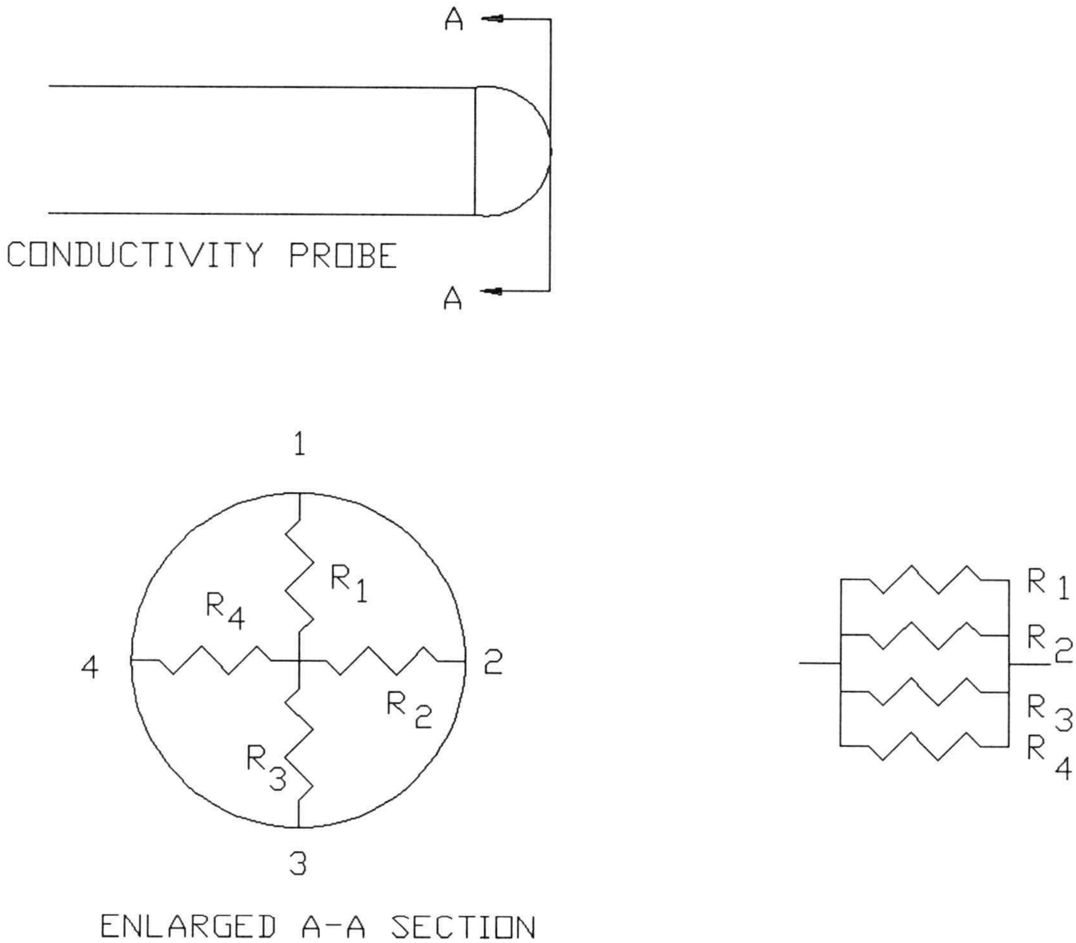

Figure A-2. Cross section of conductivity probe and electrical circuit which is an analog to the conductance measured by the probe.

At the edge of the conductivity probe, positions 1, 2, 3 and 4 shown in Figure A.2, the concentrations deviate from the value at the center due to the gradient of the concentration. Thus with $C_2=C_4=C+\Delta S_h$ and $C_1=C_3=C+\Delta S_v$, equation A-4 becomes

$$R_T=\frac{K}{(4C+2\Delta S_h+2\Delta S_v)} \qquad \text{(A-5)}$$

where ΔS_h is concentration difference between center and edges of the conductivity probe due to horizontal concentration gradient. And ΔS_v is concentration difference due to vertical concentration gradient. For the ideal case, zero size probe, $\Delta S_v=\Delta S_h=0$ and equation A-5 becomes

$$R_i=\frac{K}{4}C \qquad \text{(A-6)}$$

Therefore the error caused by the finite sizal probe can be represented as

$$\frac{\omega_{cp}}{C}=\frac{\Delta R}{R_i}=\frac{|R_i-R_T|}{R_i}=1-\frac{4C}{4C+2\Delta S_h+2\Delta S_v} \qquad \text{(A-7)}$$

where ω_{cp} is the uncertainty due to concentration gradient.

In order to have maximum uncertainty, vertical concentration gradient and horizontal concentration gradient are assumed to be the same. Thus right at the center of the plume where the concentration gradient is maximum, equation A-7 becomes

$$\frac{\omega_{cp}}{C}=\Delta\frac{R}{R_i}=1-\frac{4C}{4(C+\Delta S)} \tag{A-8}$$

where $\Delta S=\Delta S_h=\Delta S_v$.

Table A-1 shows the computation of ω_{cp}/C by using equation A-8 for Fr=25, H/D=15, θ=0° and velocity ratio R=0.11 at different downstream locations. It is noted that the error due to the concentration gradient is significant only in the region near the discharge. In the region far downstream as the plume is greatly diluted, this error is insignificant compared to the uncertainty given by equation A-2. The total uncertainty due to probe calibration and concentration gradient then can be computed from

$$\frac{\omega_c}{C}=[(\frac{\omega_{cc}}{C})^2+(\frac{\omega_{cp}}{C})^2]^{1/2} \tag{A-9}$$

The errors of measurement of the ratio of concentration deficit $\Delta C/\Delta C_0$ are the primary concern in this error analysis. The ratio of concentration deficit is calculated from

$$\frac{\Delta C}{\Delta C_0}=\frac{C-C_\infty}{C_0-C_\infty}=1-\frac{C}{C_\infty}$$

and the uncertainty of $\Delta C/\Delta C_0$ is written as

$$\frac{\omega_{(\Delta C/\Delta C_0)}}{\Delta C/\Delta C_0}=[(\frac{\omega_C}{C})^2+(\frac{\omega_{C_\infty}}{C_\infty})^2]^{1/2} \tag{A-10}$$

X/D	$\Delta C_m/\Delta C_0$	C_∞*	C_m*	b**(cm)	ΔS***	ω_{cp}/C
10	0.617	17.4	6.664	1.27	1.268	0.159
20	0.325	17.4	11.745	1.61	0.537	0.044
30	0.252	17.4	13.015	3.81	0.173	0.013
40	0.191	17.4	14.077	5.08	0.098	7.0E-3
50	0.161	17.4	14.599	6.35	0.066	4.6E-3
60	0.134	17.4	15.068	7.62	0.045	3.0E-3
70	0.112	17.4	15.451	8.89	0.033	2.2E-3

* Unit of C_∞ and C_m is ppt.

** b is half width of the plume

*** $\Delta S=(\Delta C_m/b)*(\text{radius of conductivity probe})$

Table A-1. Errors due to concentration gradient for Fr=25, H/D=15, θ=0° and velocity ratio R=0.11.

The uncertainty of the ratio of concentration deficit can be calculated from equation A-9 by using the values obtained from equations A-2 and A-7.

A.2 Independent Variables

In this study, the dimensionless independent variables are obtained based on several other measurements. Each measurement has its associated error. The propagation of these measurement errors depends on the form of the mathematical expression being used to calculate the dimensionless independent variables. The uncertainty for several different mathematical operation R=f(x,y,z...) are given by Dally et.al. (1984) as:

$$R=XY^nZ^{-k}$$

$$\frac{\omega_R}{R}=\left[\left(\frac{\omega_x}{X}\right)^2+\left(\frac{n\omega_y}{Y}\right)^2+\left(\frac{-k\omega_z}{Z}\right)^2\right]^{1/2} \qquad \text{(A-11)}$$

and

$$R=X\mp Y$$

$$\frac{\omega_R}{R}=\left[\frac{\omega_x^2+\omega_y^2}{(X\mp Y)^2}\right]^{1/2} \qquad \text{(A-12)}$$

By using equations A-11 and A-12, the uncertainty of independent variables Froude number, Fr, velocity ratio, R, submerged depth, H/D and downstream distance, X/D, can be obtained by employing the uncertainty in each measurements.

Velocity Ratio R

$$R=U_\infty/U_0$$

$$\left(\frac{\omega_R}{R}\right)_{max}=\pm\left[\left(\frac{\omega_{U_0}}{U_0}\right)^2+\left(-\frac{\omega_{U_\infty}}{U_\infty}\right)^2\right]^{1/2}=\pm[(0.032)^2+(0.034)^2]^{1/2}=\pm 0.046$$

Submerged Depth H/D

$$\left(\frac{\omega_{(H/D)}}{H/D}\right)_{max}=\pm\left[\left(\frac{\omega_H}{H}\right)^2+\left(-\frac{\omega_D}{D}\right)^2\right]^{1/2}=\pm[(0.033)^2+(0.002)^2]^{1/2}=\pm 0.033$$

Downstream Distance X/D

$$\left(\frac{\omega_{(X/D)}}{X/D}\right)_{max}=\pm\left[\left(\frac{\omega_X}{X}\right)^2+\left(-\frac{\omega_D}{D}\right)^2\right]^{1/2}=\pm[(0.02)^2+(0.002)^2]=\pm 0.02$$

Densimetric Froude Number Fr

$$Fr=U_0/(gD\Delta\rho/\rho)^{1/2}=U_0(gD)^{-1/2}(\rho_\infty-\rho_0)^{-1/2}(\rho_0)^{1/2}$$

$$\left(\frac{\omega_{Fr}}{Fr}\right)_{max}=\pm\left[\left(\frac{\omega_{U_0}}{U_0}\right)^2+\left(-\frac{1}{2}\frac{\omega_D}{D}\right)^2+\left(-\frac{1}{2}\frac{\omega_{\rho_0}}{\rho_0}\right)^2+\frac{1}{4}\frac{\omega_{\rho_\infty}{}^2+\omega_{\rho_0}{}^2}{(\rho_\infty-\rho_0)^2}\right]^{1/2}$$

$$=\pm[(0.032)^2+(0.001)^2+(0.001)^2+0.000256]^{1/2}=\pm 0.036$$

APPENDIX B

Curves of Maximum Concentration Deficit and Trajectory

This appendix contains all the curves of maximum concentration deficit and trajectory obtained in the experiments. Major concerns in the experiments were the effect of densimetric Froude number, Fr, water depth, H/D, velocity ratio, R, and discharge angle, θ, on dilution and trajectories. The results are best illustrated by showing the maximum concentration deficit $\Delta C_m/\Delta C_0$ and trajectories Y/D plotted as a function of horizontal distance X/D for various combinations of Fr, H/D, R and θ.

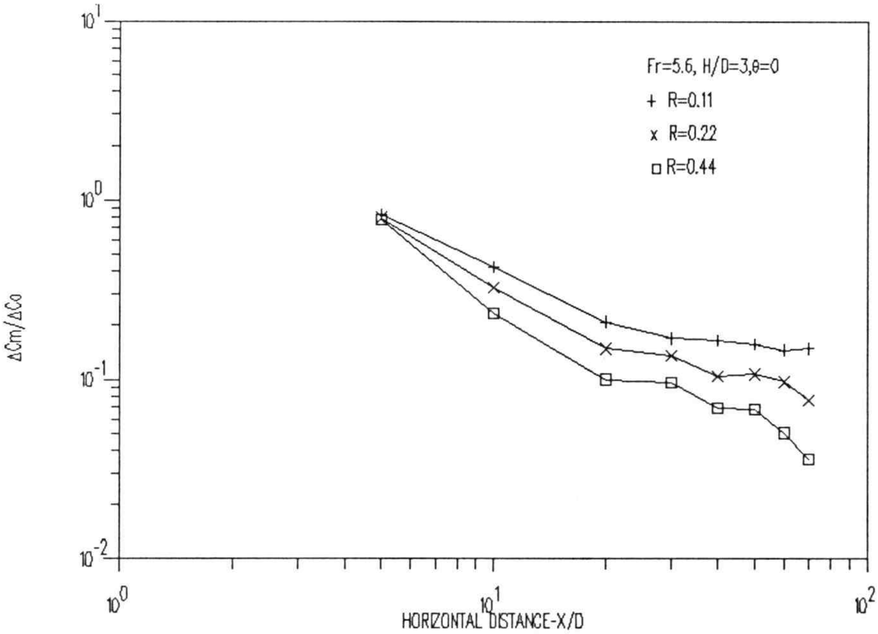

Figure B-1. Effect of varying R on maximum concentration deficit for Fr=5.6, H/D=3 and Θ=0°.

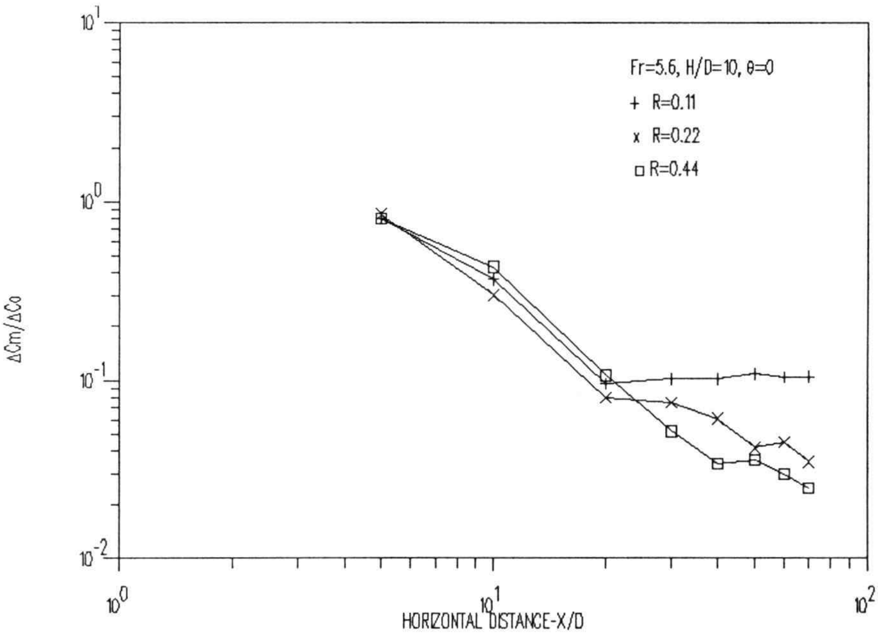

Figure B-2. Effect of varying R on maximum concentration deficit for Fr=5.6, H/D=10 and Θ=0°.

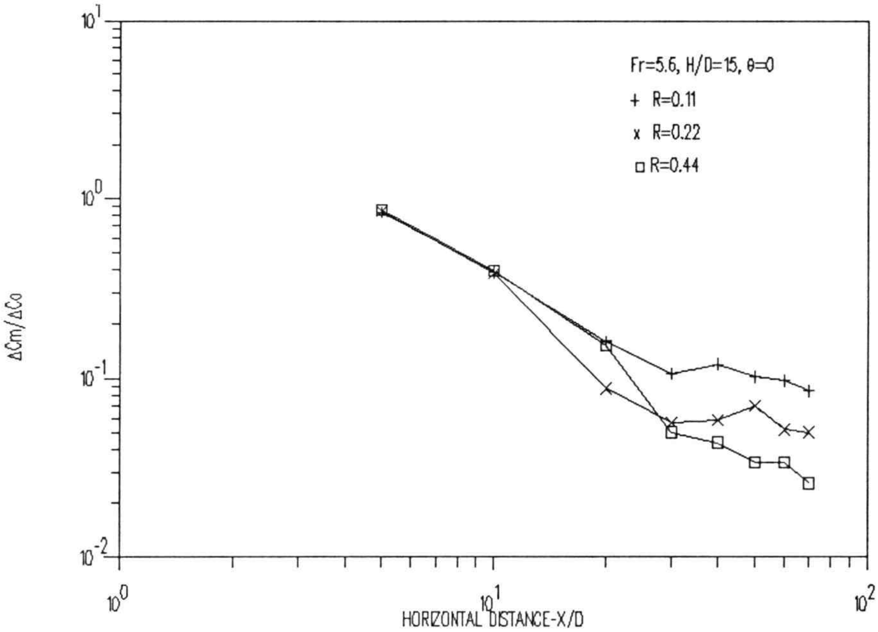

Figure B-3. Effect of varying R on maximum concentration deficit for Fr=5.6, H/D=15 and Θ=0°.

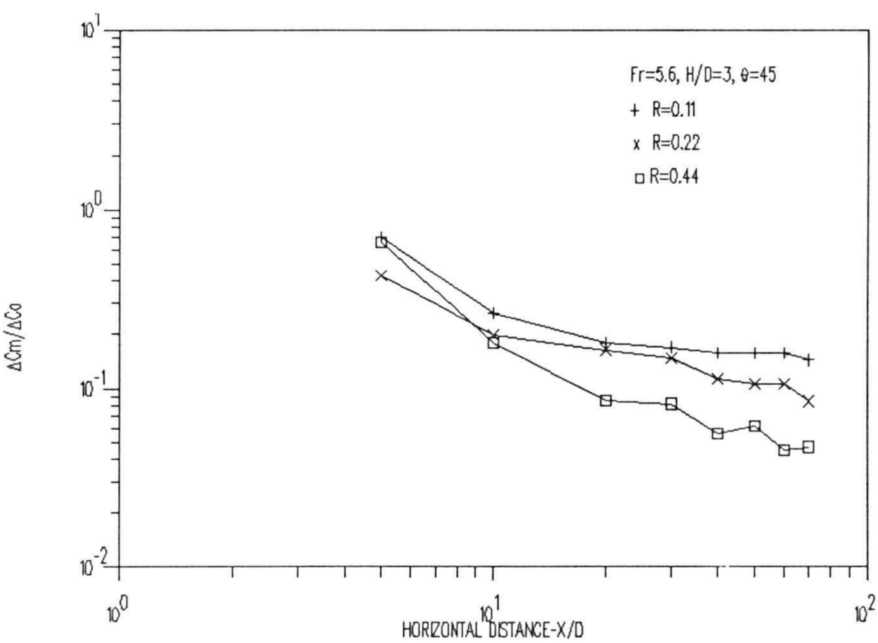

Figure B-4. Effect of varying R on maximum concentration deficit for Fr=5.6, H/D=3 and Θ=45°.

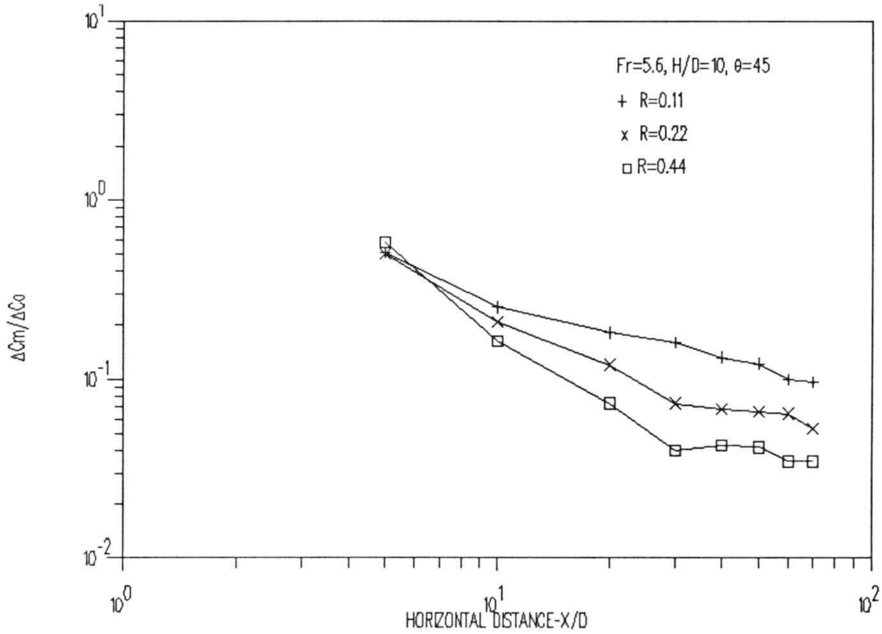

Figure B-5. Effect of varying R on maximum concentration deficit for Fr=5.6, H/D=10 and Θ=45°.

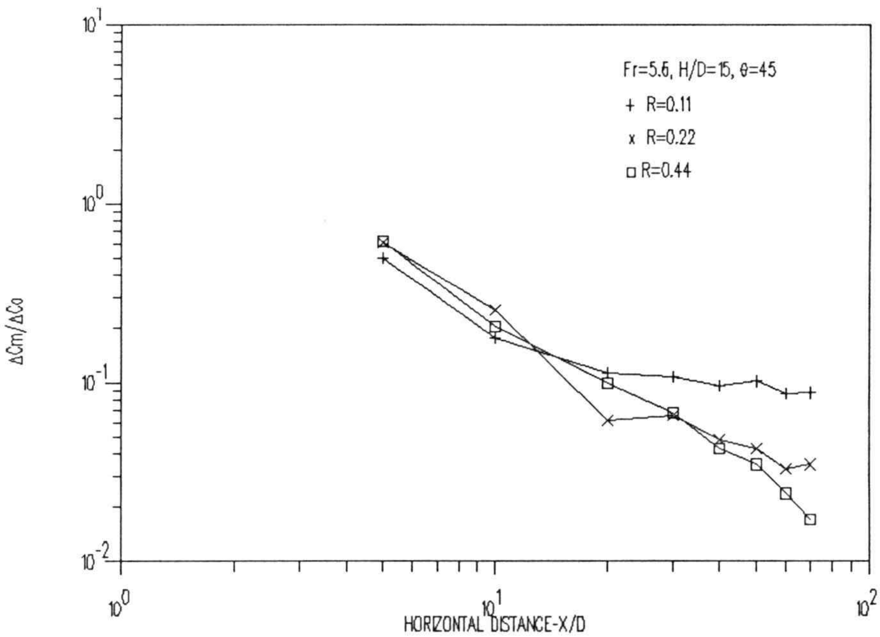

Figure B-6. Effect of varying R on maximum concentration deficit for Fr=5.6, H/D=15 and Θ=45°

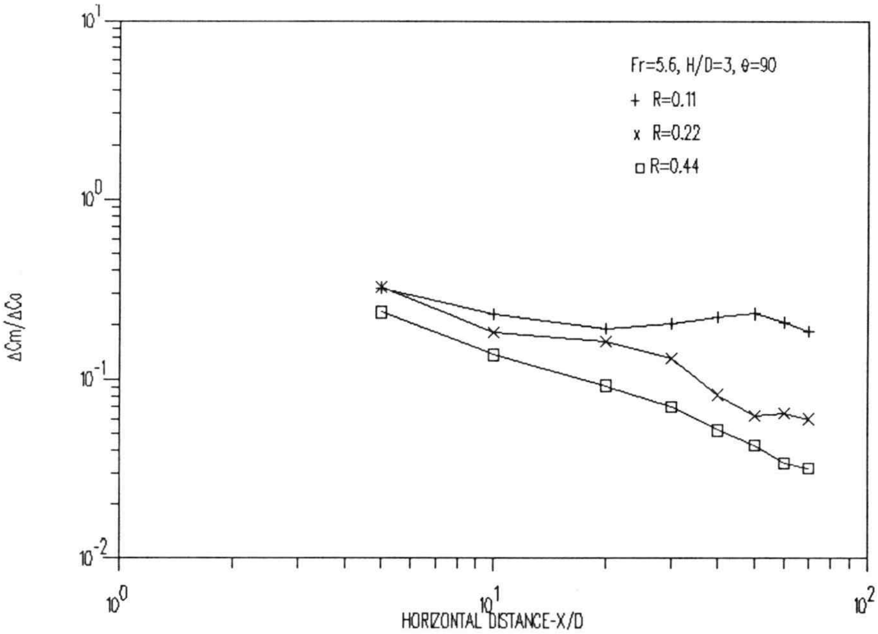

Figure B-7. Effect of varying R on maximum concentration deficit for Fr=5.6, H/D=3 and Θ=90°.

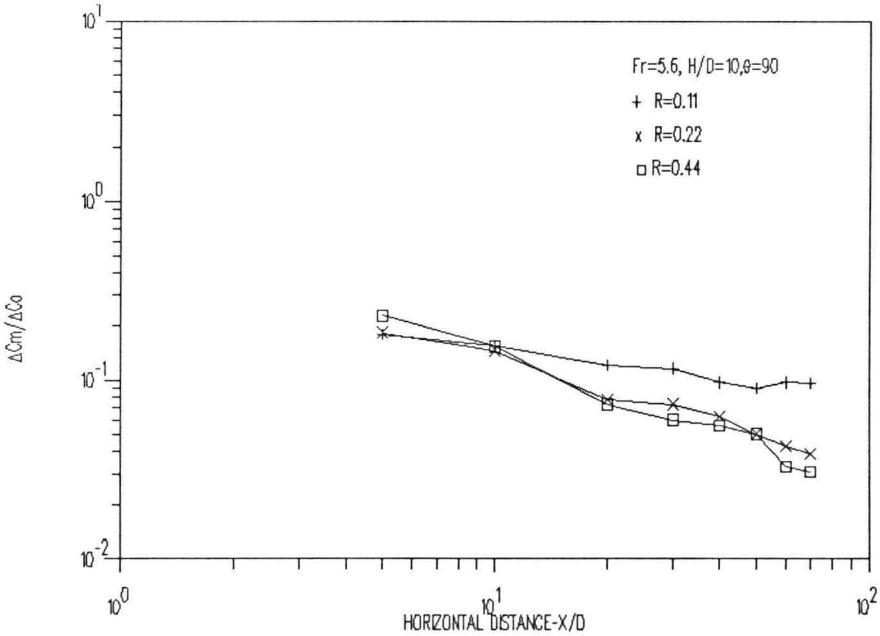

Figure B-8. Effect of varying R on maximum concentration deficit for Fr=5.6, H/D=10 and Θ=90°.

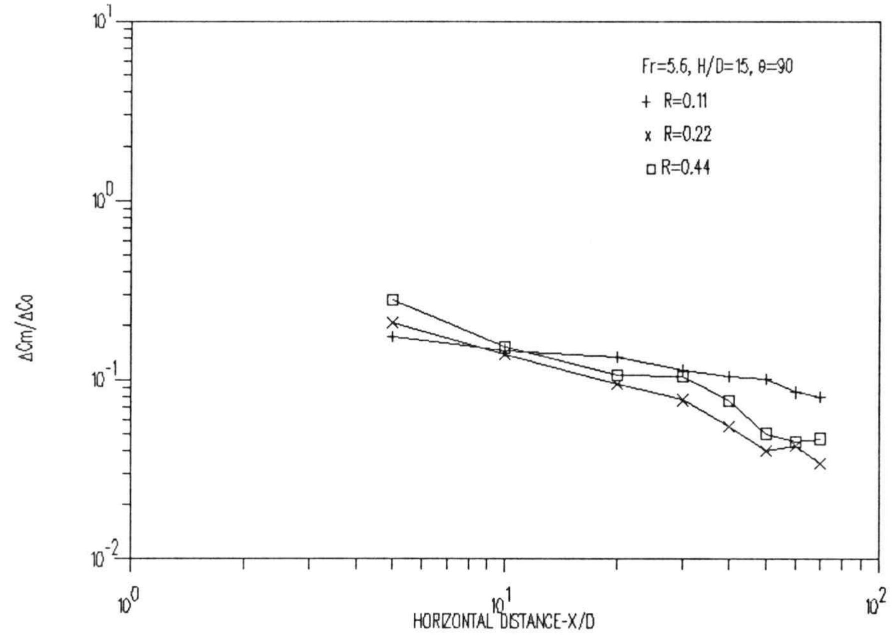

Figure B-9. Effect of varying R on maximum concentration deficit for Fr=5.6, H/D=15 and Θ=90°.

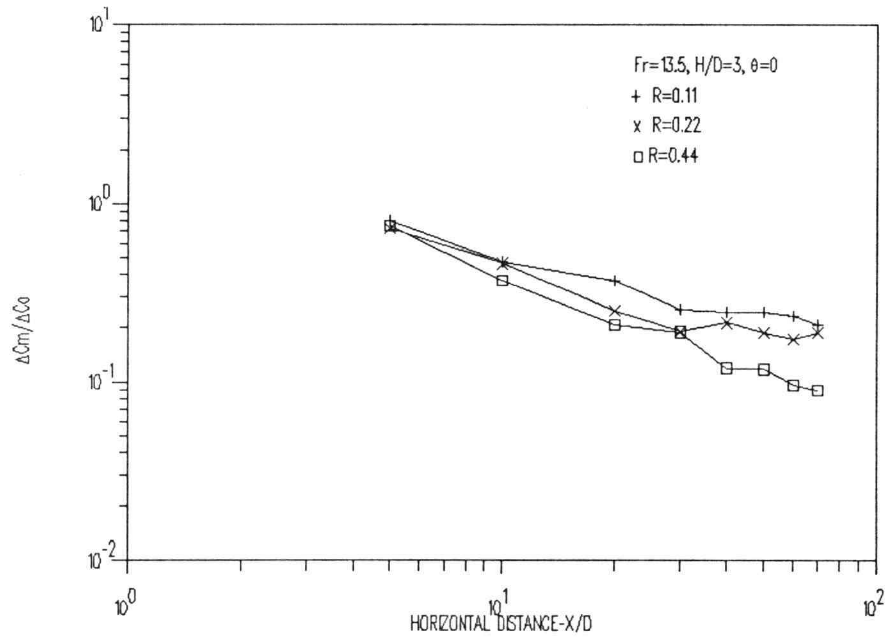

Figure B-10. Effect of varying R on maximum concentration deficit for Fr=13.5, H/D=3 and Θ=0°.

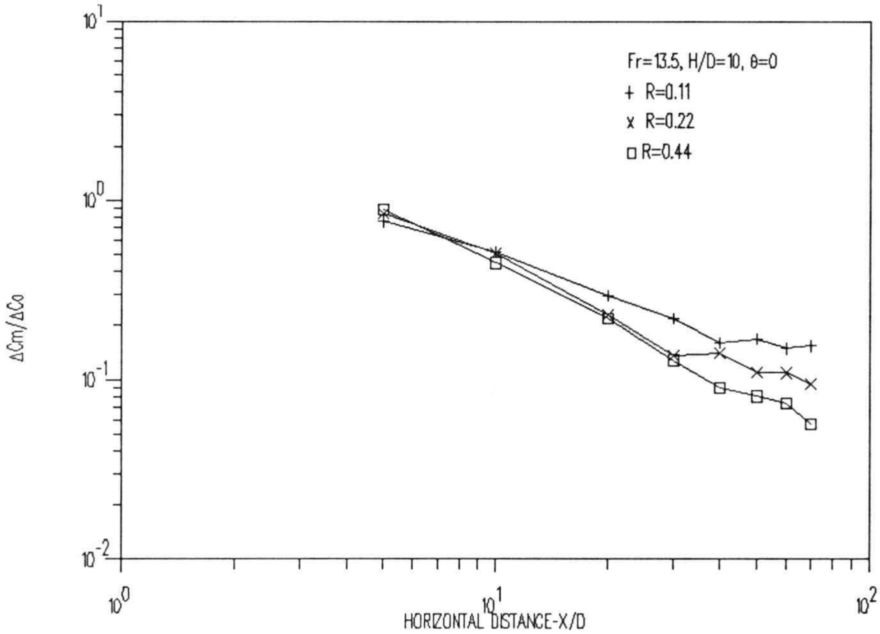

Figure B-11. Effect of varying R on maximum concentration deficit for Fr=13.5, H/D=10 and Θ=0°.

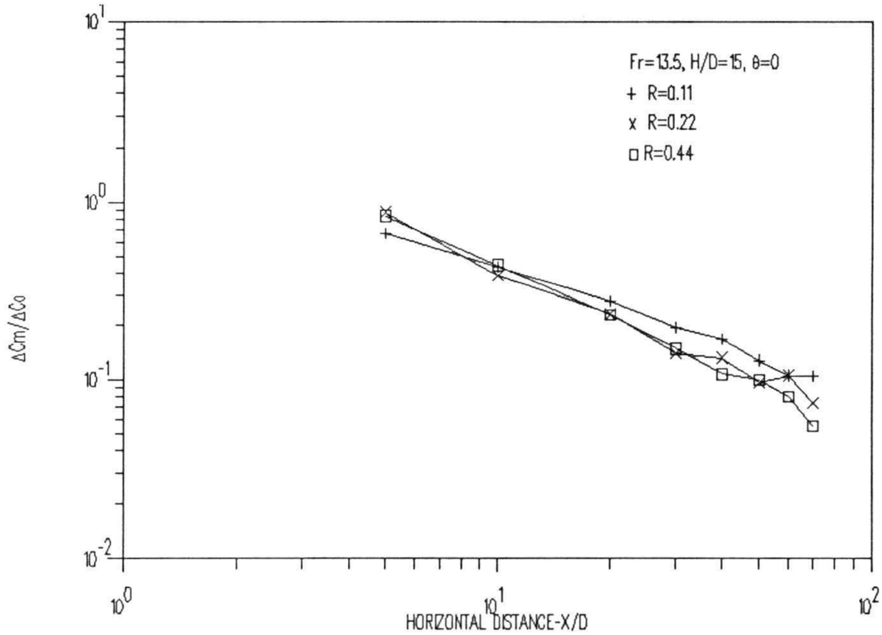

Figure B-12. Effect of varying R on maximum concentration deficit for Fr=13.5, H/D=15 and Θ=0°.

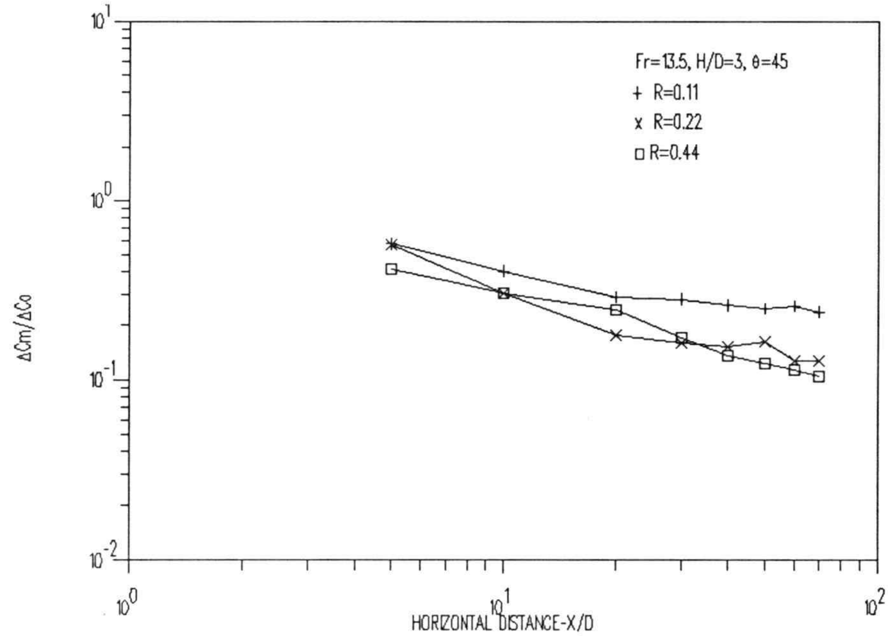

Figure B-13. Effect of varying R on maximum concentration deficit for Fr=13.5, H/D=3 and Θ=45°.

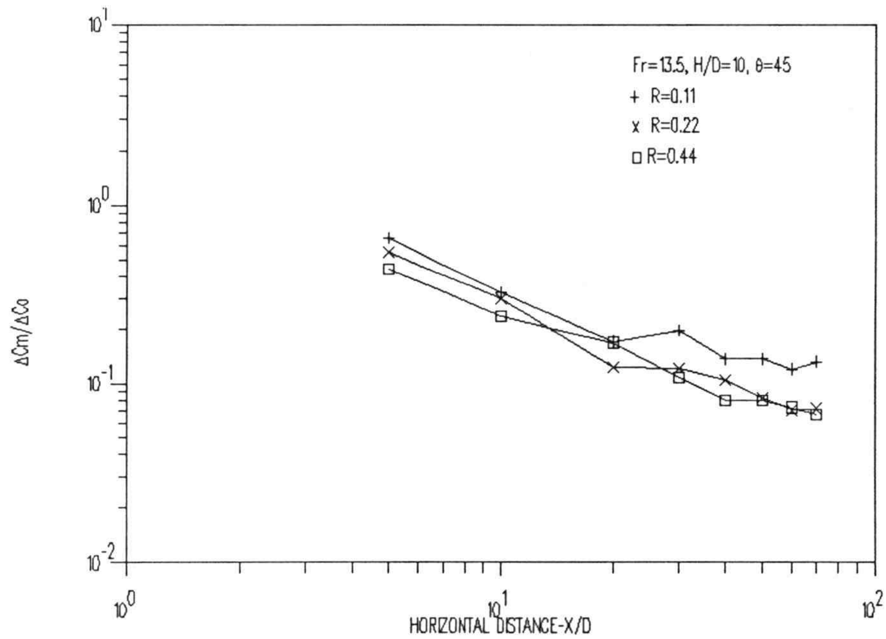

Figure B-14. Effect of varying R on maximum concentration deficit for Fr=13.5, H/D=10 and Θ=45°.

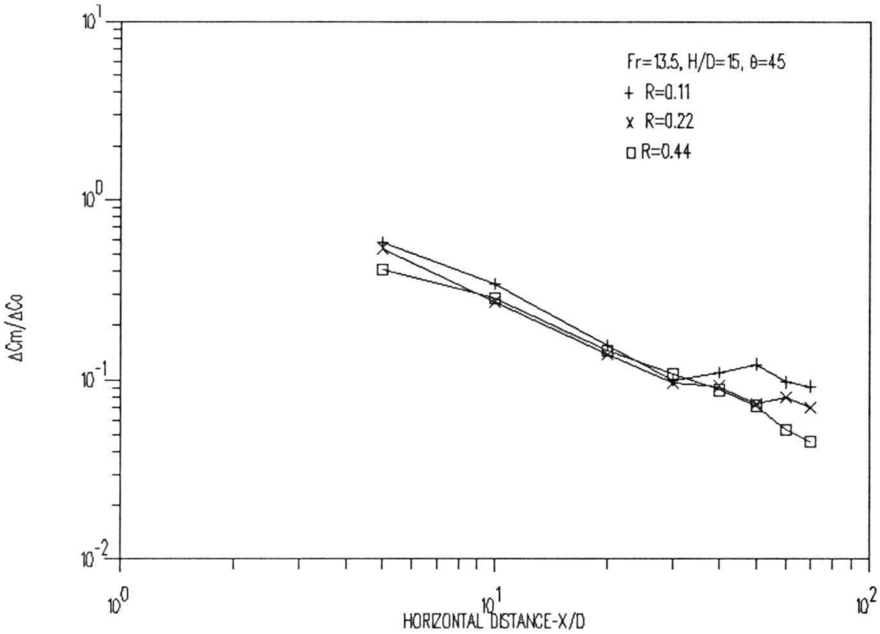

Figure B-15. Effect of varying R on maximum concentration deficit for Fr=13.5, H/D=15 and Θ=45°.

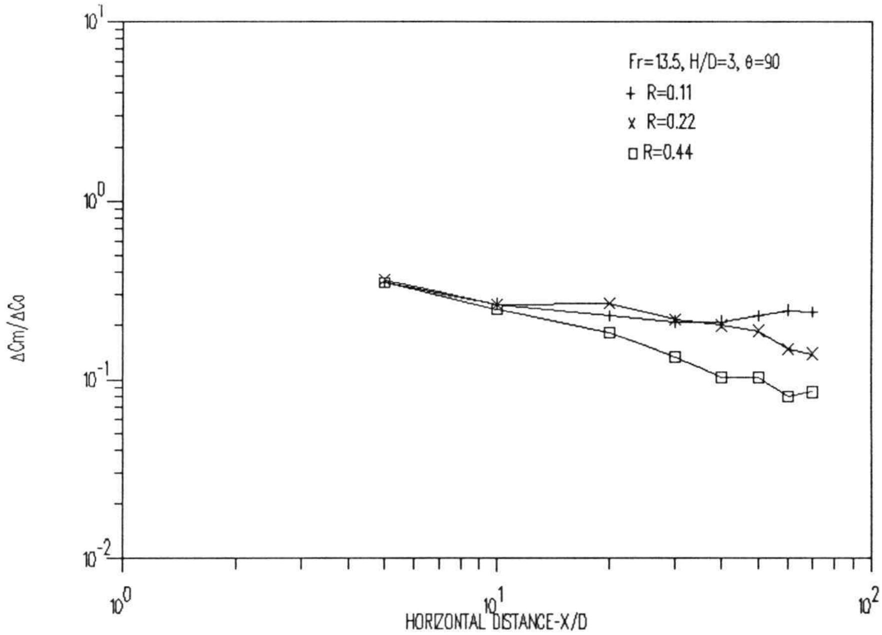

Figure B-16. Effect of varying R on maximum concentration deficit for Fr=13.5, H/D=3 and Θ=90°.

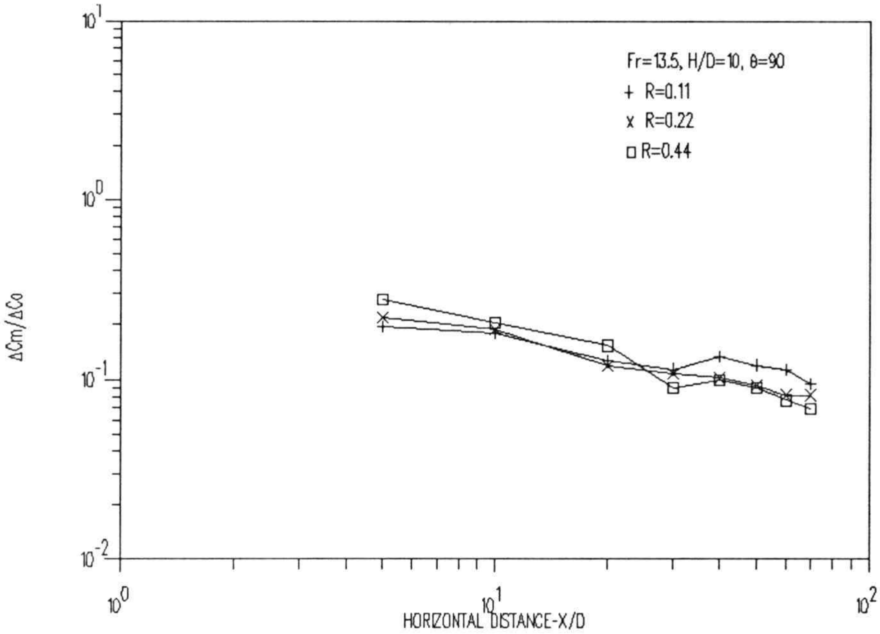

Figure B-17. Effect of varying R on maximum concentration deficit for Fr=13.5, H/D=10 and Θ=90°.

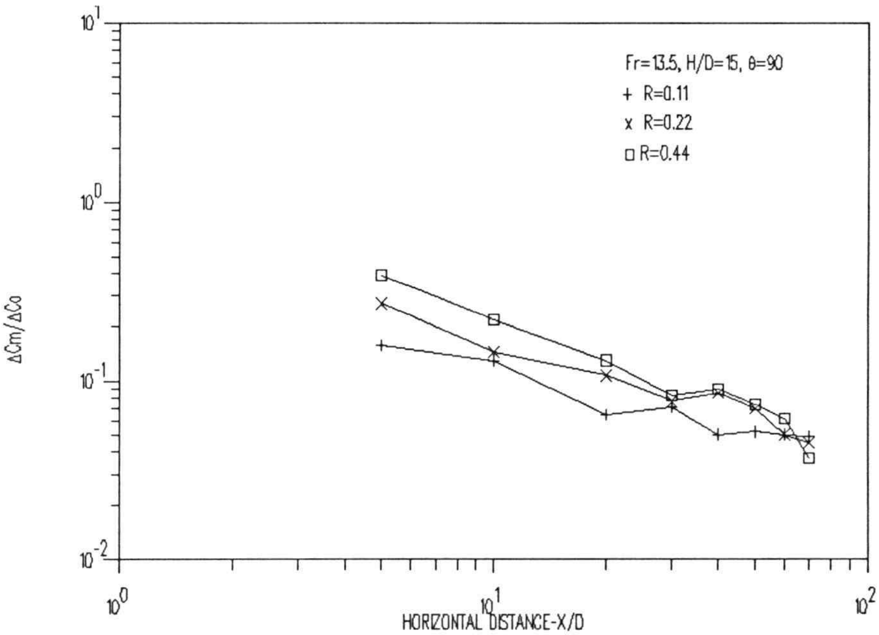

Figure B-18. Effect of varying R on maximum concentration deficit for Fr=13.5, H/D=15 and Θ=90°.

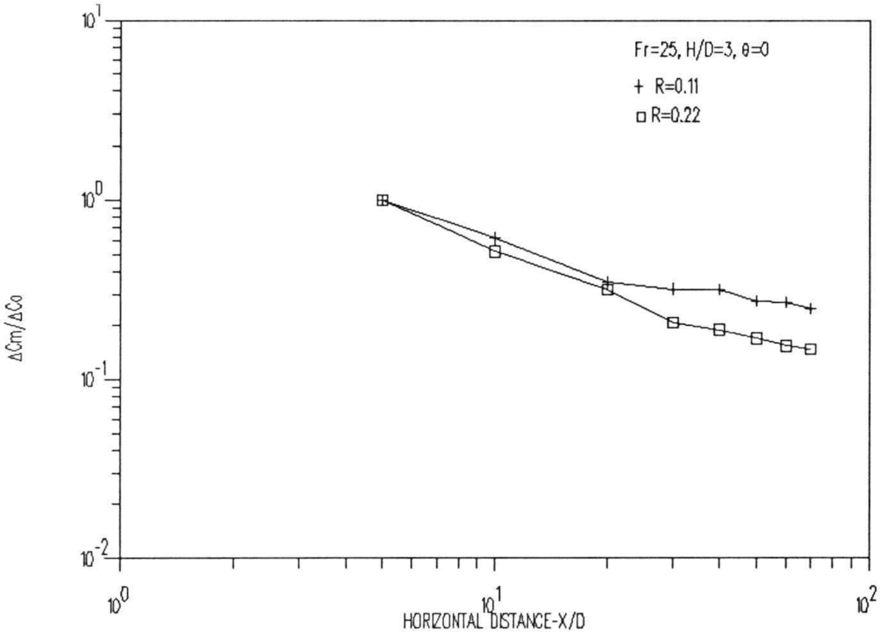

Figure B-19. Effect of varying R on maximum concentration deficit for Fr=25, H/D=3 and Θ=0°.

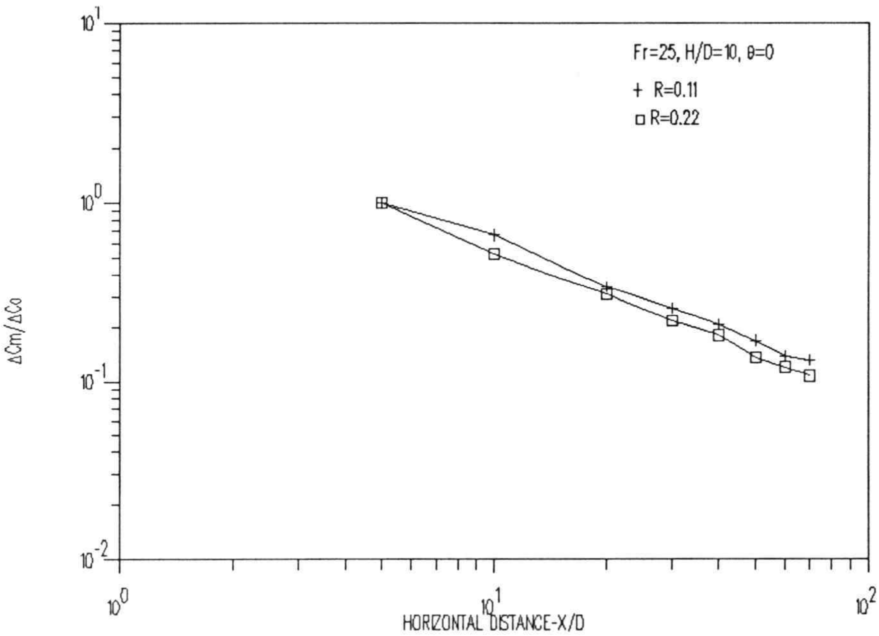

Figure B-20. Effect of varying R on maximum concentration deficit for Fr=25, H/D=10 and Θ=0°.

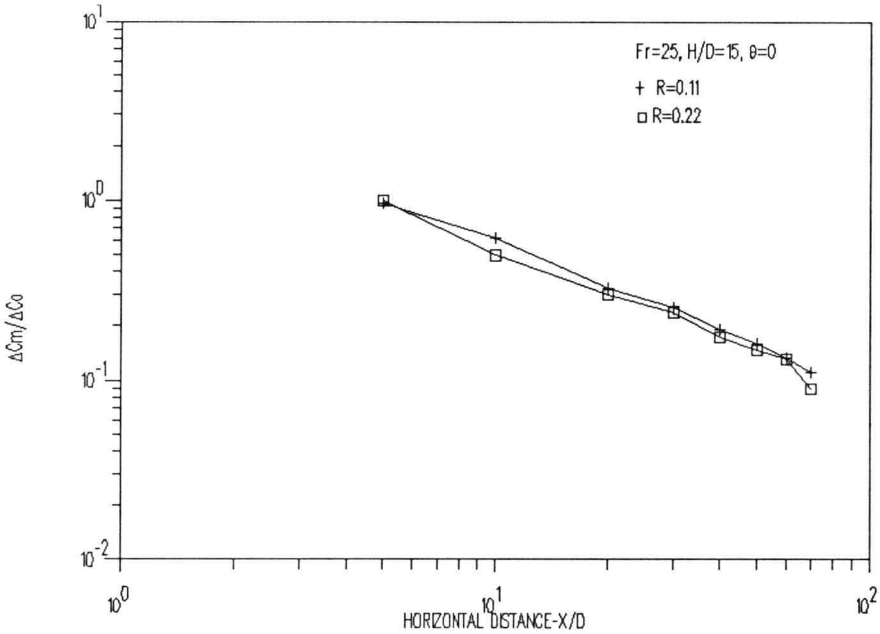

Figure B-21. Effect of varying R on maximum concentration deficit for Fr=25, H/D=15 and Θ=0°.

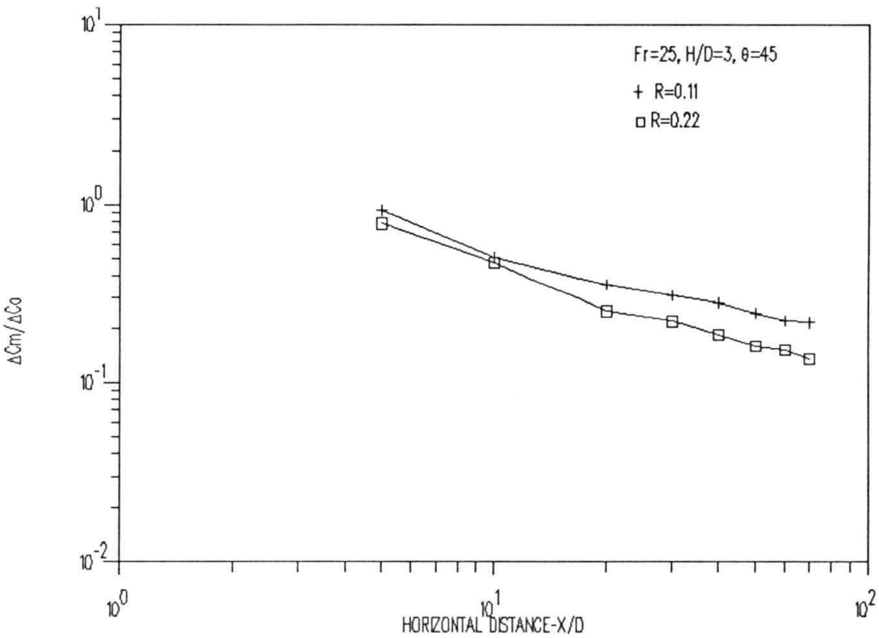

Figure B-22. Effect of varying R on maximum concentration deficit for Fr=25, H/D=3 and Θ=45°.

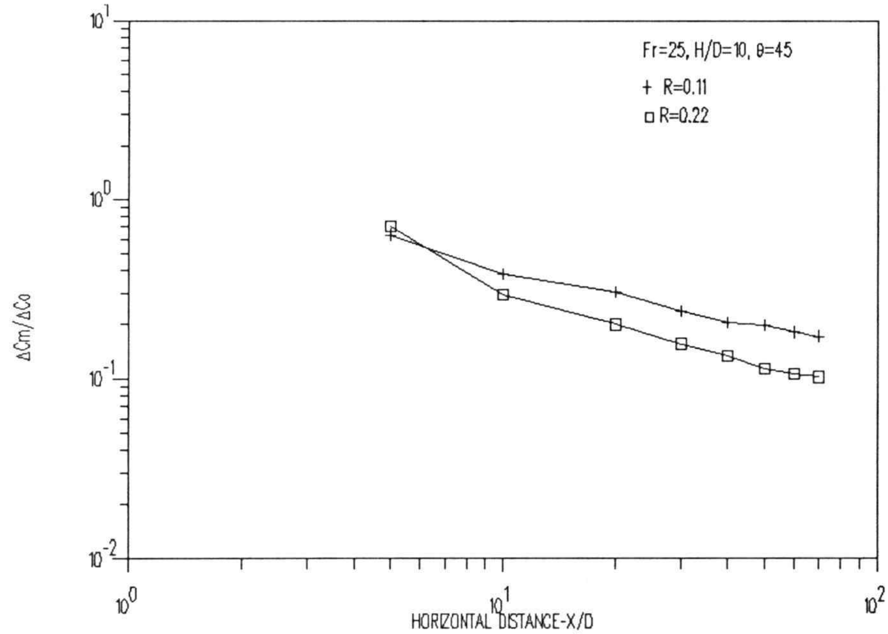

Figure B-23. Effect of varying R on maximum concentration deficit for Fr=25, H/D=10 and Θ=45°.

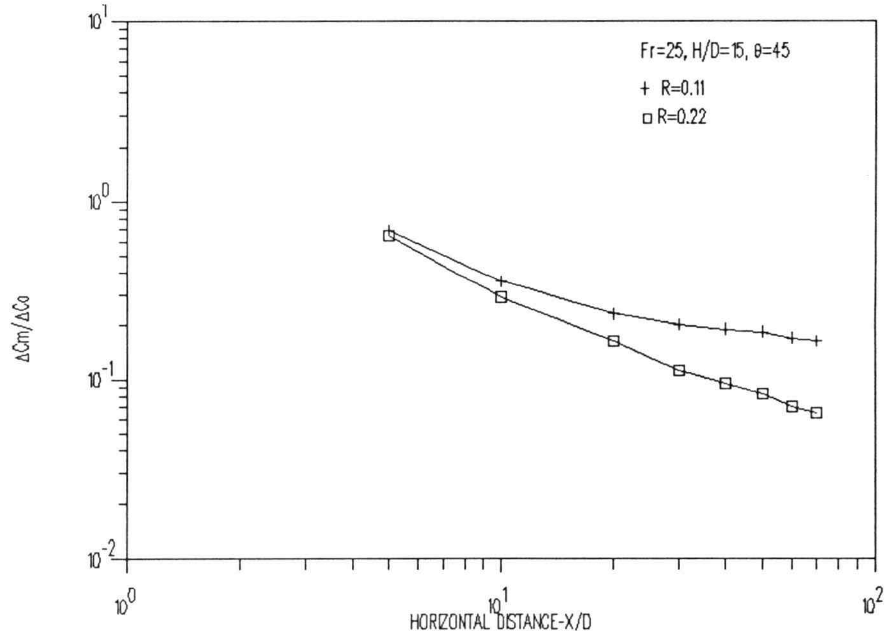

Figure B-24. Effect of varying R on maximum concentration deficit for Fr=25, H/D=15 and Θ=45°.

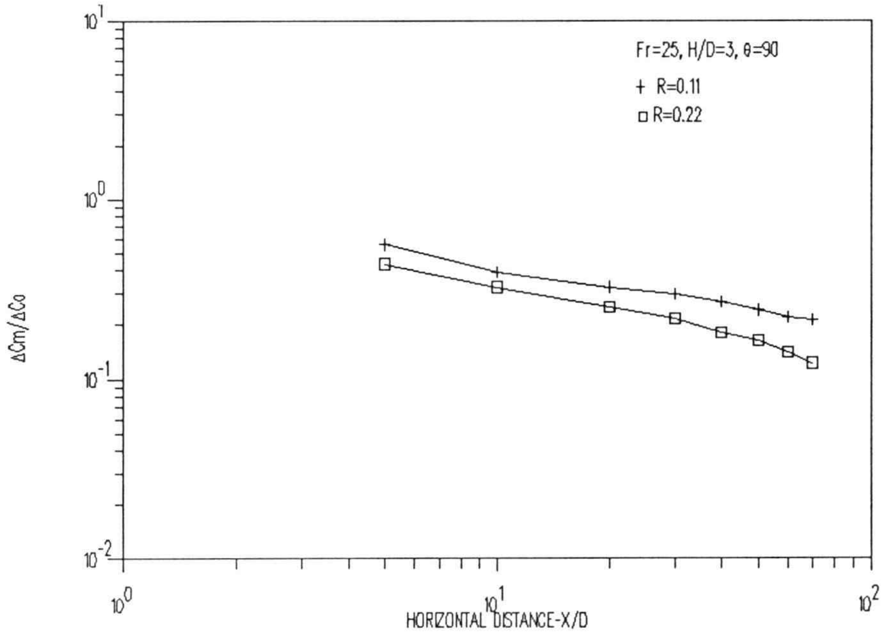

Figure B-25. Effect of varying R on maximum concentration deficit for Fr=25, H/D=3 and Θ=90°.

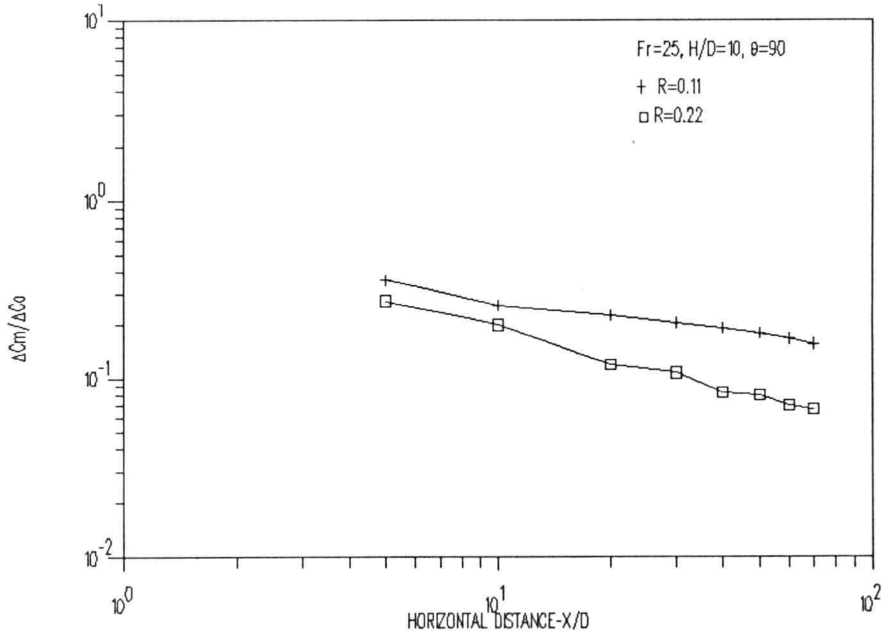

Figure B-26. Effect of varying R on maximum concentration deficit for Fr=25, H/D=10 and Θ=90°.

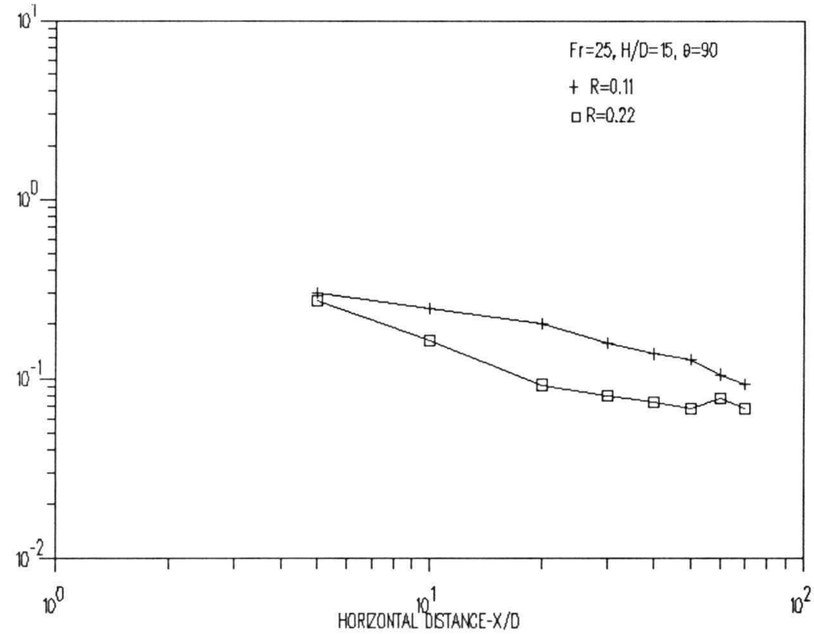

Figure B-27. Effect of varying R on maximum concentration deficit for Fr=25, H/D=15 and Θ=90°.

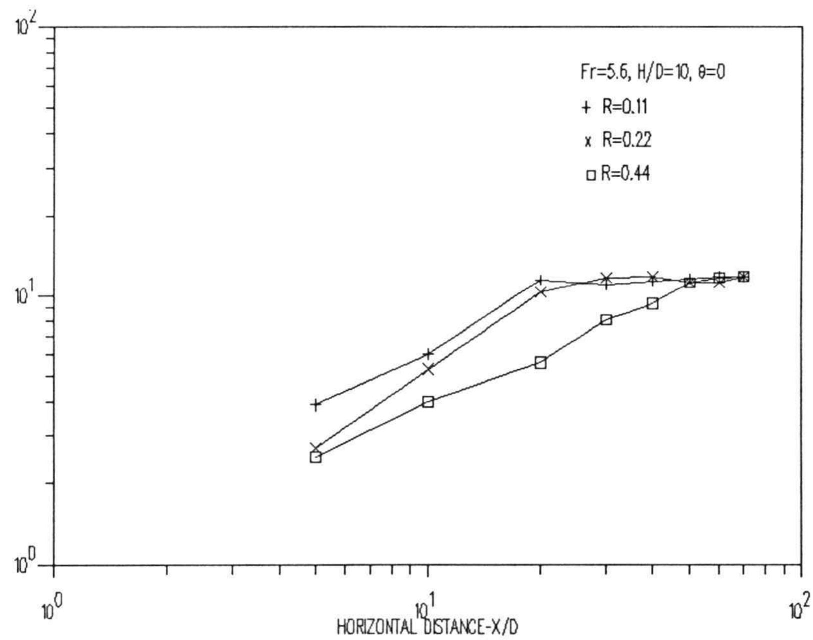

Figure B-28. Effect of varying R on trajectory for Fr=5.6, H/D=10 and Θ=0°.

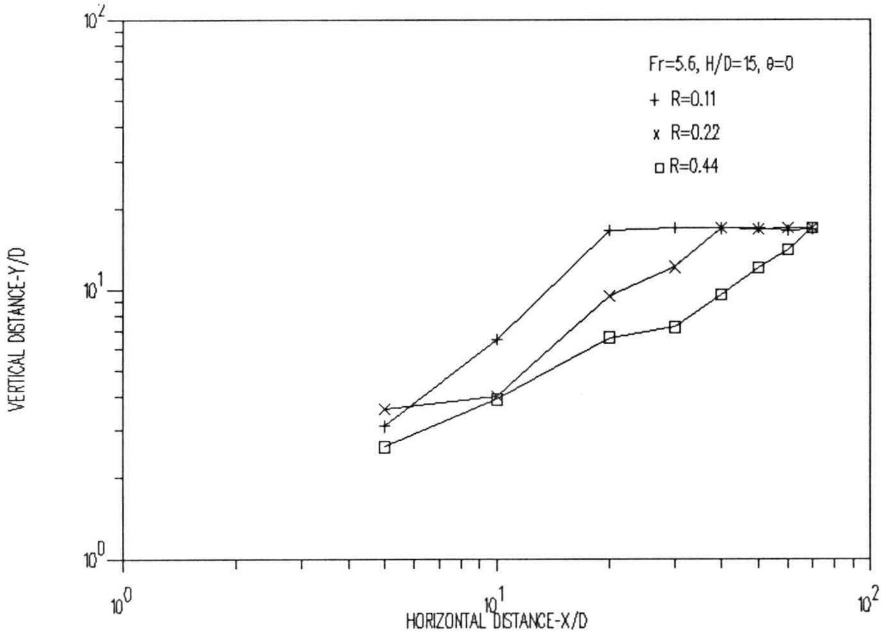

Figure B-29. Effect of varying R on trajectory for Fr=5.6, H/D=15 and Θ=0°.

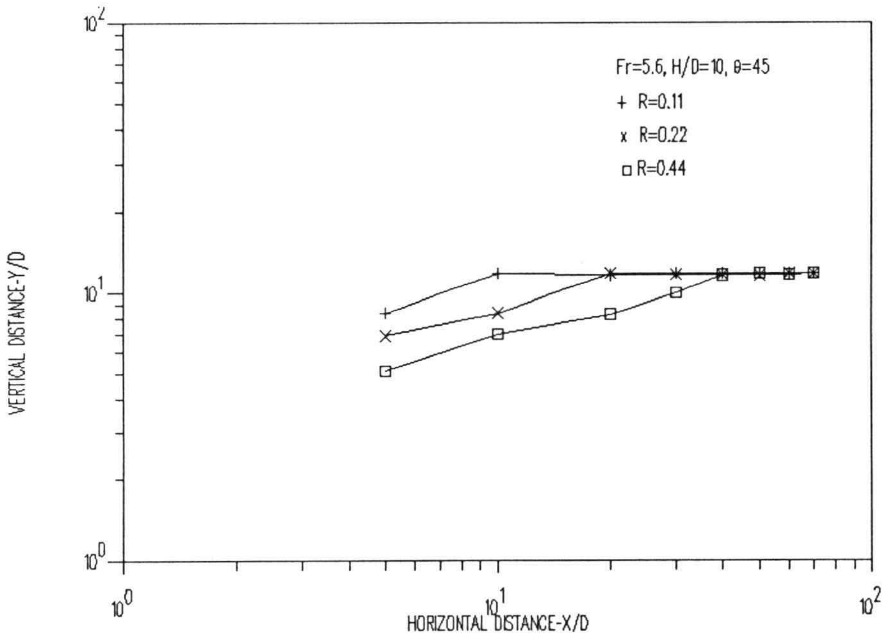

Figure B-30. Effect of varying R on trajectory for Fr=5.6, H/D=10 and Θ=45°.

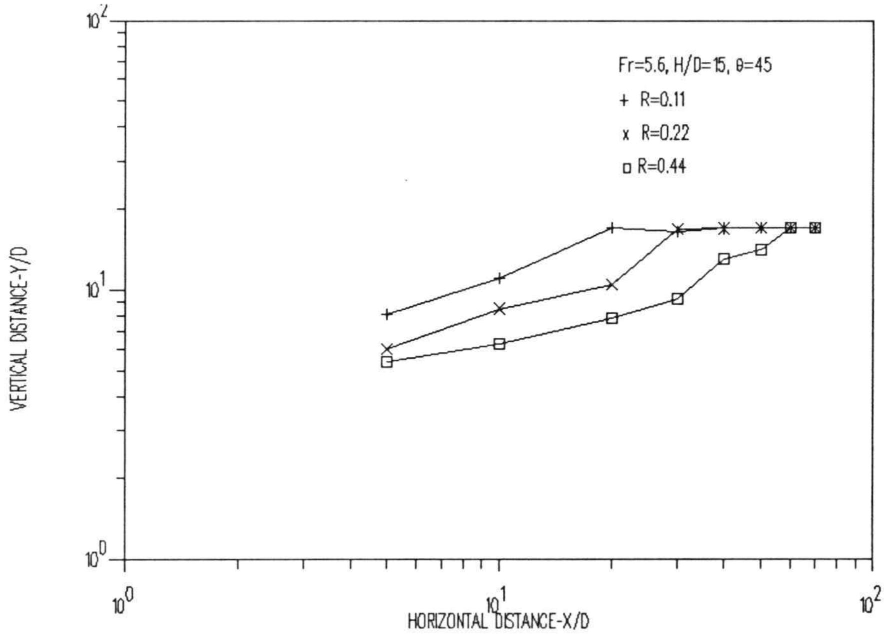

Figure B-31. Effect of varying R on trajectory for Fr=5.6, H/D=15 and Θ=45°.

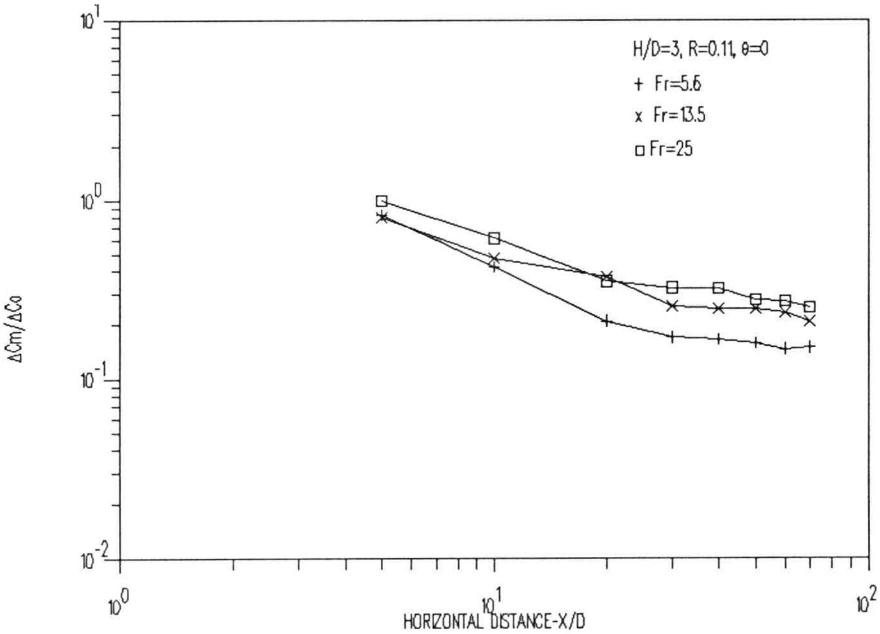

Figure B-32. Effect of varying Fr on maximum concentration deficit for H/D=3, R=0.11 and Θ=0°.

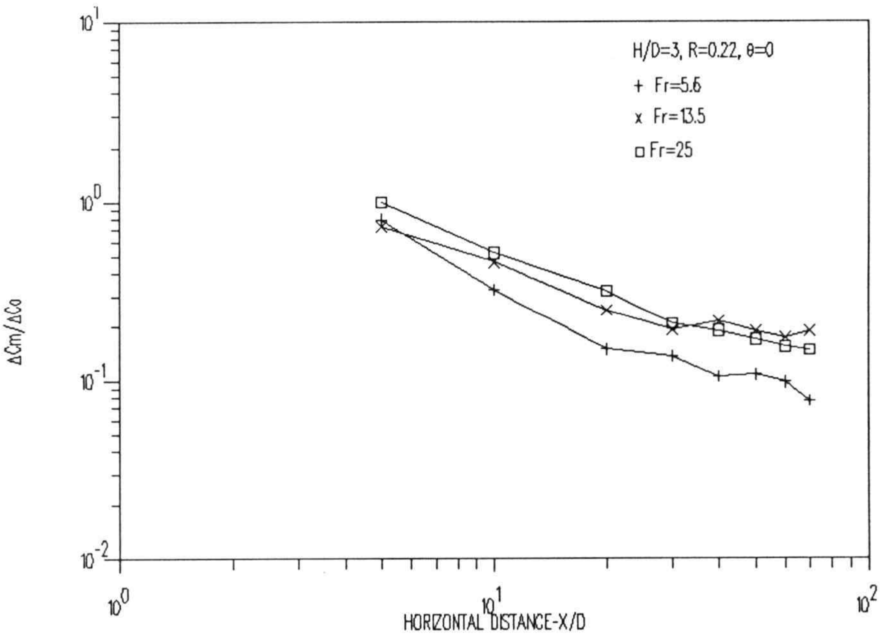

Figure B-33. Effect of varying Fr on maximum concentration deficit for H/D=3, R=0.22 and Θ=0°.

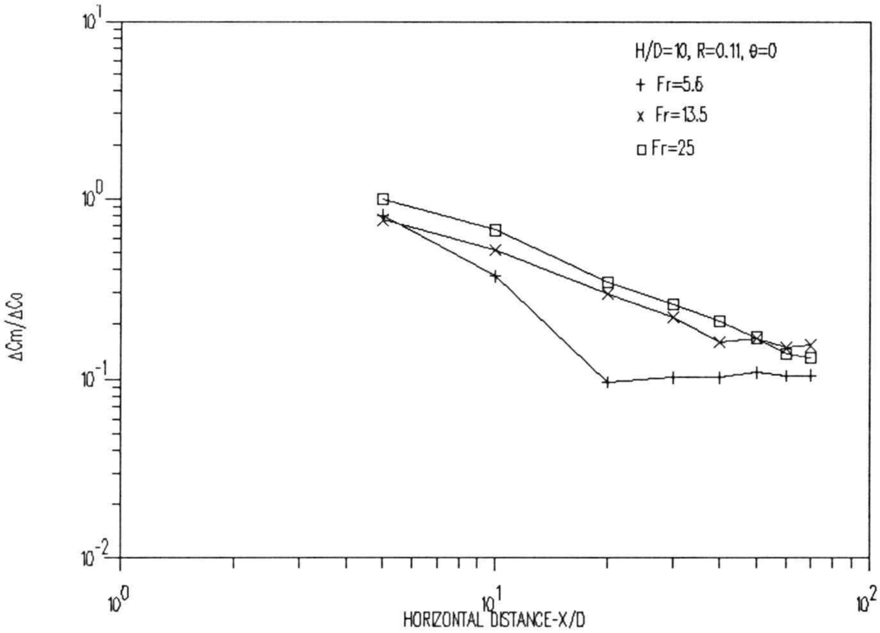

Figure B-34. Effect of varying Fr on maximum concentration deficit for H/D=10, R=0.11 and Θ=0°.

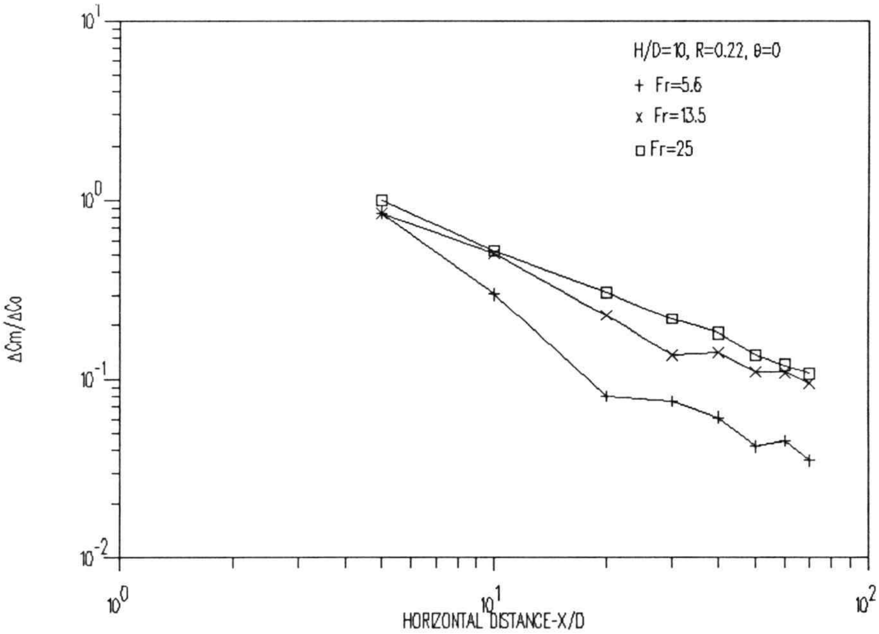

Figure B-35. Effect of varying Fr on maximum concentration deficit for H/D=10, R=0.22 and Θ=0°.

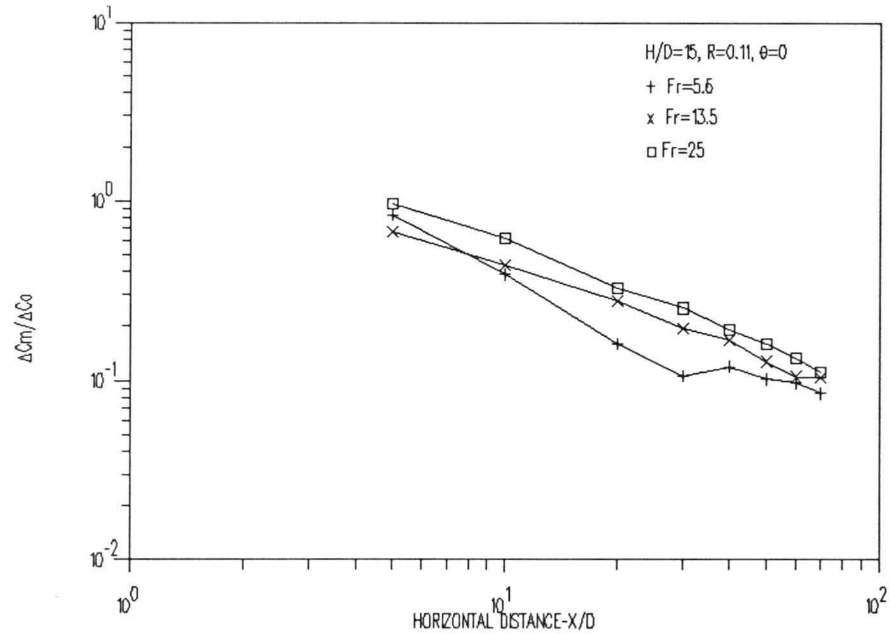

Figure B-36. Effect of varying Fr on maximum concentration deficit for H/D=15, R=0.11 and Θ=0°.

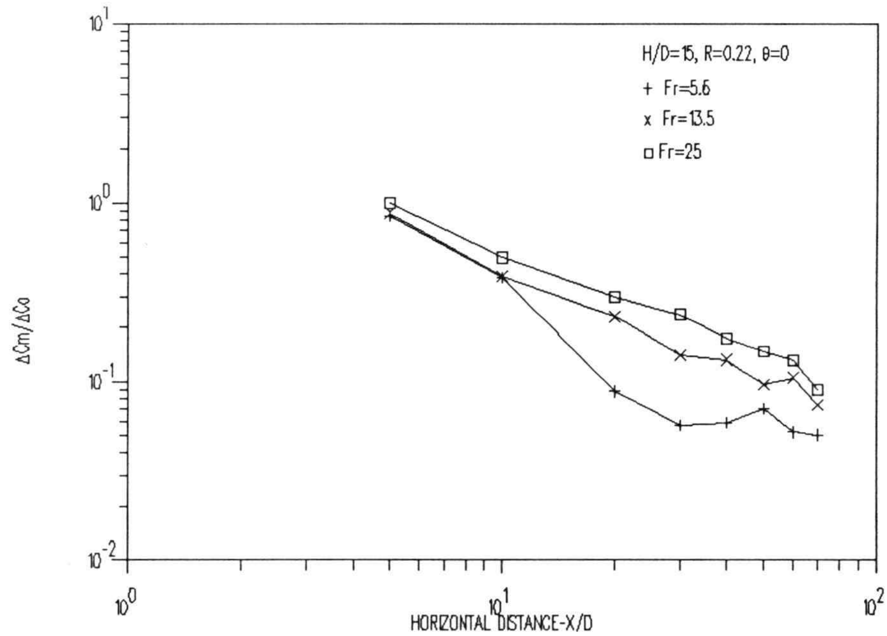

Figure B-37. Effect of varying Fr on maximum concentration deficit for H/D=15, R=0.22 and Θ=0°.

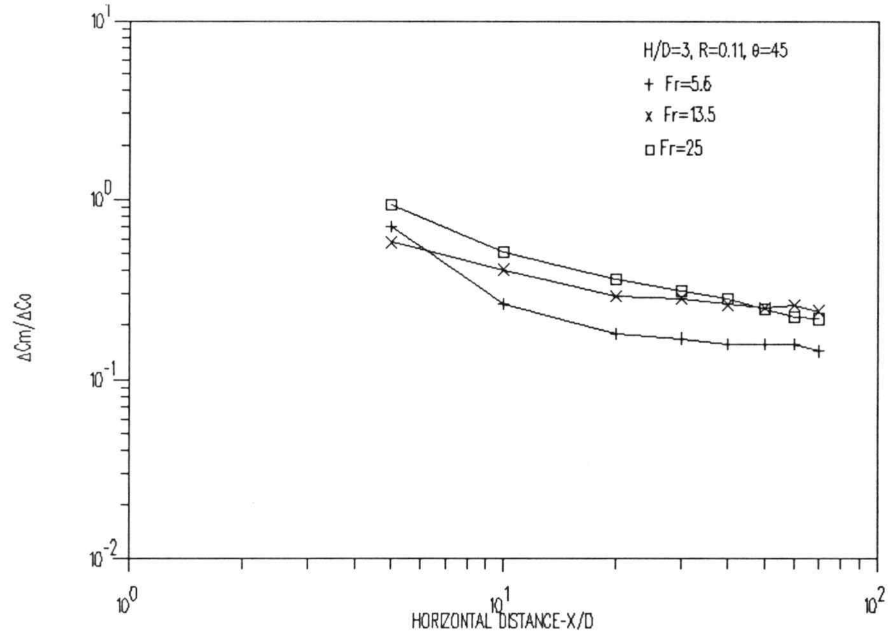

Figure B-38. Effect of varying Fr on maximum concentration deficit for H/D=3, R=0.11 and Θ=45°.

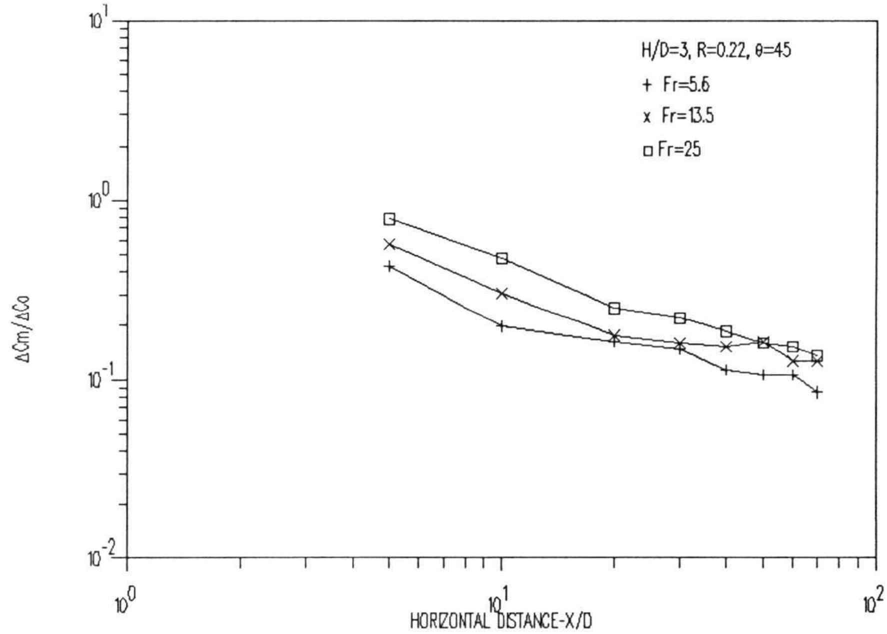

Figure B-39. Effect of varying Fr on maximum concentration deficit for H/D=3, R=0.22 and Θ=45°.

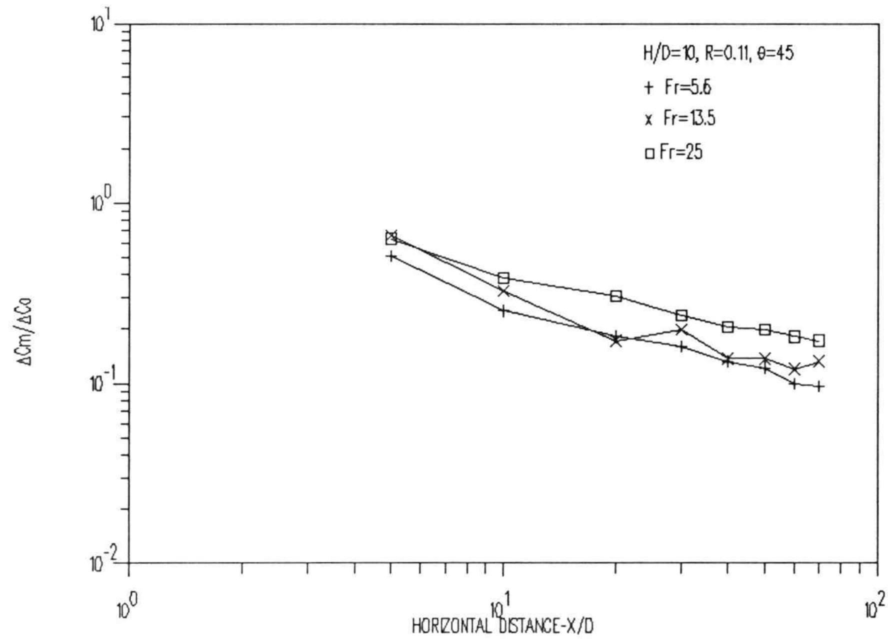

Figure B-40. Effect of varying Fr on maximum concentration deficit for H/D=10, R=0.11 and Θ=45°.

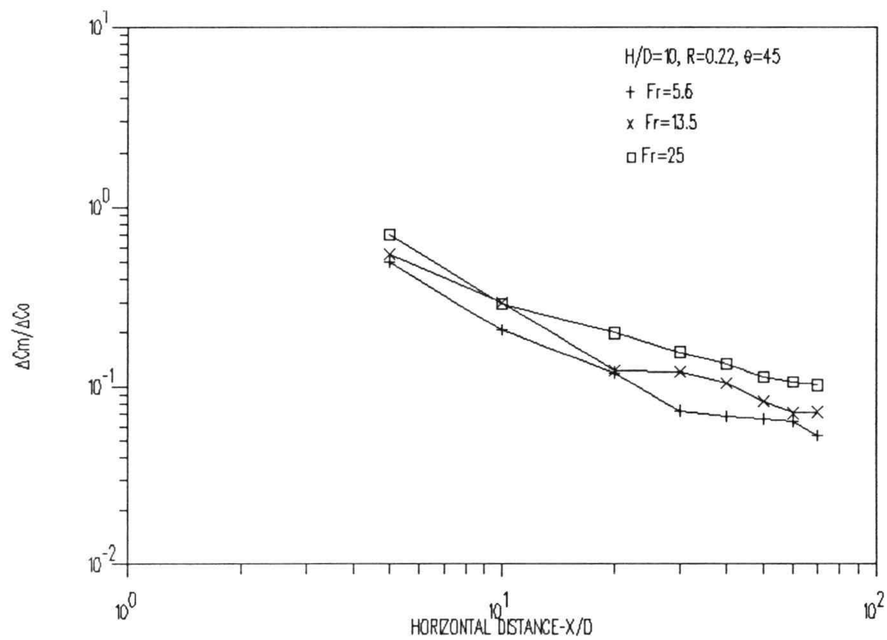

Figure B-41. Effect of varying Fr on maximum concentration deficit for H/D=10, R=0.22 and Θ=45°.

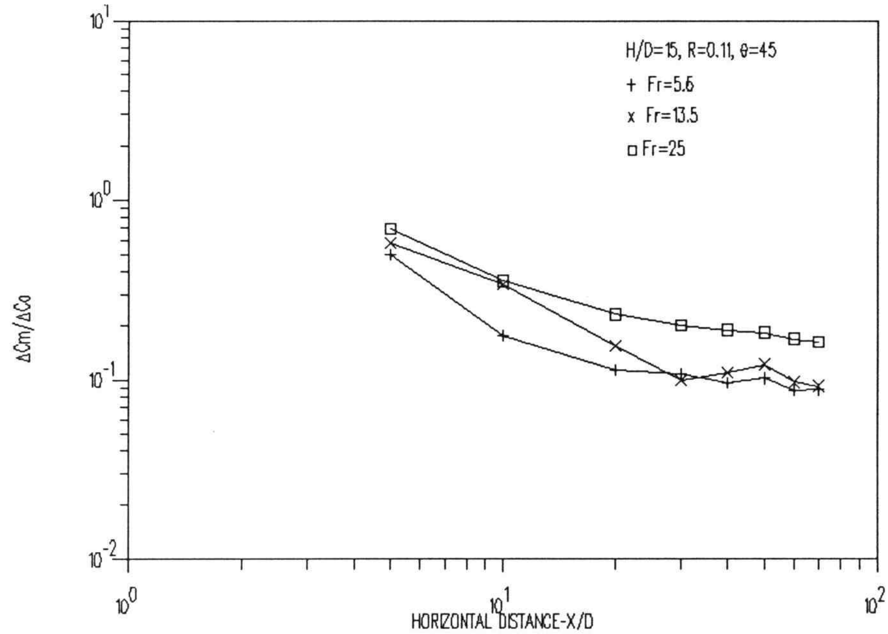

Figure B-42. Effect of varying Fr on maximum concentration deficit for H/D=15, R=0.11 and Θ=45°.

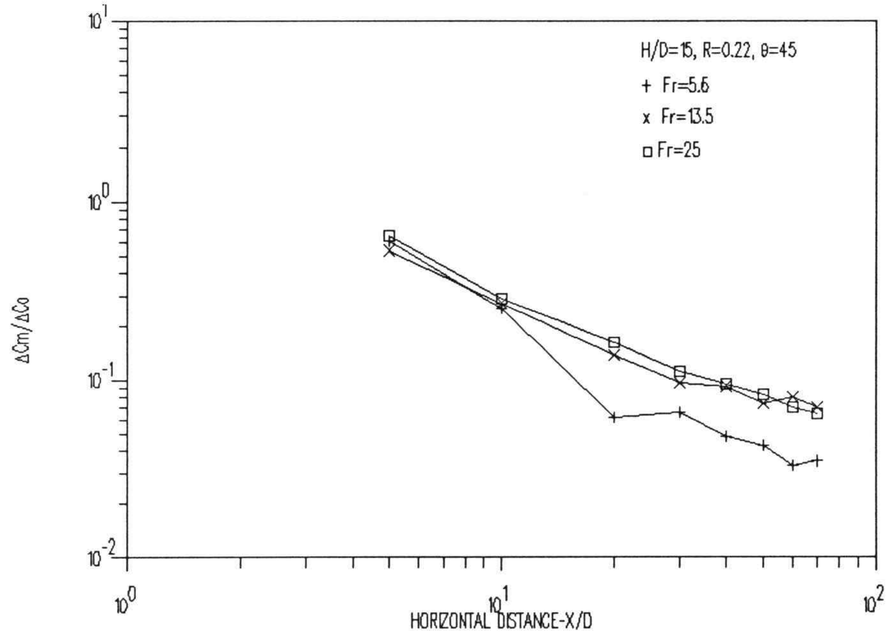

Figure B-43. Effect of varying Fr on maximum concentration deficit for H/D=15, R=0.22 and Θ=45°.

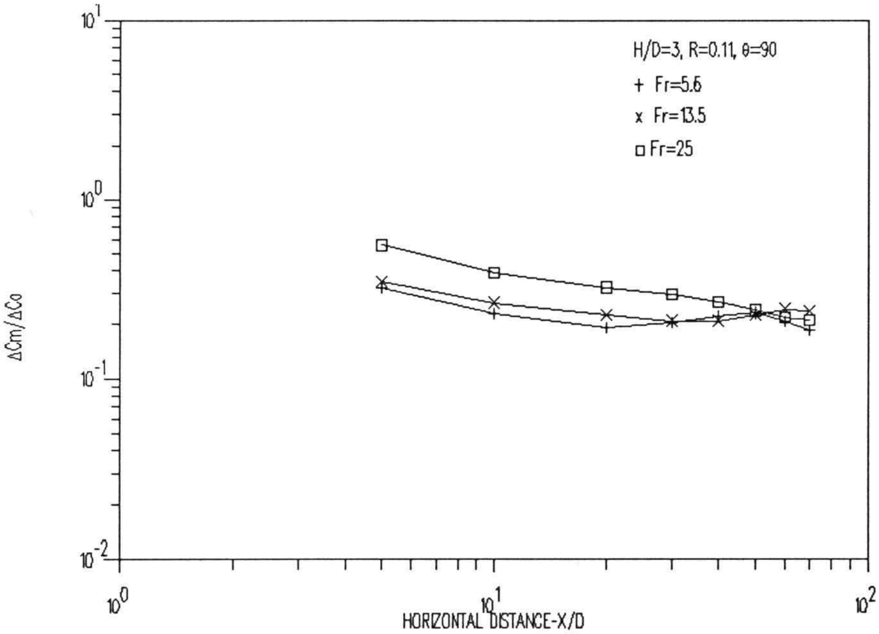

Figure B-44. Effect of varying Fr on maximum concentration deficit for H/D=3, R=0.11 and Θ=90°.

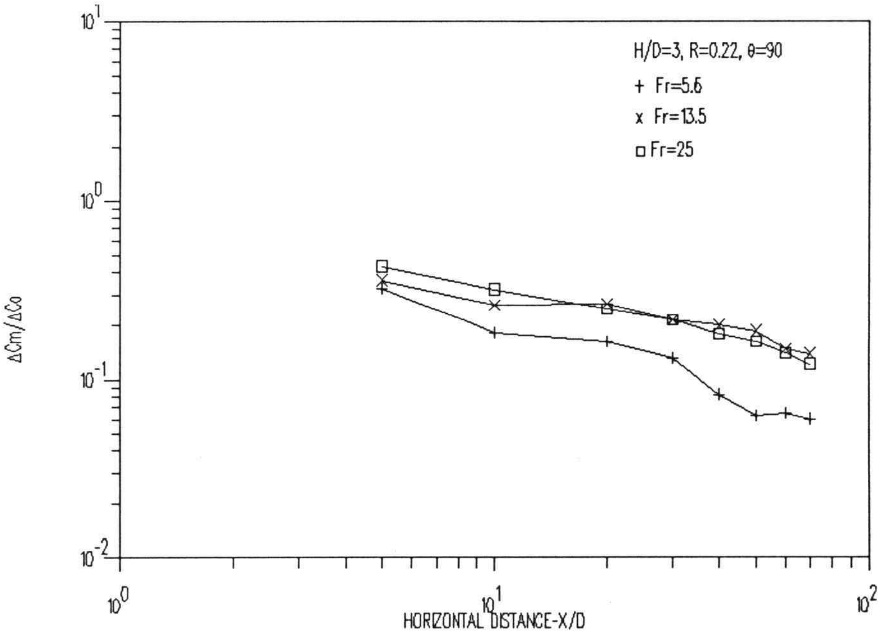

Figure B-45. Effect of varying Fr on maximum concentration deficit for H/D=3, R=0.22 and Θ=90°.

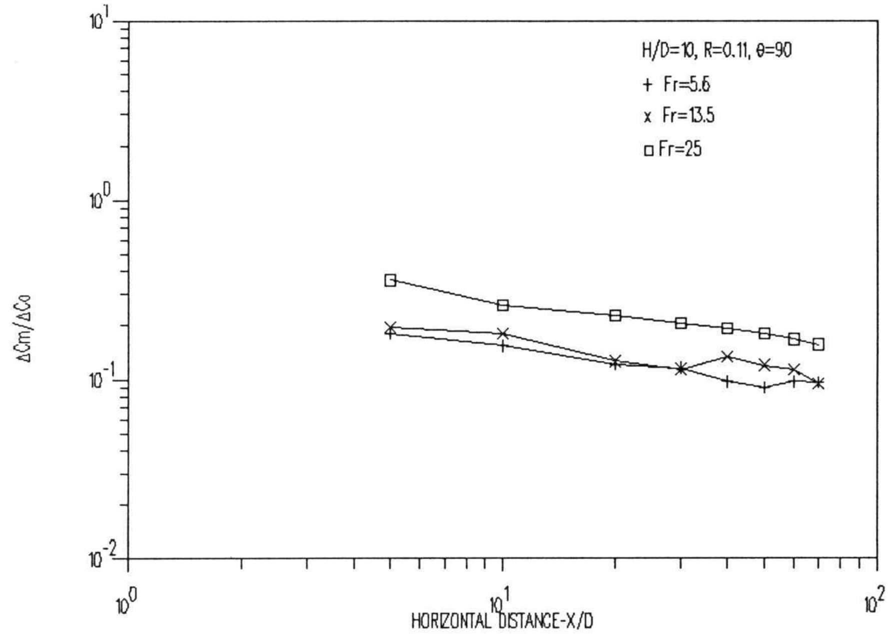

Figure B-46. Effect of varying Fr on maximum concentration deficit for H/D=10, R=0.11 and Θ=90°.

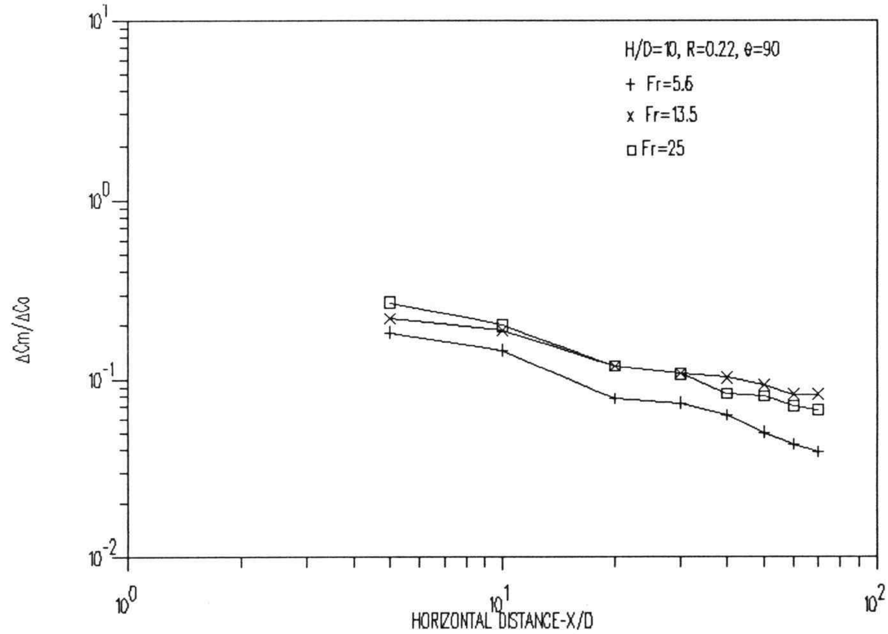

Figure B-47. Effect of varying Fr on maximum concentration deficit for H/D=10, R=0.22 and Θ=90°.

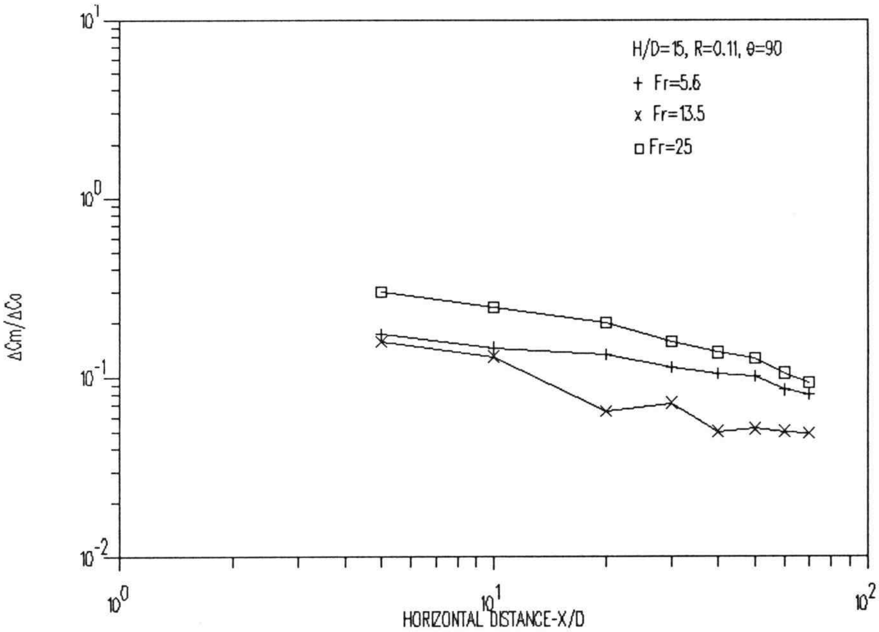

Figure B-48. Effect of varying Fr on maximum concentration deficit for H/D=15, R=0.11 and Θ=90°.

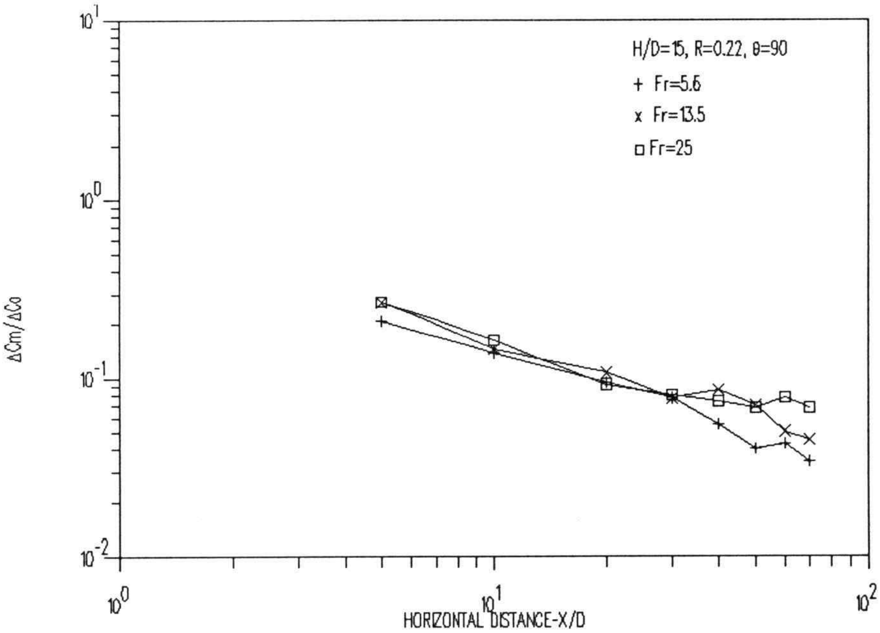

Figure B-49. Effect of varying Fr on maximum concentration deficit for H/D=15, R=0.22 and Θ=90°.

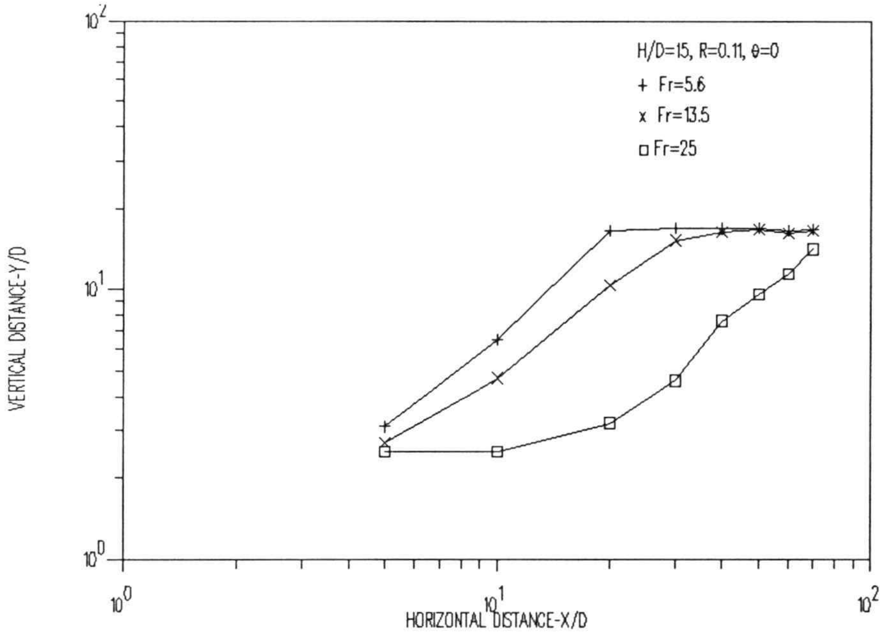

Figure B-50. Effect of varying Fr on trajectory for H/D=15, R=0.11 and Θ=0°.

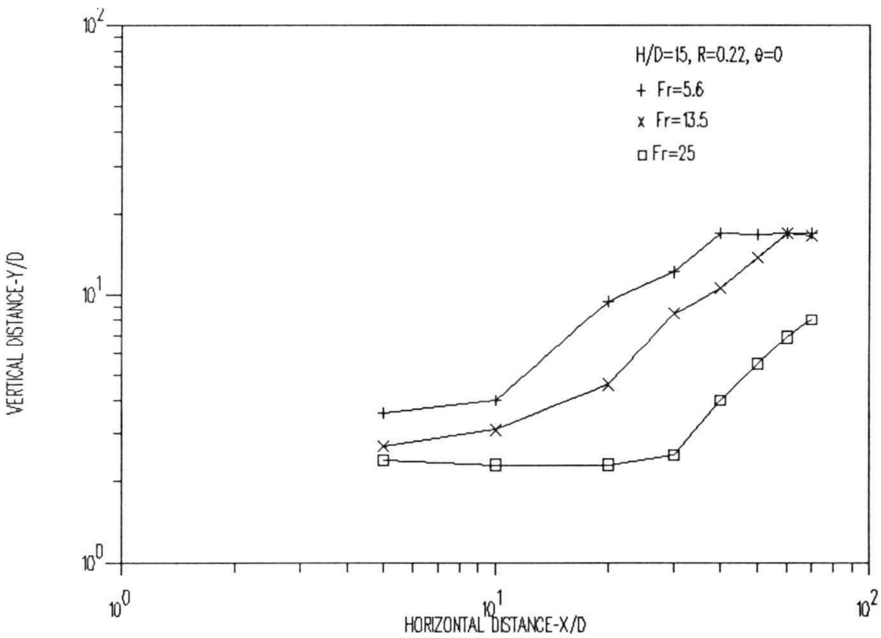

Figure B-51. Effect of varying Fr on trajectory for H/D=15, R=0.22 and Θ=0°.

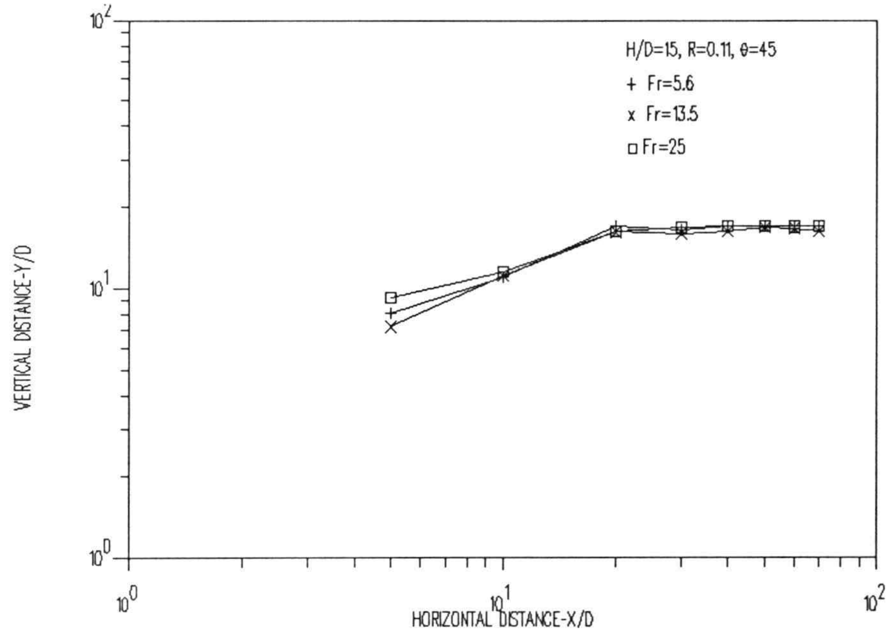

Figure B-52. Effect of varying Fr on trajectory for H/D=15, R=0.11 and Θ=45°.

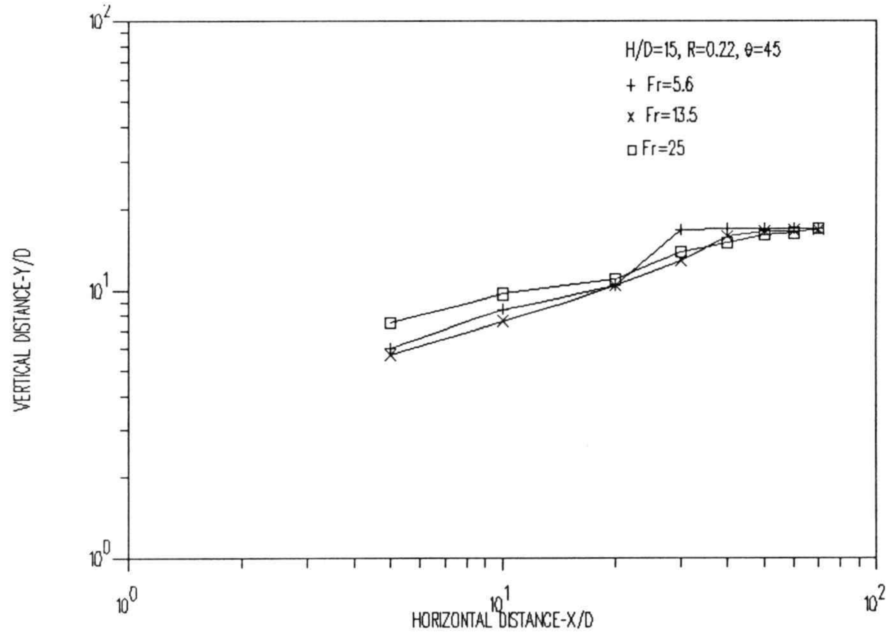

Figure B-53. Effect of varying Fr on trajectory for H/D=15, R=0.22 and Θ=45°.

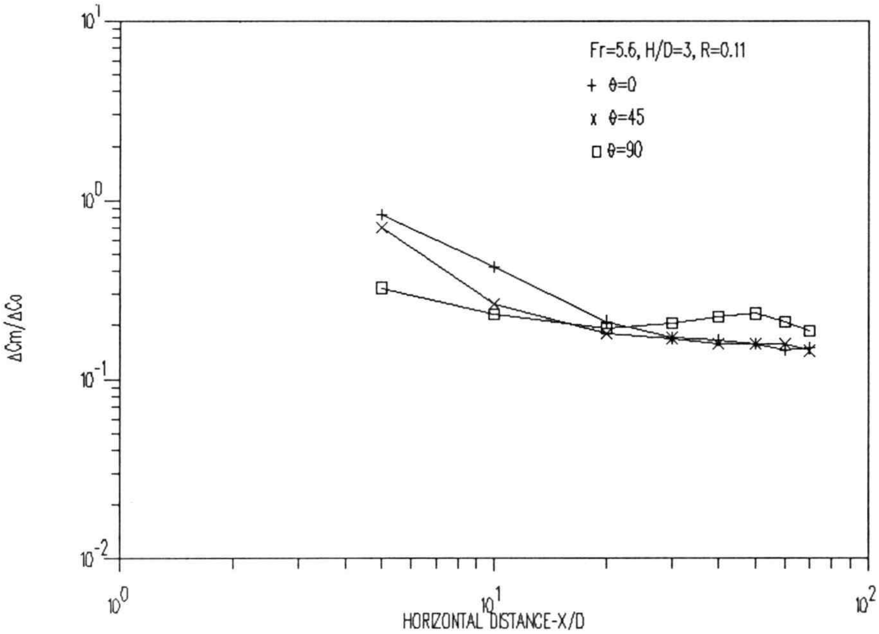

Figure B-54. Effect of varying Θ on maximum concentration deficit for Fr=5.6, H/D=3 and R=0.11.

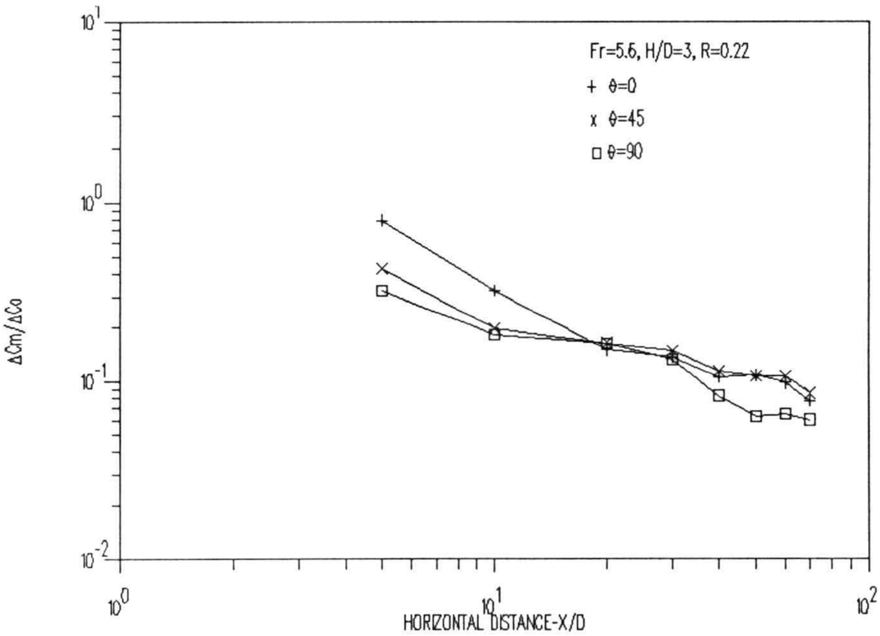

Figure B-55. Effect of varying Θ on maximum concentration deficit for Fr=5.6, H/D=3 and R=0.22.

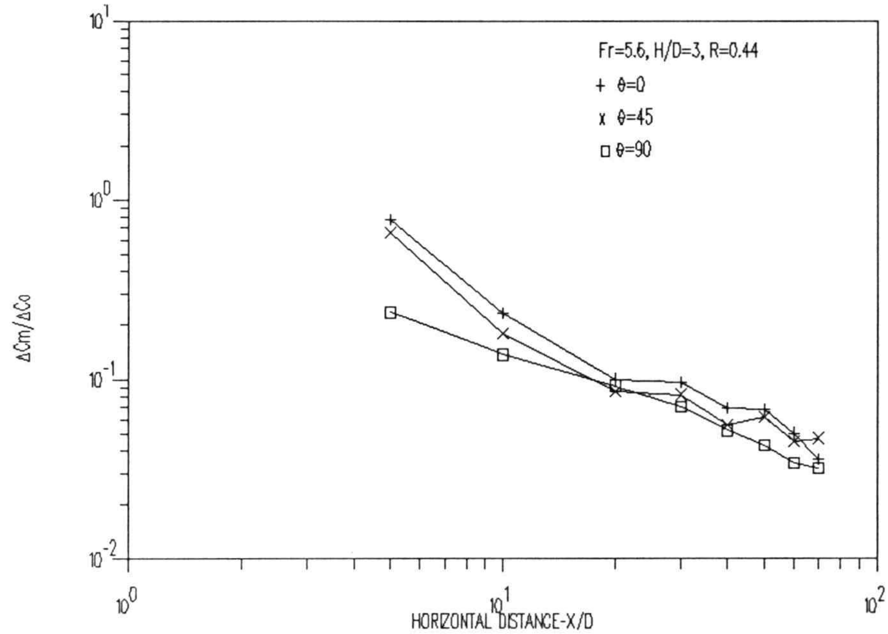

Figure B-56. Effect of varying Θ on maximum concentration deficit for Fr=5.6, H/D=3 and R=0.44.

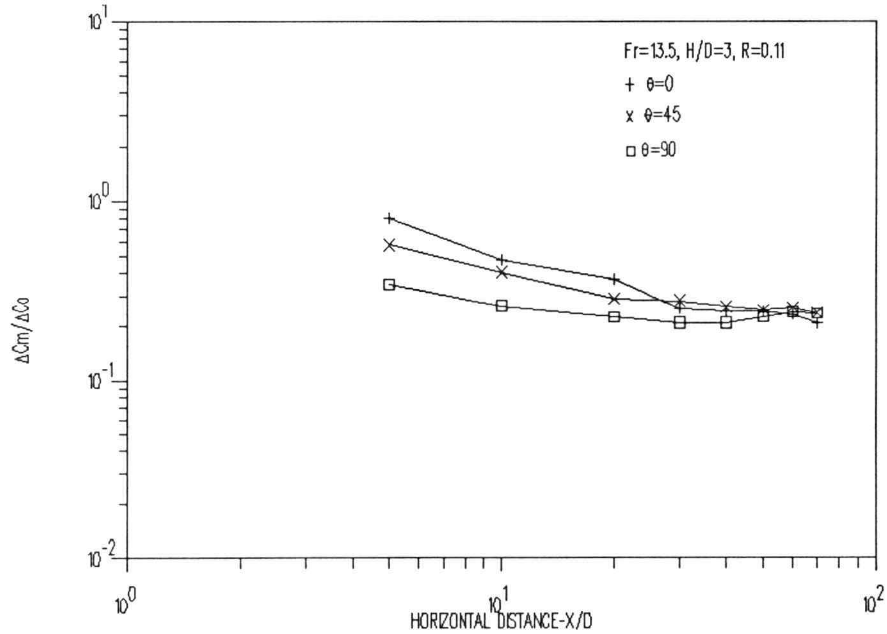

Figure B-57. Effect of varying Θ on maximum concentration deficit for Fr=13.5, H/D=3 and R=0.11.

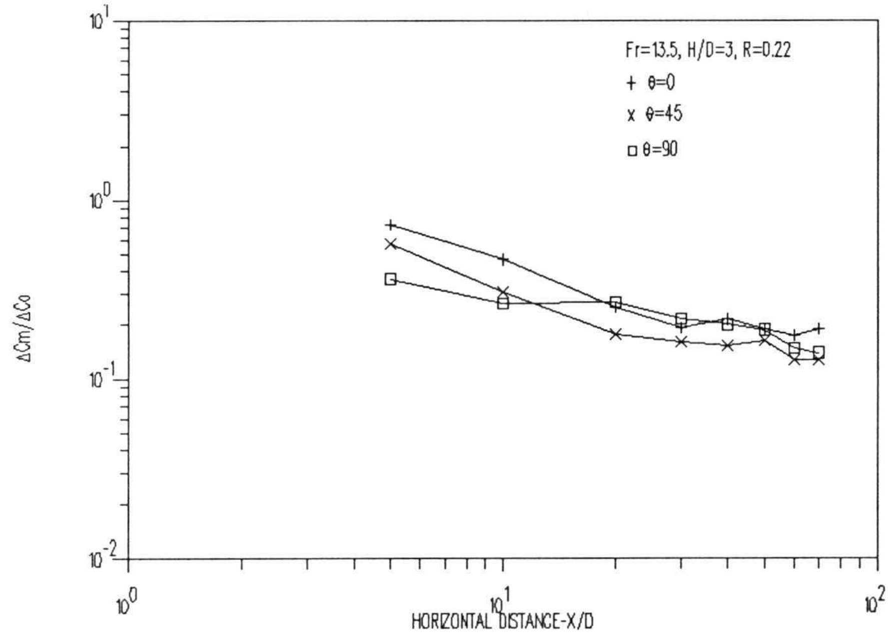

Figure B-58. Effect of varying Θ on maximum concentration deficit for Fr=13.5, H/D=3 and R=0.22.

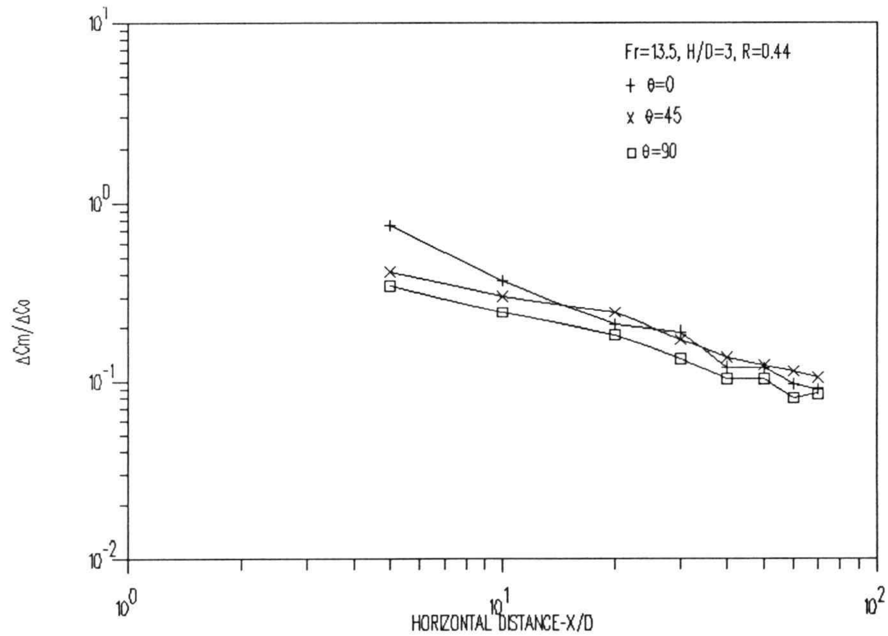

Figure B-59. Effect of varying Θ on maximum concentration deficit for Fr=13.5, H/D=3 and R=0.44.

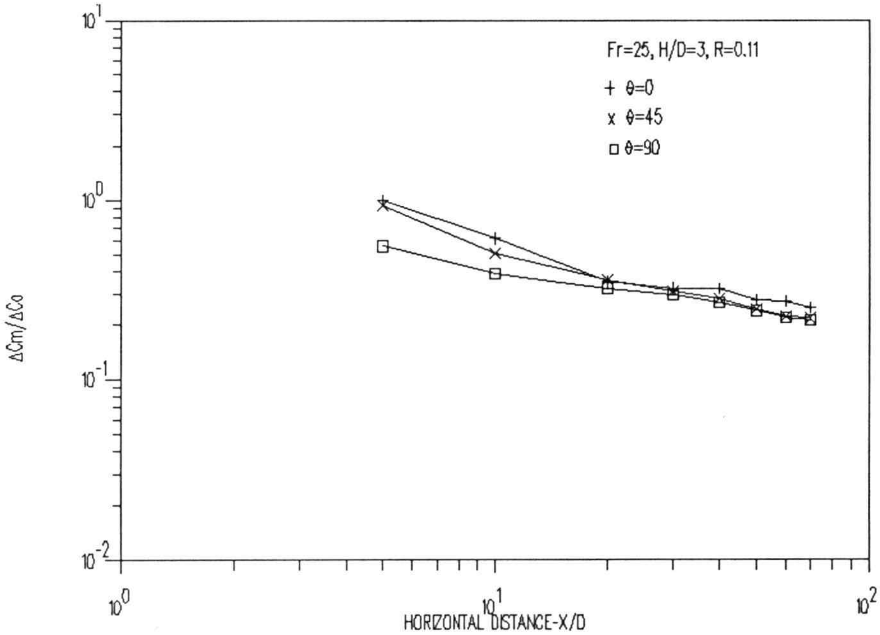

Figure B-60. Effect of varying Θ on maximum concentration deficit for Fr=25, H/D=3 and R=0.11.

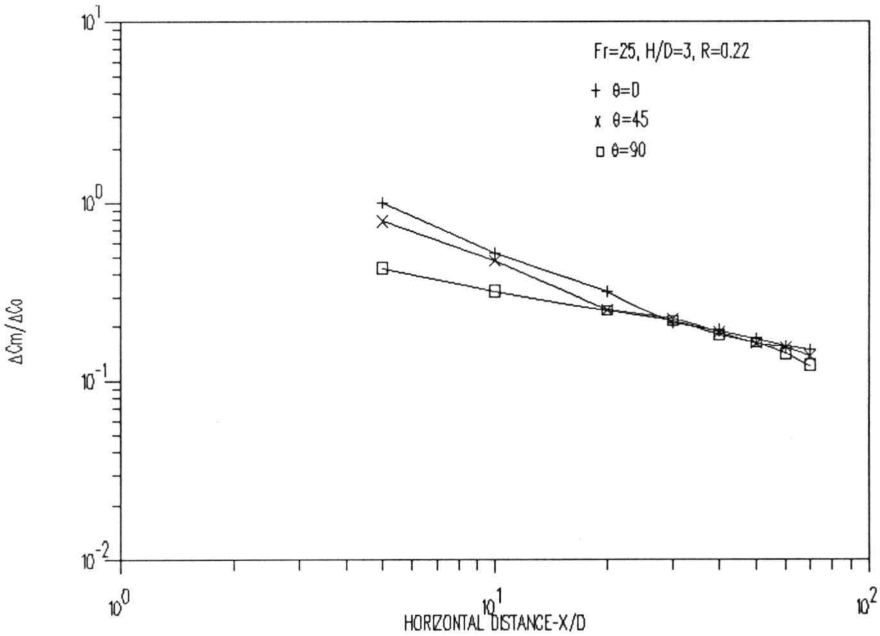

Figure B-61. Effect of varying Θ on maximum concentration deficit for Fr=25, H/D=3 and R=0.22.

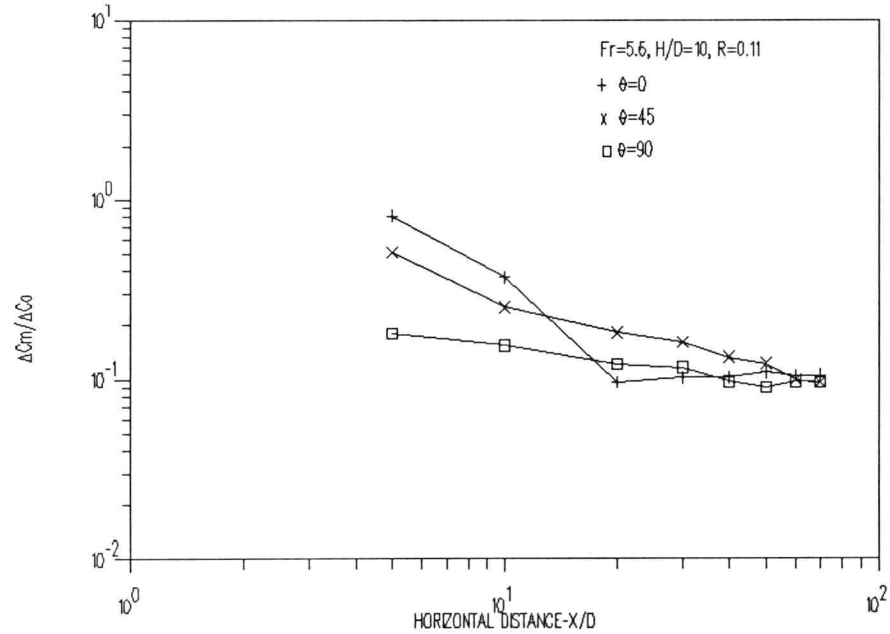

Figure B-62. Effect of varying Θ on maximum concentration deficit for Fr=5.6, H/D=10 and R=0.11.

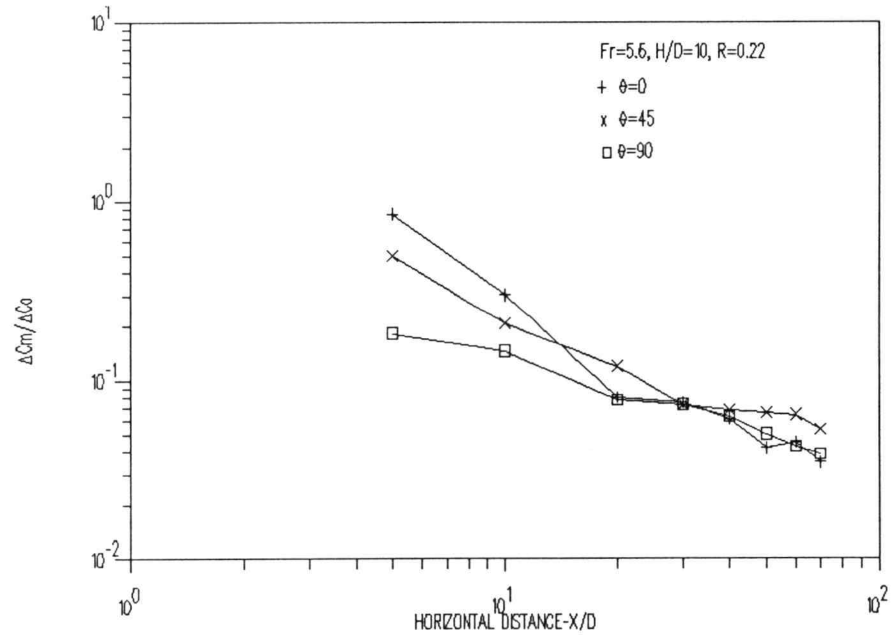

Figure B-63. Effect of varying Θ on maximum concentration deficit for Fr=5.6, H/D=10 and R=0.22.

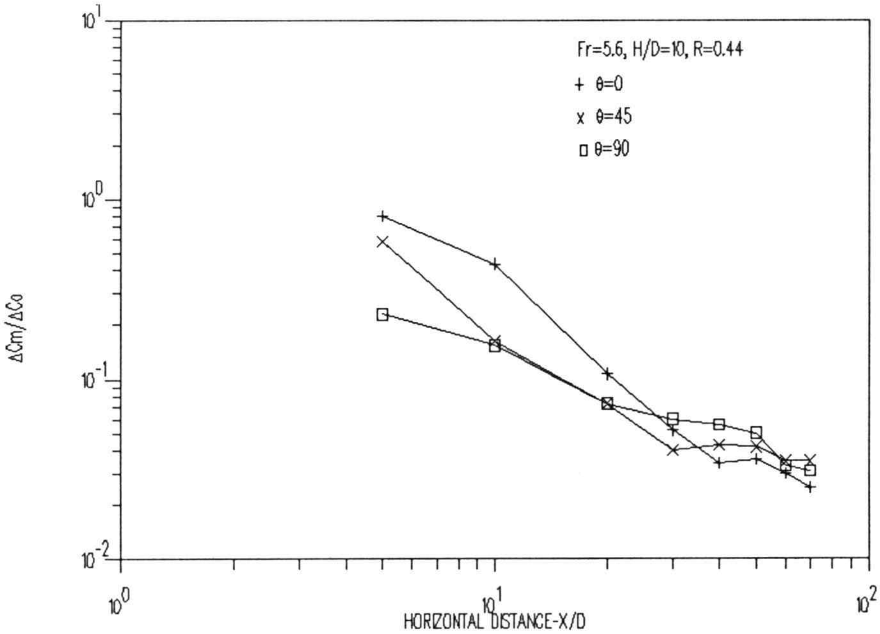

Figure B-64. Effect of varying Θ on maximum concentration deficit for Fr=5.6, H/D=10 and R=0.44.

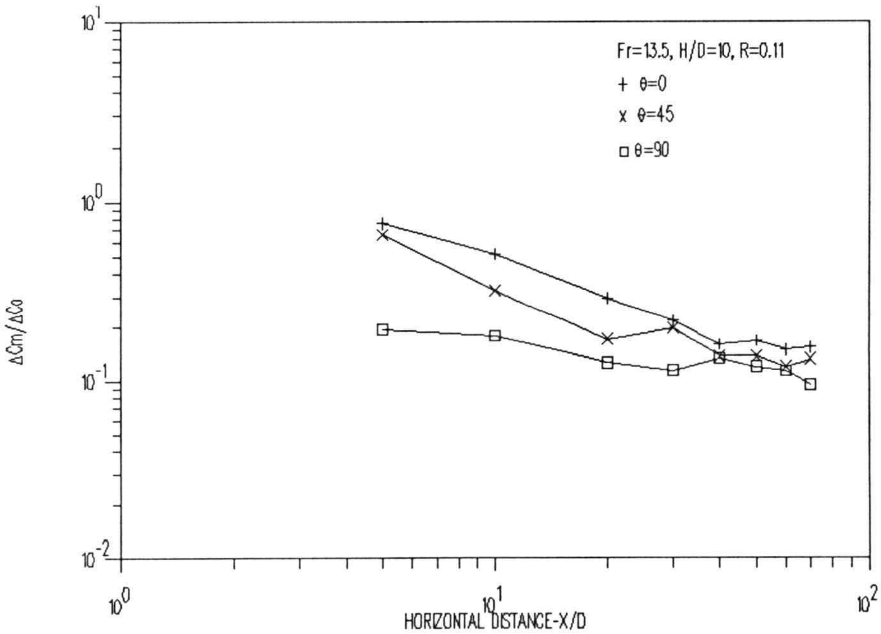

Figure B-65. Effect of varying Θ on maximum concentration deficit for Fr=13.5, H/D=10 and R=0.11.

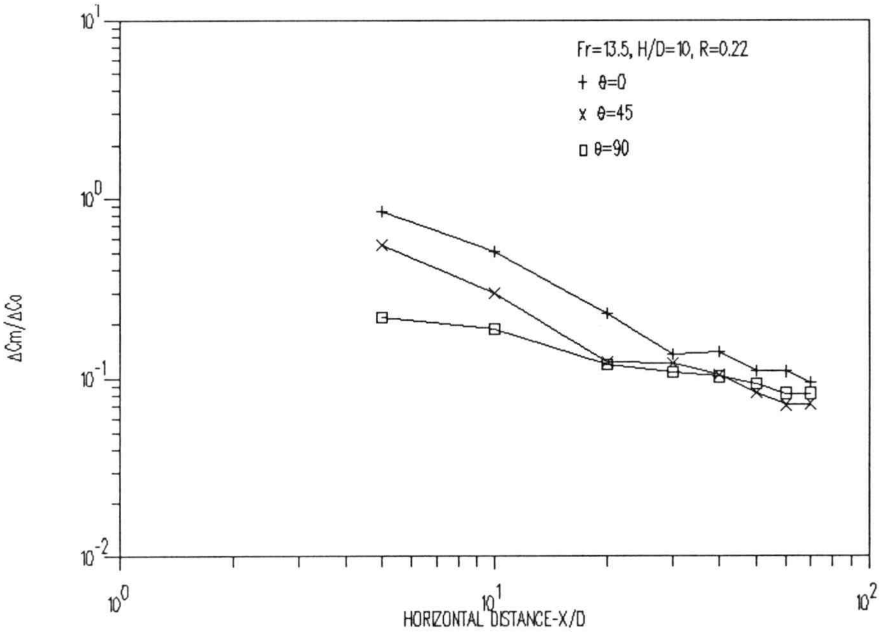

Figure B-66. Effect of varying Θ on maximum concentration deficit for Fr=13.5, H/D=10 and R=0.22.

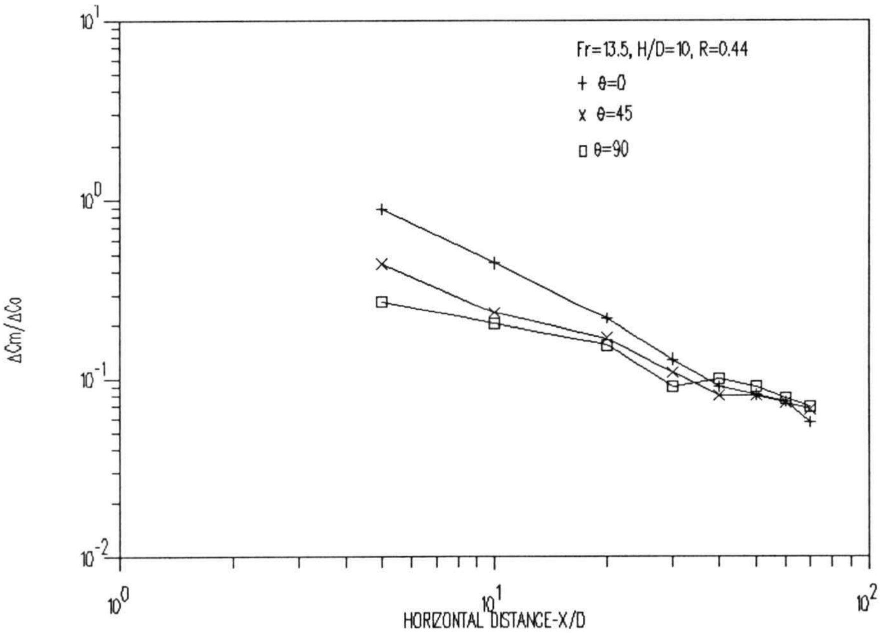

Figure B-67. Effect of varying Θ on maximum concentration deficit for Fr=13.5, H/D=10 and R=0.44.

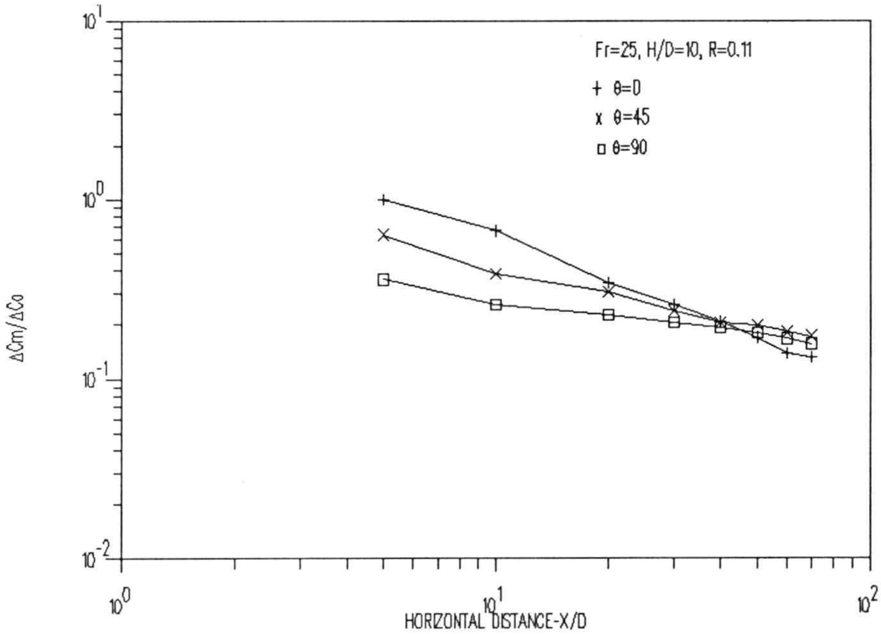

Figure B-68. Effect of varying Θ on maximum concentration deficit for Fr=25, H/D=10 and R=0.11.

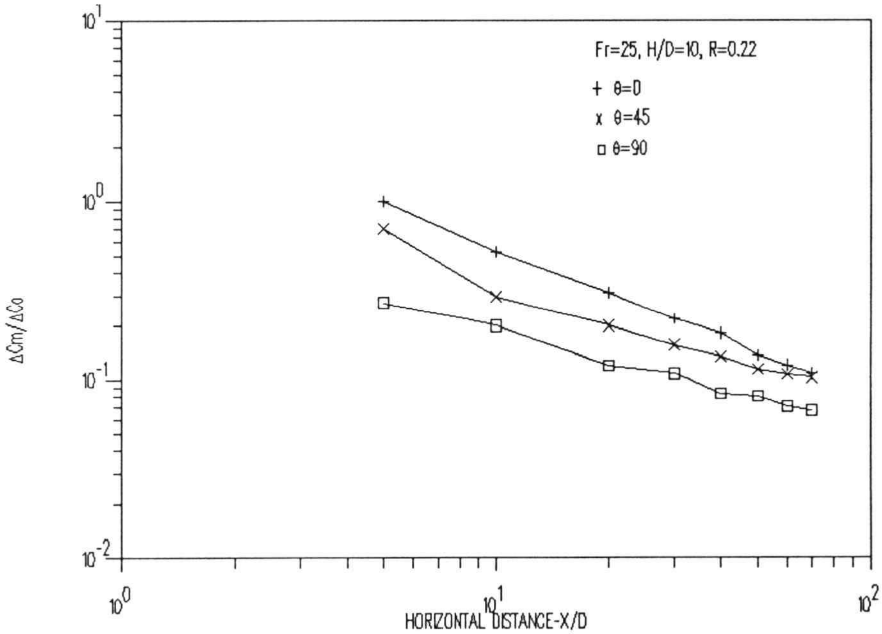

Figure B-69. Effect of varying Θ on maximum concentration deficit for Fr=25, H/D=10 and R=0.22.

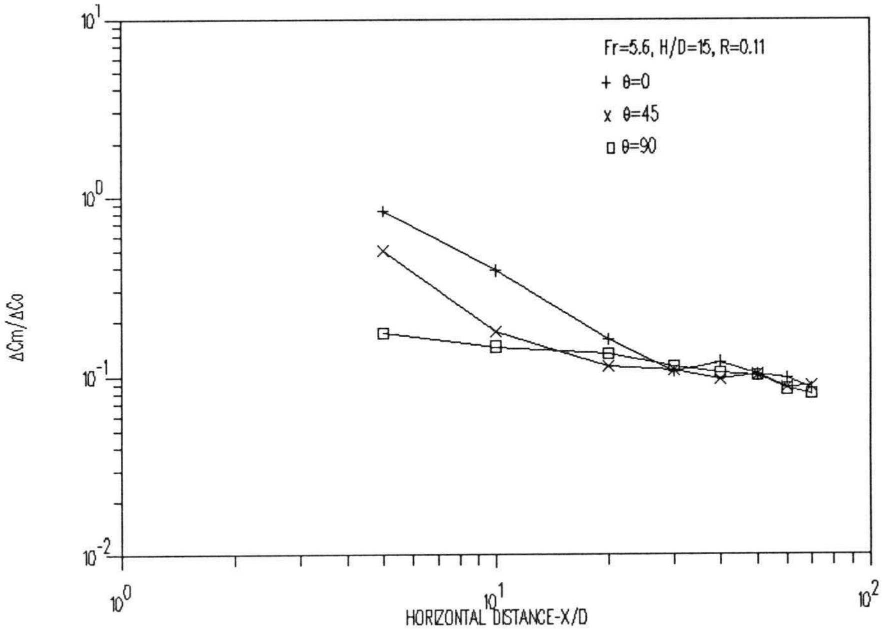

Figure B-70. Effect of varying Θ on maximum concentration deficit for Fr=5.6, H/D=15 and R=0.11.

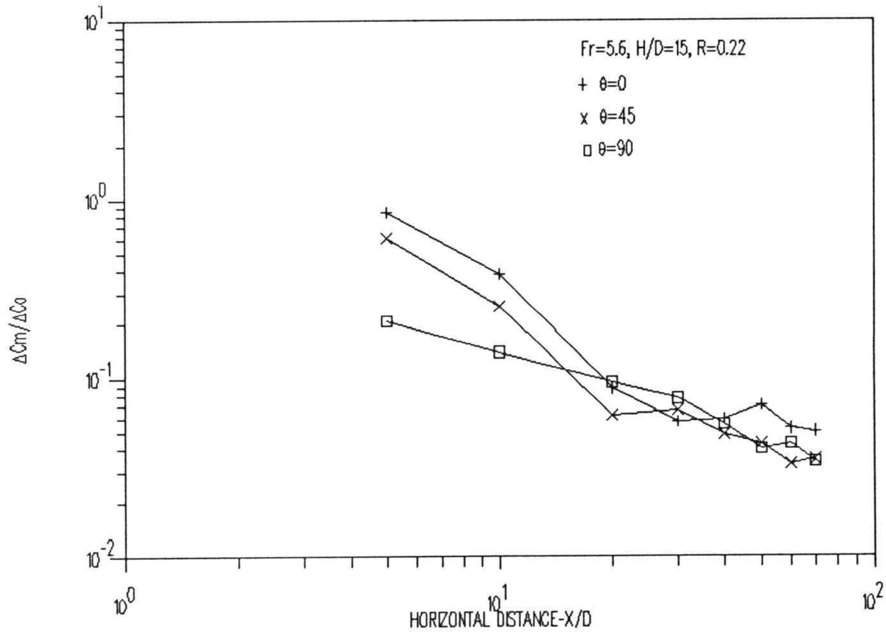

Figure B-71. Effect of varying Θ on maximum concentration deficit for Fr=5.6, H/D=15 and R=0.22.

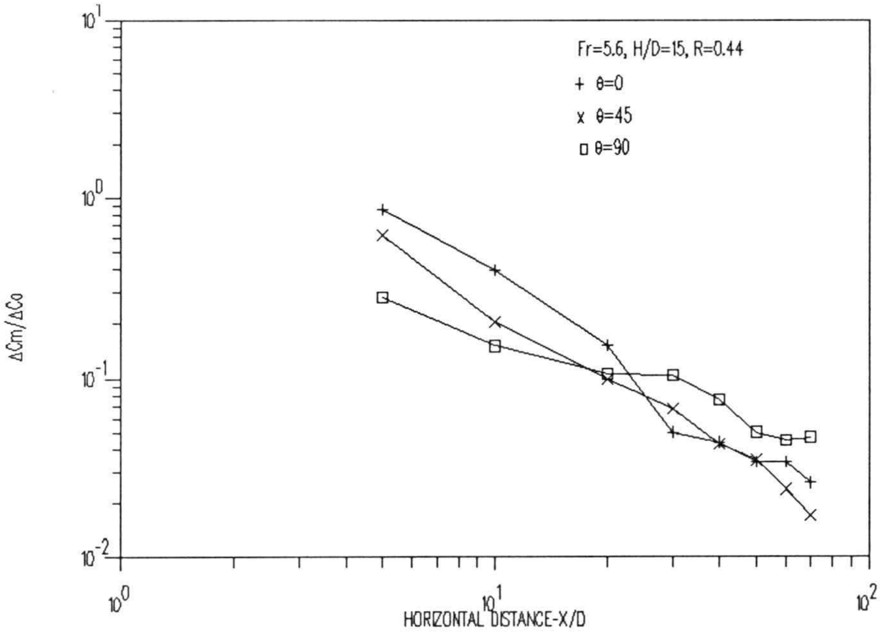

Figure B-72. Effect of varying Θ on maximum concentration deficit for Fr=5.6, H/D=15 and R=0.44.

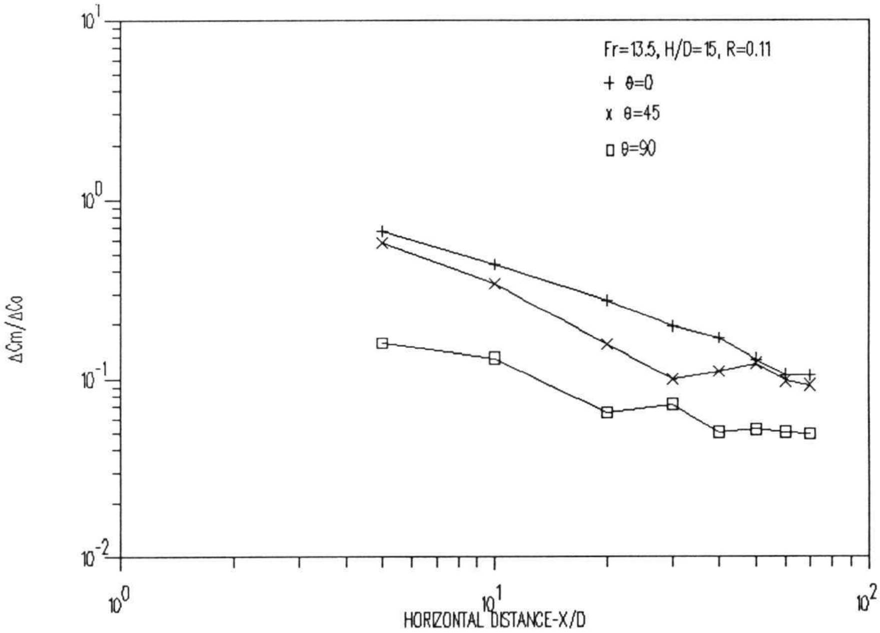

Figure B-73. Effect of varying Θ on maximum concentration deficit for Fr=13.5, H/D=15 and R=0.11.

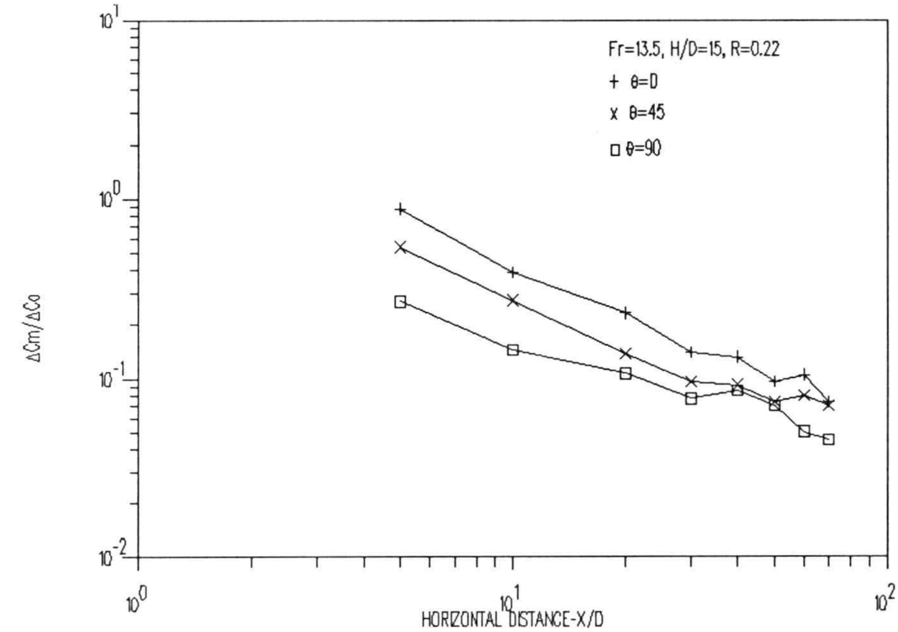

Figure B-74. Effect of varying Θ on maximum concentration deficit for Fr=13.5, H/D=15 and R=0.22.

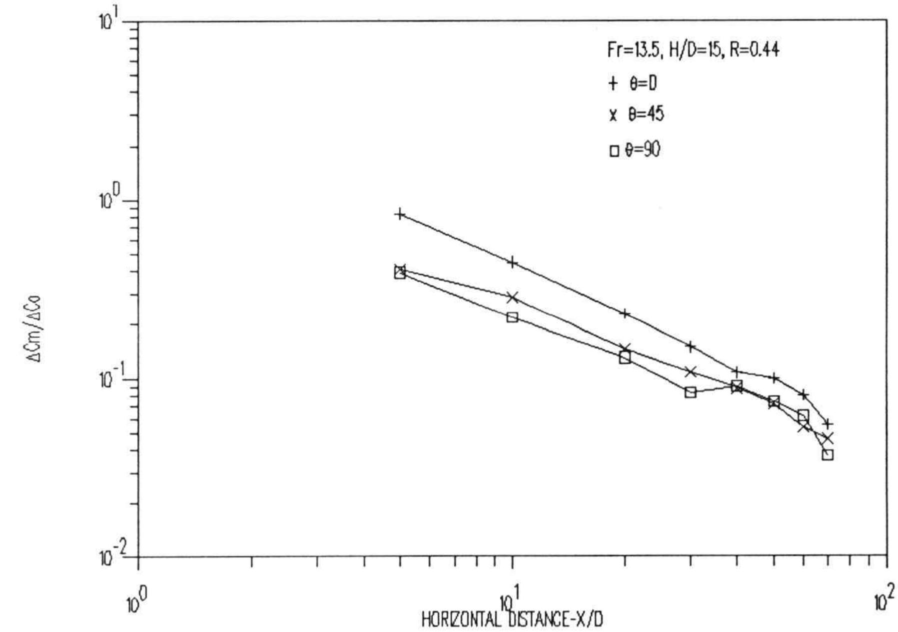

Figure B-75. Effect of varying Θ on maximum concentration deficit for Fr=13.5, H/D=15 and R=0.44.

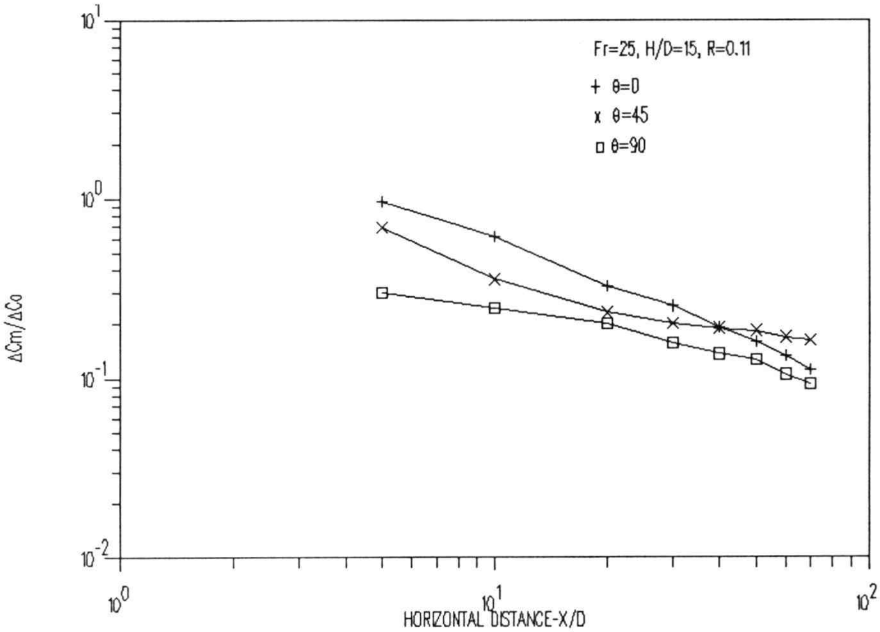

Figure B-76. Effect of varying Θ on maximum concentration deficit for Fr=25, H/D=15 and R=0.11.

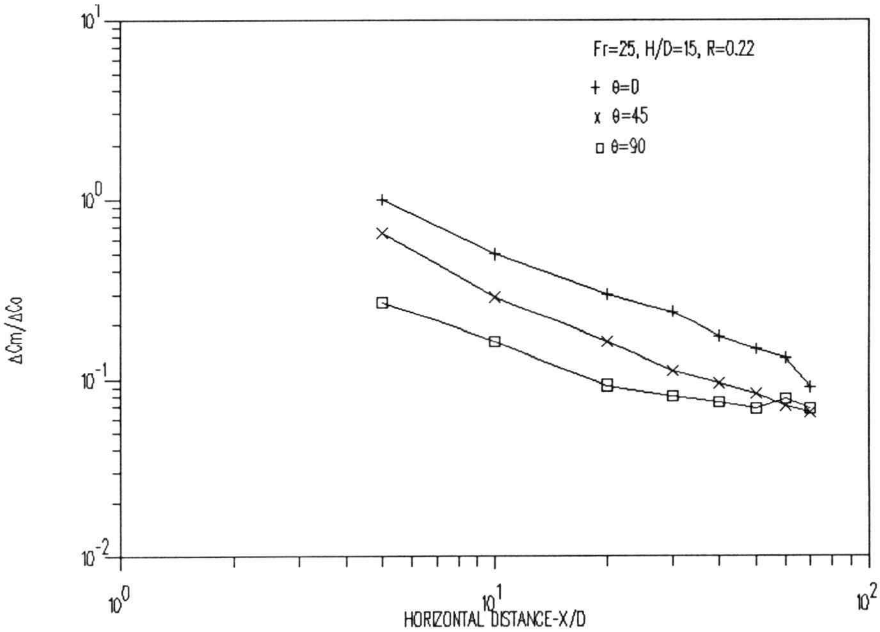

Figure B-77. Effect of varying Θ on maximum concentration deficit for Fr=25, H/D=15 and R=0.22.

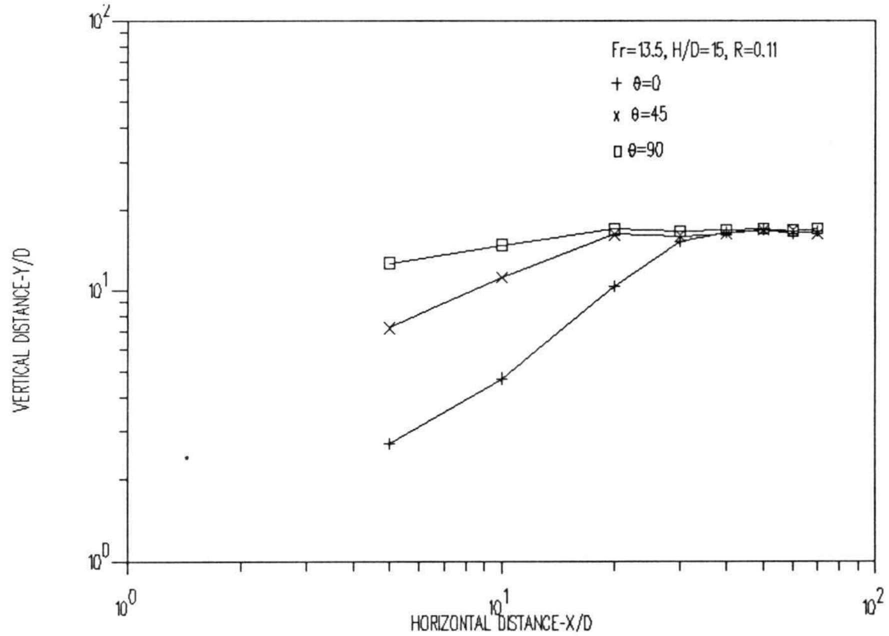

Figure B-78. Effect of varying Θ on trajectory for Fr=13.5, H/D=15 and R=0.11.

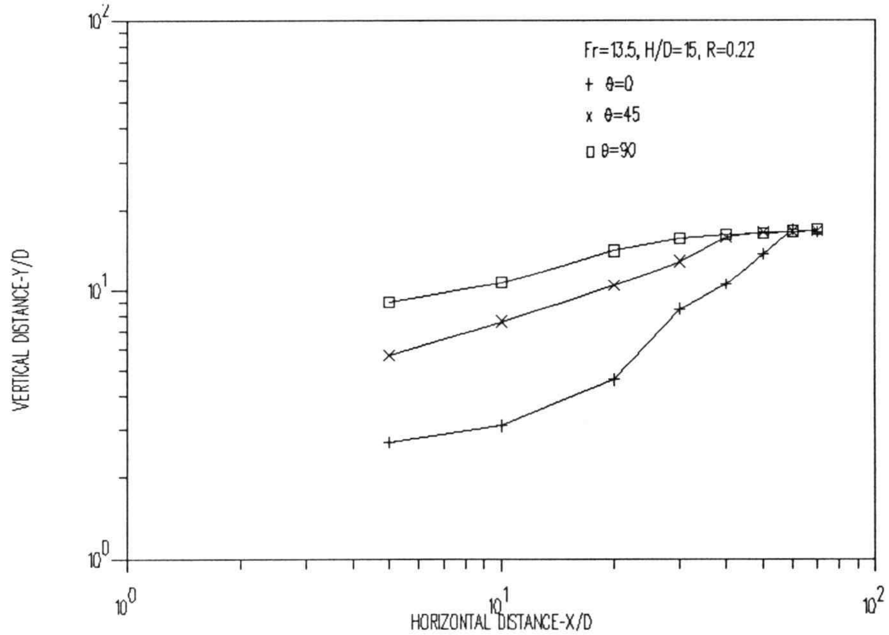

Figure B-79. Effect of varying Θ on trajectory for Fr=13.5, H/D=15 and R=0.22.

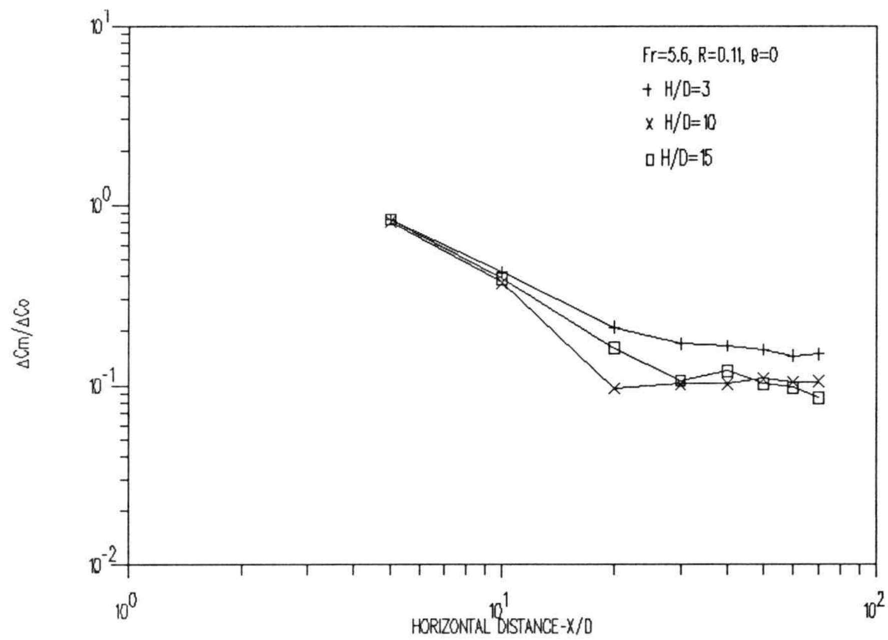

Figure B-80. Effect of varying H/D on maximum concentration deficit for Fr=5.6, R=0.11 and Θ=0°.

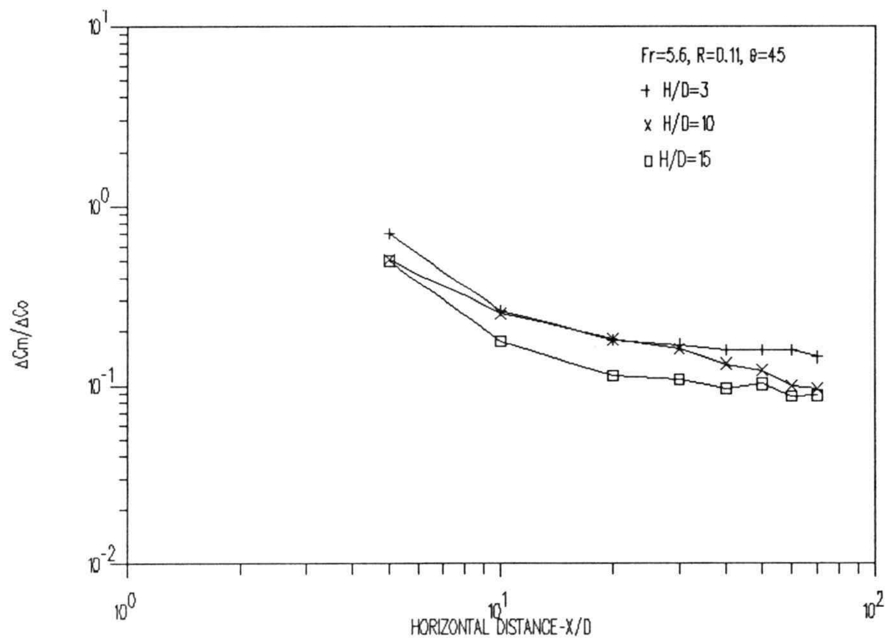

Figure B-81. Effect of varying H/D on maximum concentration deficit for Fr=5.6, R=0.11 and Θ=45°.

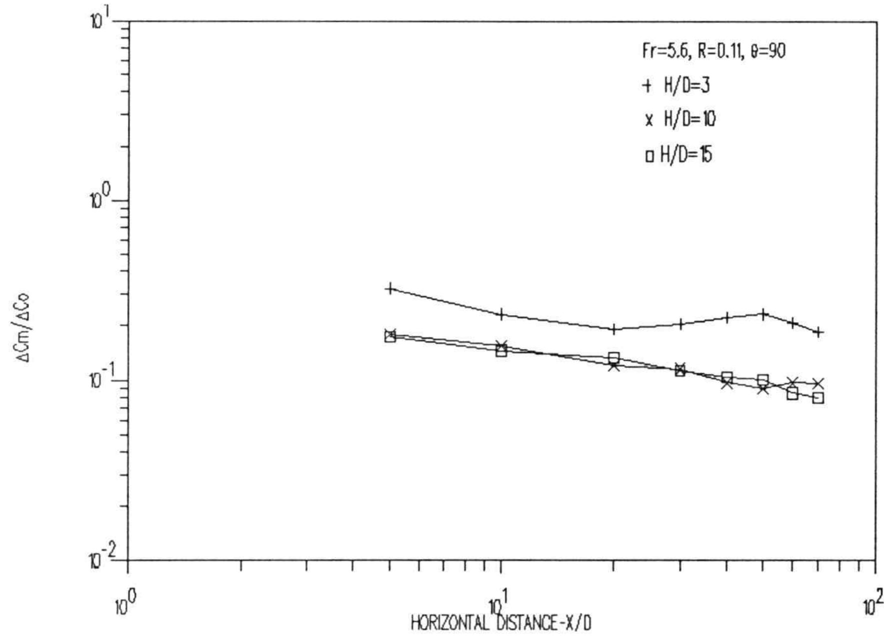

Figure B-82. Effect of varying H/D on maximum concentration deficit for Fr=5.6, R=0.11 and Θ=90°.

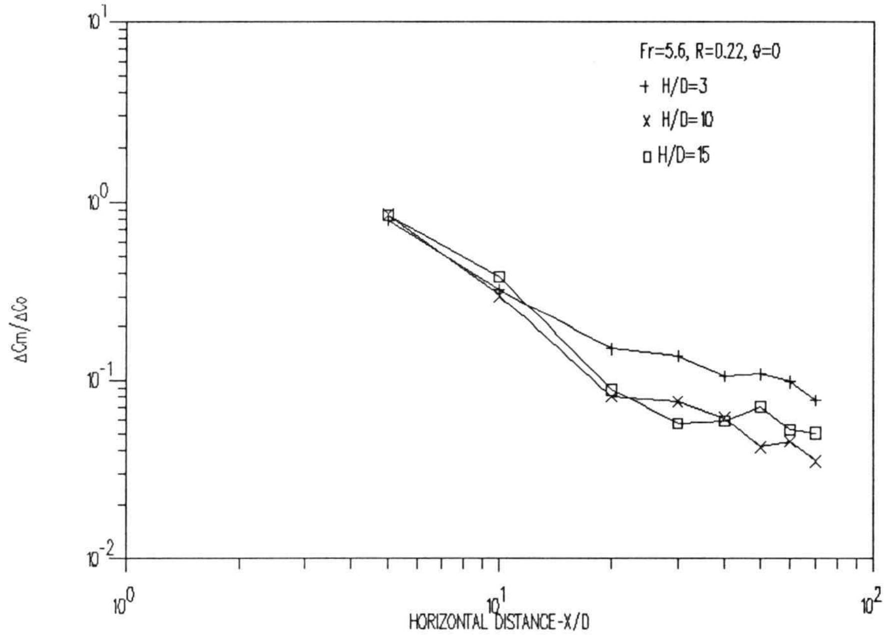

Figure B-83. Effect of varying H/D on maximum concentration deficit for Fr=5.6, R=0.22 and Θ=0°.

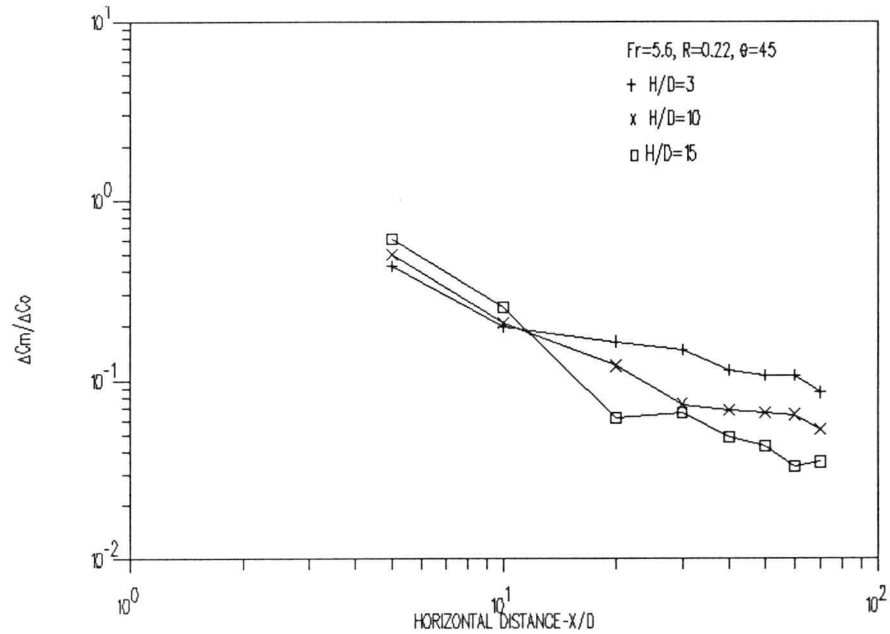

Figure B-84. Effect of varying H/D on maximum concentration deficit for Fr=5.6, R=0.22 and Θ=45°.

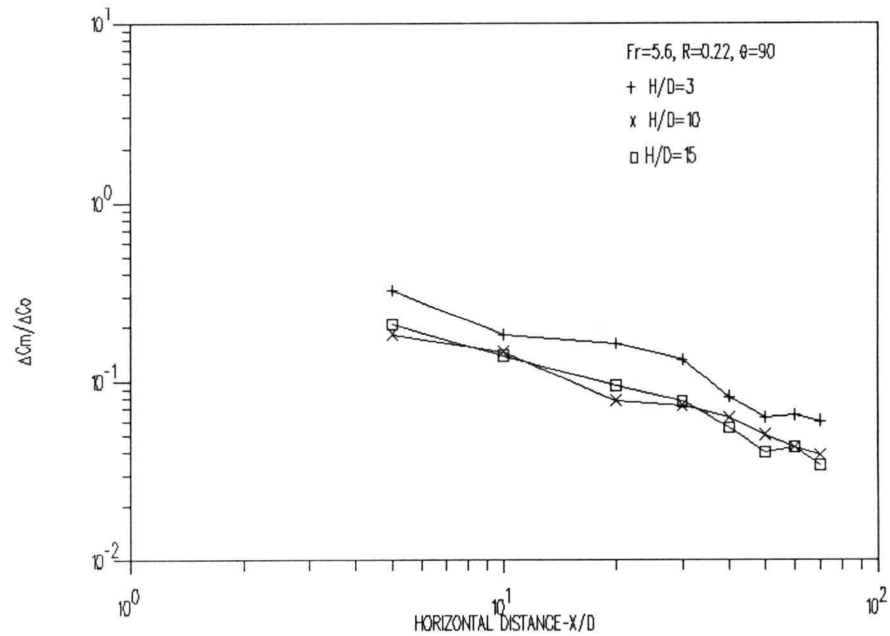

Figure B-85. Effect of varying H/D on maximum concentration deficit for Fr=5.6, R=0.22 and Θ=90°.

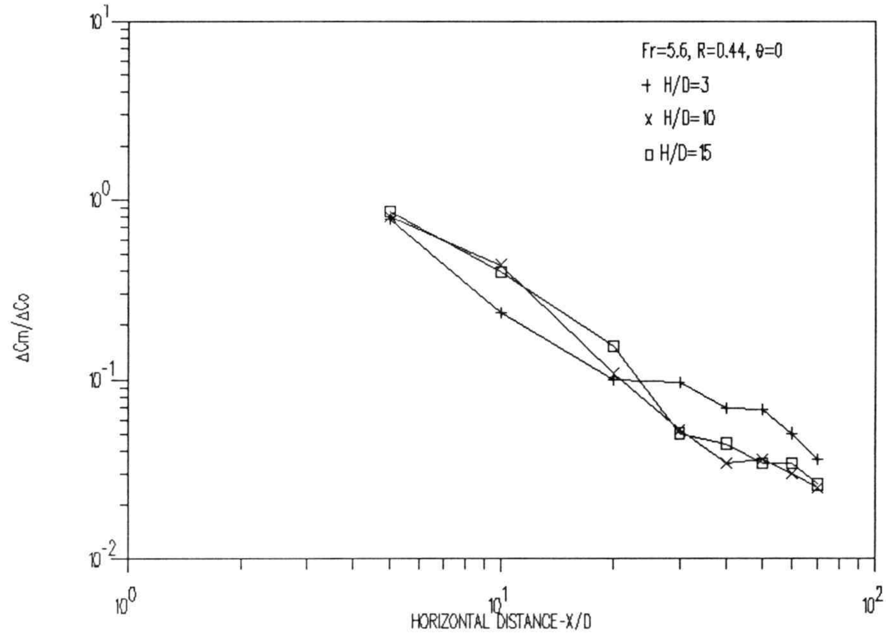

Figure B-86. Effect of varying H/D on maximum concentration deficit for Fr=5.6, R=0.44 and Θ=0°.

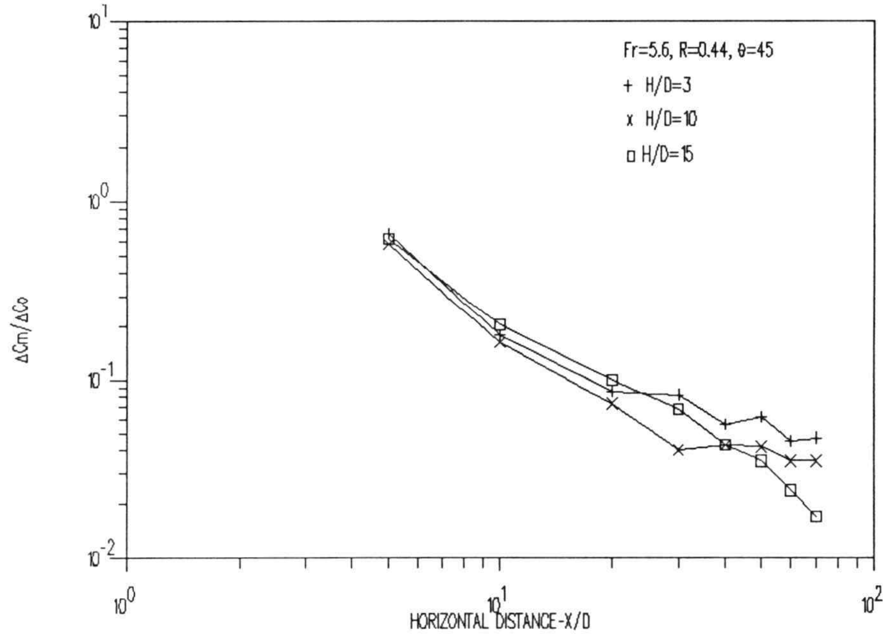

Figure B-87. Effect of varying H/D on maximum concentration deficit for Fr=5.6, R=0.44 and Θ=45°.

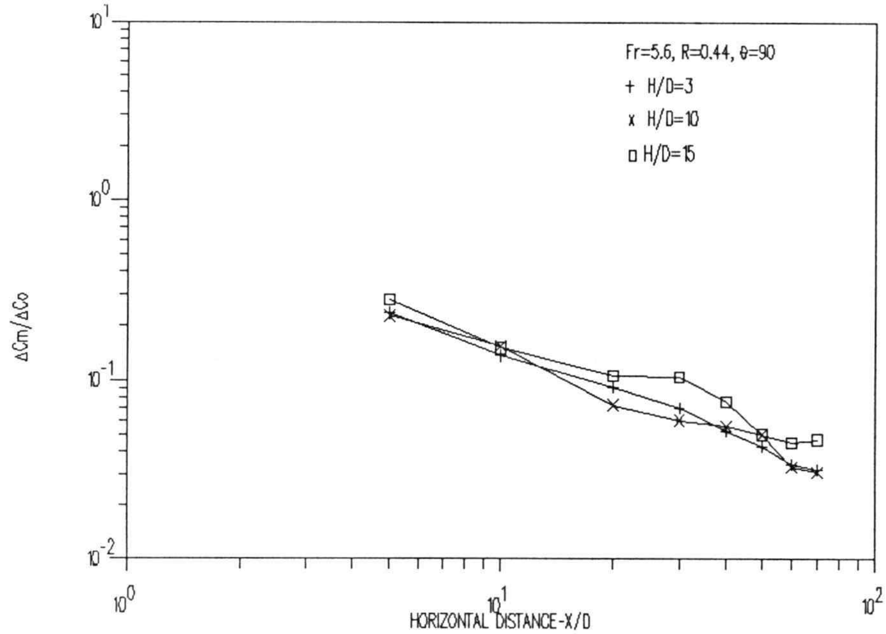

Figure B-88. Effect of varying H/D on maximum concentration deficit for Fr=5.6, R=0.44 and Θ=90°.

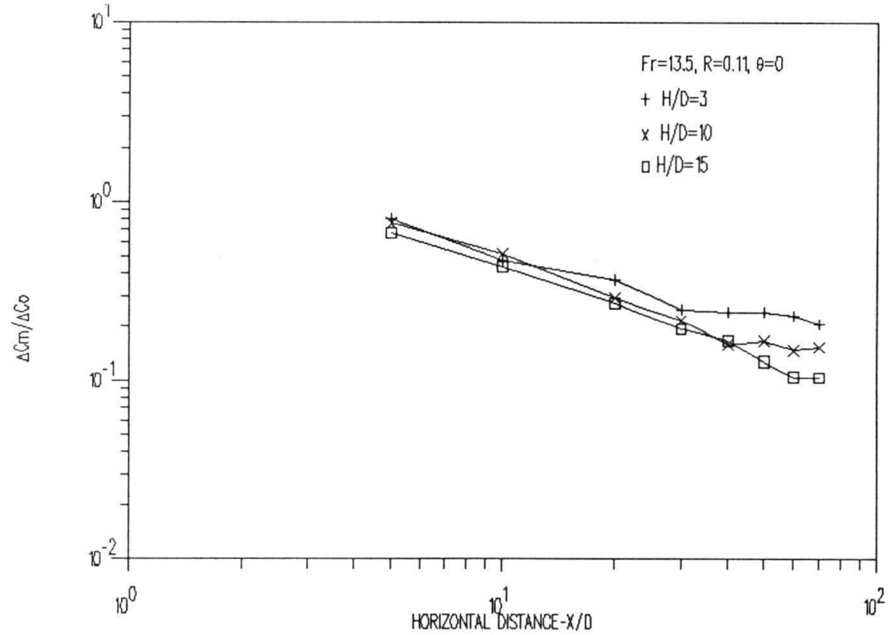

Figure B-89. Effect of varying H/D on maximum concentration deficit for Fr=13.5, R=0.11 and Θ=0°.

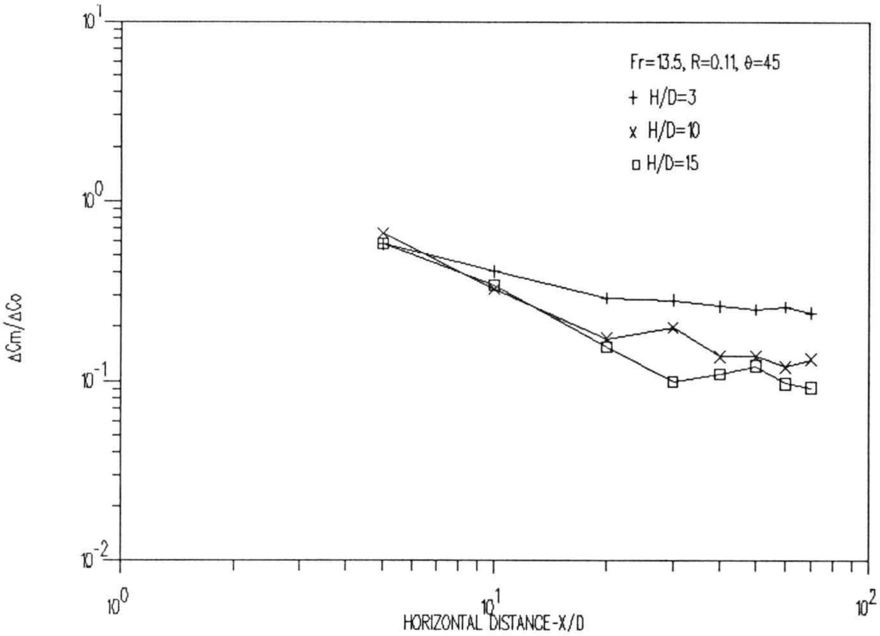

Figure B-90. Effect of varying H/D on maximum concentration deficit for Fr=13.5, R=0.11 and Θ=45°.

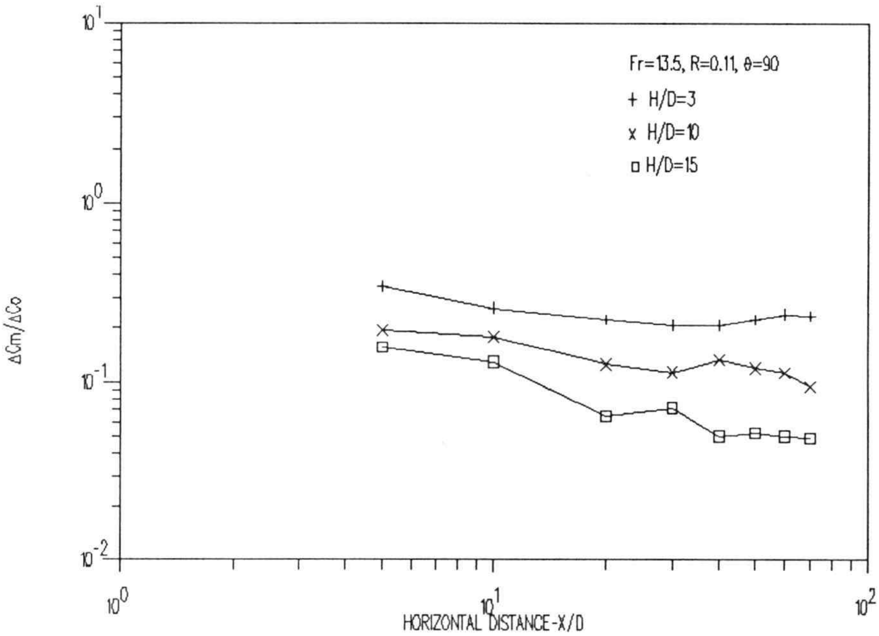

Figure B-91. Effect of varying H/D on maximum concentration deficit for Fr=13.5, R=0.11 and Θ=90°.

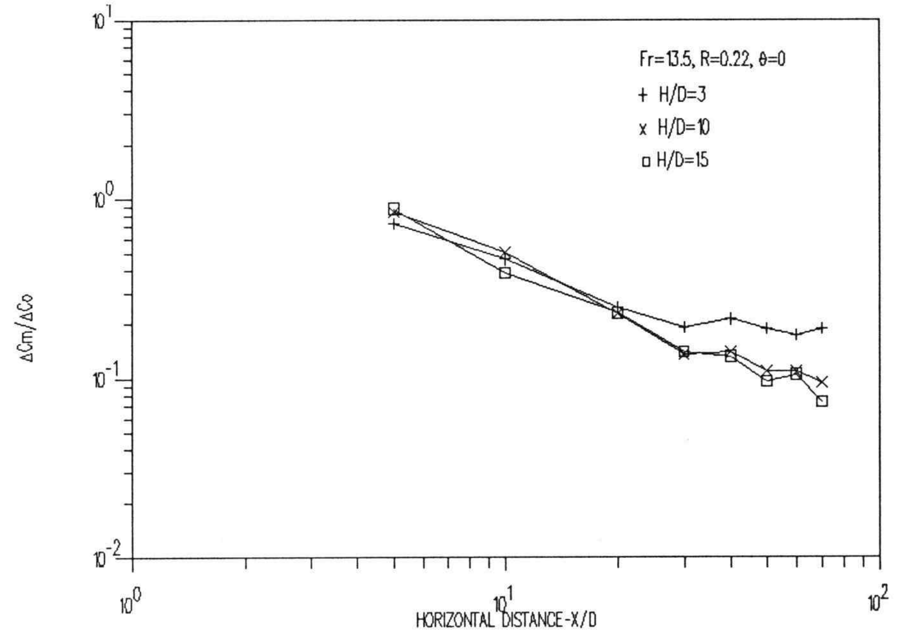

Figure B-92. Effect of varying H/D on maximum concentration deficit for Fr=13.5, R=0.22 and Θ=0°.

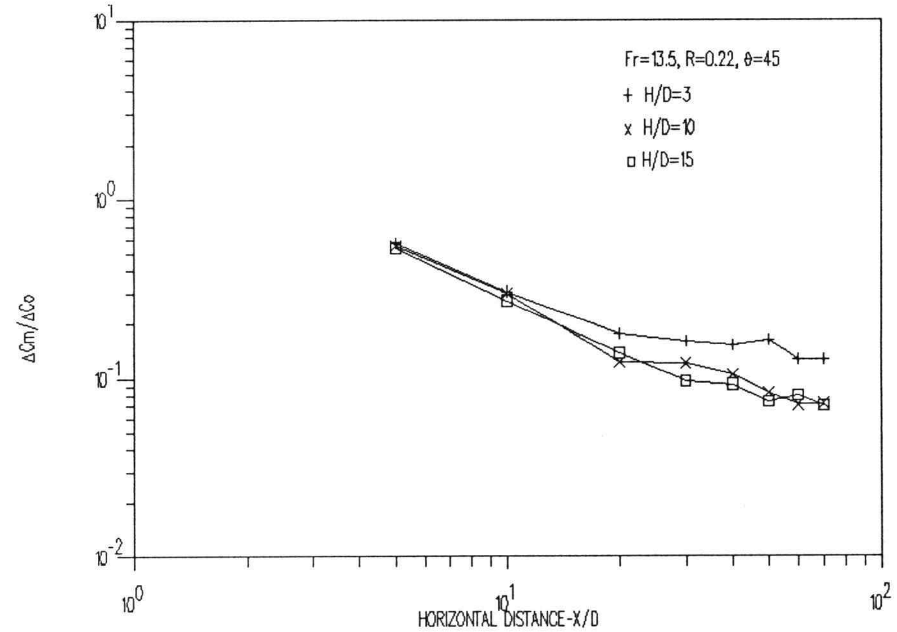

Figure B-93. Effect of varying H/D on maximum concentration deficit for Fr=13.5, R=0.22 and Θ=45°.

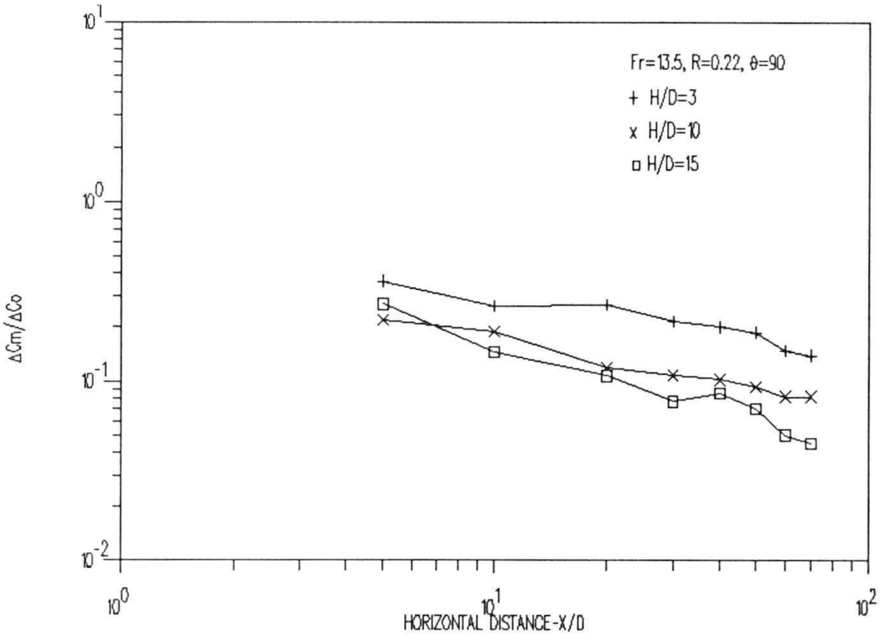

Figure B-94. Effect of varying H/D on maximum concentration deficit for Fr=13.5, R=0.22 and Θ=90°.

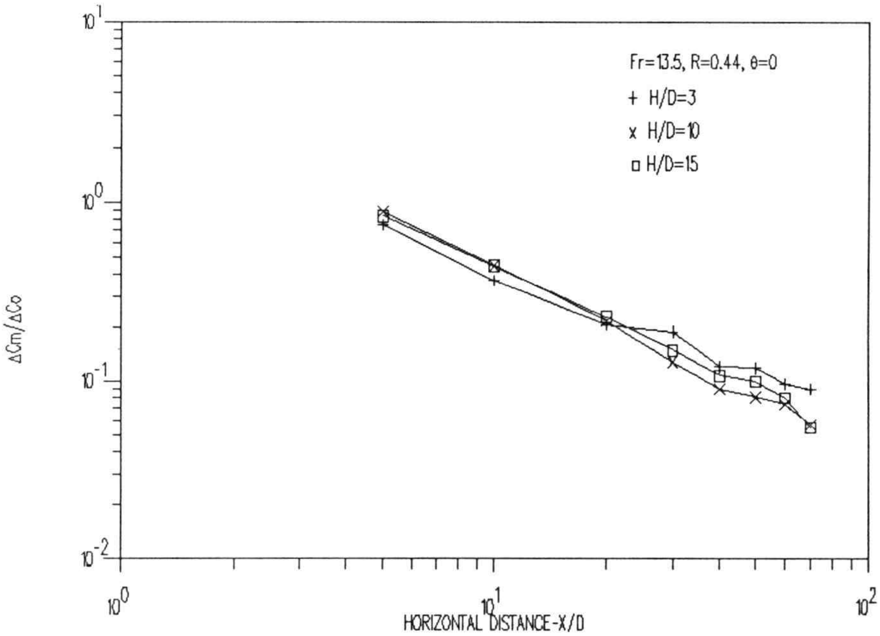

Figure B-95. Effect of varying H/D on maximum concentration deficit for Fr=13.5, R=0.44 and Θ=0°.

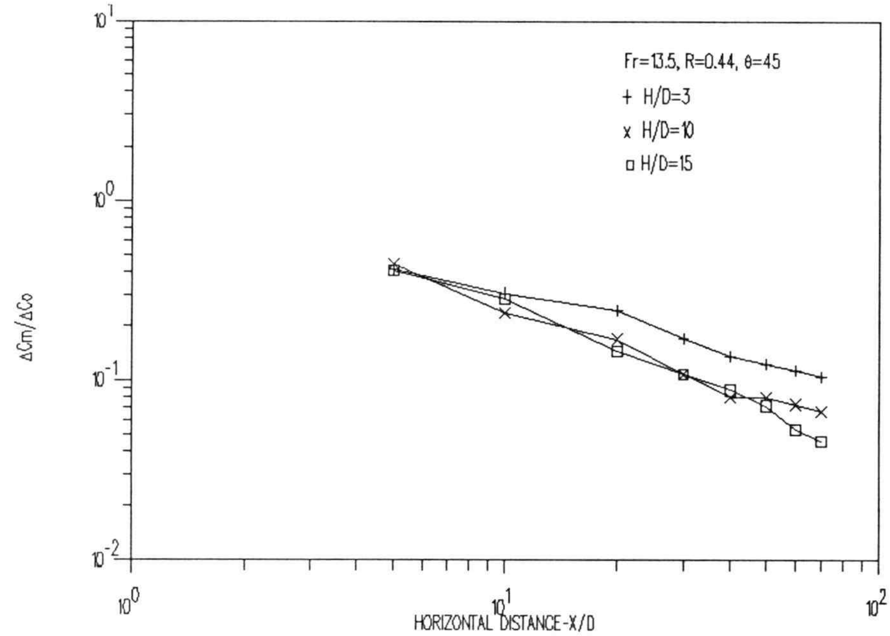

Figure B-96. Effect of varying H/D on maximum concentration deficit for Fr=13.5, R=0.44 and Θ=45°..

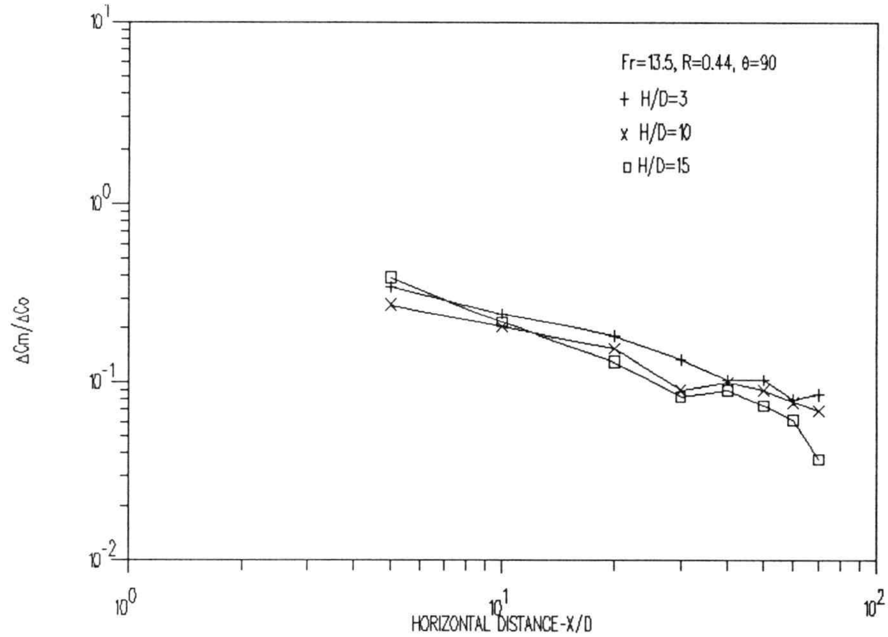

Figure B-97. Effect of varying H/D on maximum concentration deficit for Fr=13.5, R=0.44 and Θ=90.

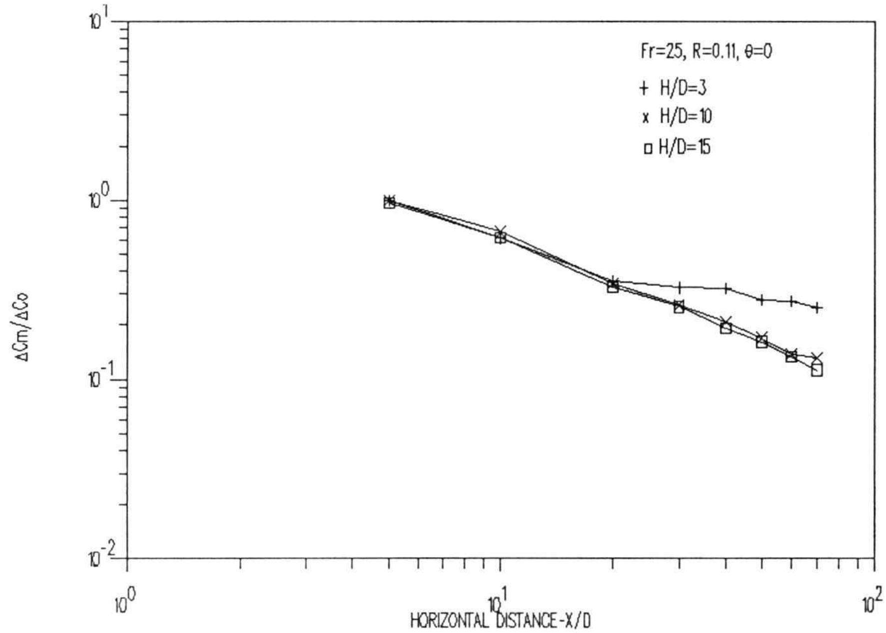

Figure B-98. Effect of varying H/D on maximum concentration deficit for Fr=25, R=0.11 and Θ=0°.

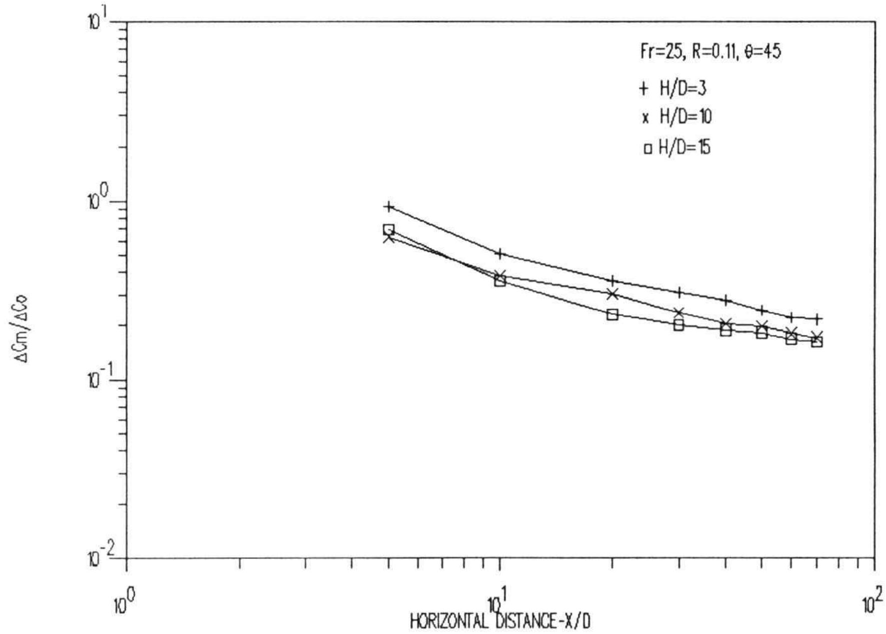

Figure B-99. Effect of varying H/D on maximum concentration deficit for Fr=25, R=0.11 and Θ=45°.

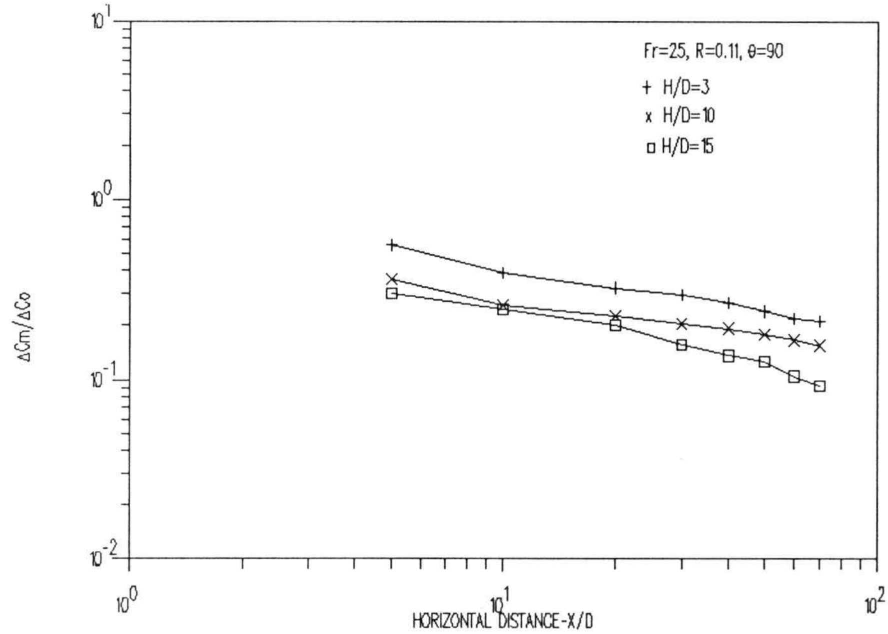

Figure B-100. Effect of varying H/D on maximum concentration deficit for Fr=25, R=0.11 and Θ=90°.

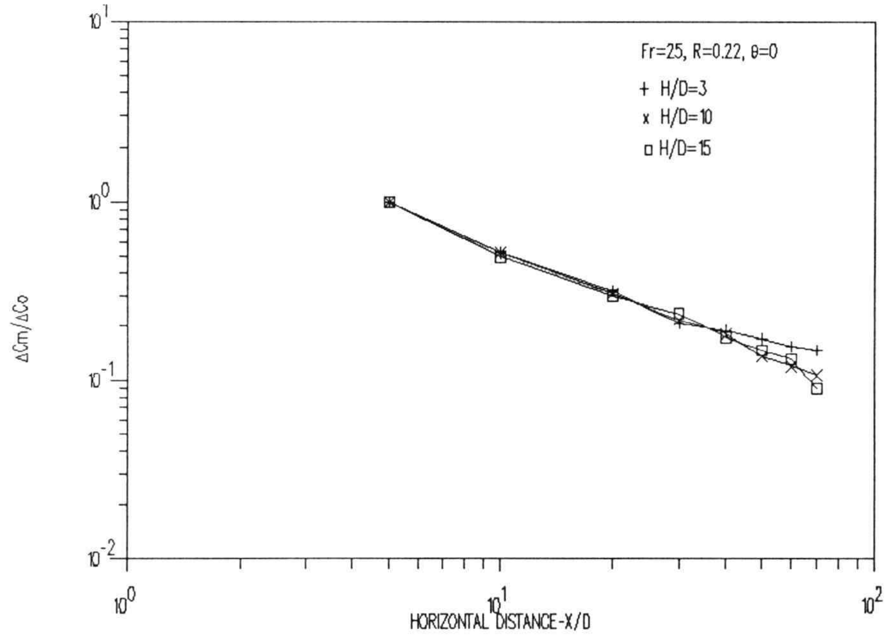

Figure B-101. Effect of varying H/D on maximum concentration deficit for Fr=25, R=0.22 and Θ=0°.

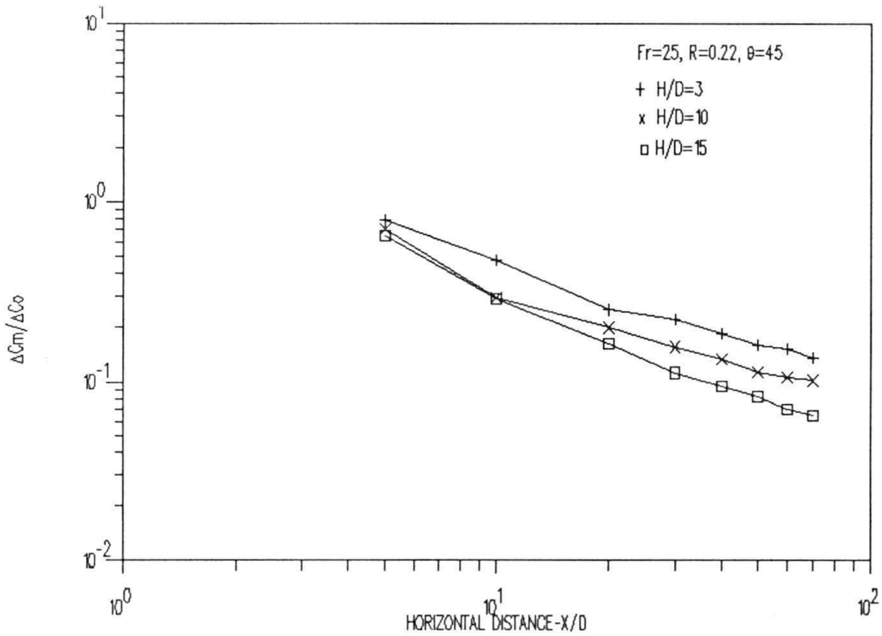

Figure B-102. Effect of varying H/D on maximum concentration deficit for Fr=25, R=0.22 and Θ=45°.

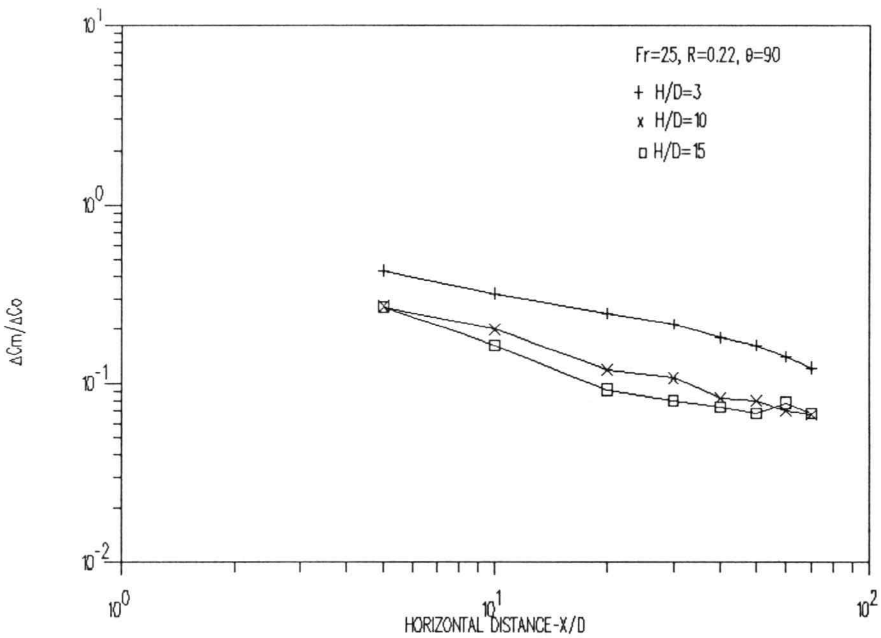

Figure B-103. Effect of varying H/D on maximum concentration deficit for Fr=25, R=0.22 and Θ=90°.

APPENDIX C.

Tabulated Data

θ	Fr	H/D	R	X/D	Y/D	$\Delta C_m/\Delta C_0$
0	5.6	3	0.11	5	2.9	0.833
				10	2.5	0.423
				20	2.8	0.210
				30	2.9	0.170
				40	2.8	0.165
				50	2.8	0.157
				60	2.9	0.146
				70	2.9	0.149
0	5.6	3	0.22	5	2.5	0.796
				10	2.9	0.324
				20	2.9	0.149
				30	2.9	0.135
				40	2.9	0.104
				50	2.9	0.107
				60	2.8	0.097
				70	2.9	0.076
0	5.6	3	0.44	5	0.7	0.780
				10	2.0	0.233
				20	2.8	0.100
				30	2.8	0.096
				40	2.9	0.069
				50	2.9	0.068
				60	2.9	0.050
				70	2.9	0.036
0	5.6	10	0.11	5	1.9	0.809
				10	4.0	0.368
				20	9.5	0.096
				30	9.0	0.102
				40	9.4	0.102
				50	9.6	0.109
				60	9.9	0.104
				70	9.9	0.105
0	5.6	10	0.22	5	0.7	0.850
				10	3.3	0.302
				20	8.3	0.080
				30	9.8	0.075
				40	9.9	0.061
				50	9.3	0.042
				60	9.3	0.045
				70	9.9	0.035
0	5.6	10	0.44	5	0.5	0.802

θ	Fr	H/D	R	X/D	Y/D	$\Delta C_m/\Delta C_0$
0	5.6	10	0.44	10	2.0	0.434
				20	3.6	0.107
				30	6.1	0.052
				40	7.3	0.034
				50	9.3	0.036
				60	9.8	0.030
				70	9.9	0.025
0	5.6	15	0.11	5	1.1	0.832
				10	4.5	0.387
				20	14.5	0.161
				30	14.9	0.106
				40	14.8	0.120
				50	14.9	0.102
				60	14.5	0.097
				70	14.7	0.085
0	5.6	15	0.22	5	1.6	0.845
				10	2.0	0.382
				20	7.4	0.088
				30	10.1	0.057
				40	14.9	0.059
				50	14.7	0.070
				60	14.9	0.052
				70	14.9	0.050
0	5.6	15	0.44	5	0.6	0.863
				10	1.9	0.397
				20	4.6	0.152
				30	5.2	0.050
				40	7.5	0.044
				50	10.0	0.034
				60	12.0	0.034
				70	14.9	0.026
0	13.5	3	0.11	5	1.0	0.808
				10	2.8	0.474
				20	2.9	0.371
				30	2.9	0.255
				40	2.9	0.245
				50	2.9	0.245
				60	2.9	0.233
				70	2.9	0.209
0	13.5	3	0.22	5	0.8	0.730
				10	1.4	0.465
				20	2.8	0.250
				30	2.8	0.192
				40	2.9	0.214

θ	Fr	H/D	R	X/D	Y/D	$\Delta C_m/\Delta C_0$
0	13.5	3	0.22	50	2.8	0.188
				60	2.9	0.173
				70	2.9	0.188
0	13.5	3	0.44	5	0.6	0.751
				10	1.1	0.372
				20	2.5	0.207
				30	2.8	0.190
				40	2.9	0.120
				50	2.7	0.118
				60	2.8	0.096
				70	2.9	0.090
0	13.5	10	0.11	5	1.3	0.759
				10	2.9	0.518
				20	8.0	0.293
				30	9.9	0.220
				40	9.7	0.161
				50	9.9	0.168
				60	9.5	0.149
				70	9.8	0.154
0	13.5	10	0.22	5	0.9	0.847
				10	0.8	0.508
				20	4.3	0.229
				30	6.5	0.136
				40	9.0	0.140
				50	9.9	0.110
				60	9.6	0.109
				70	9.9	0.095
0	13.5	10	0.44	5	0.4	0.886
				10	0.8	0.449
				20	1.1	0.219
				30	2.2	0.128
				40	2.7	0.090
				50	3.5	0.081
				60	4.8	0.074
				70	5.9	0.057
0	13.5	15	0.11	5	0.7	0.670
				10	2.7	0.438
				20	8.3	0.276
				30	13.2	0.194
				40	14.4	0.168
				50	14.7	0.128
				60	14.2	0.105
				70	14.5	0.104

θ	Fr	H/D	R	X/D	Y/D	$\Delta C_m/\Delta C_0$
0	13.5	15	0.22	5	0.7	0.878
				10	1.1	0.391
				20	2.6	0.232
				30	6.5	0.140
				40	8.5	0.132
				50	11.7	0.096
				60	14.9	0.105
				70	14.5	0.074
0	13.5	15	0.44	5	0.0	0.837
				10	1.2	0.448
				20	2.5	0.231
				30	2.8	0.149
				40	3.1	0.107
				50	4.3	0.099
				60	5.8	0.080
				70	7.5	0.055
0	25.0	3	0.11	5	0.3	0.990
				10	0.5	0.612
				20	1.0	0.351
				30	2.5	0.323
				40	2.9	0.320
				50	2.9	0.276
				60	2.9	0.271
				70	2.9	0.248
0	25.0	3	0.22	5	0.1	0.999
				10	0.3	0.520
				20	1.0	0.319
				30	1.0	0.208
				40	2.5	0.190
				50	2.9	0.170
				60	2.9	0.154
				70	2.9	0.148
0	25.0	10	0.11	5	0.5	0.999
				10	0.5	0.666
				20	1.6	0.343
				30	3.5	0.258
				40	6.2	0.208
				50	7.0	0.169
				60	8.5	0.138
				70	9.9	0.131
0	25.0	10	0.22	5	0.3	0.999
				10	0.3	0.525
				20	0.5	0.308

θ	Fr	H/D	R	X/D	Y/D	$\Delta C_m/\Delta C_0$
0	25.0	10	0.22	30	0.5	0.218
				40	2.8	0.181
				50	3.3	0.136
				60	5.0	0.120
				70	5.5	0.107
0	25.0	15	0.11	5	0.5	0.958
				10	0.5	0.617
				20	1.2	0.325
				30	2.6	0.252
				40	5.6	0.191
				50	7.5	0.161
				60	9.4	0.134
				70	12.1	0.112
0	25.0	15	0.22	5	0.4	0.999
				10	0.3	0.496
				20	0.3	0.301
				30	0.5	0.239
				40	2.0	0.173
				50	3.5	0.148
				60	4.9	0.131
				70	6.0	0.090
45	5.6	3	0.11	10	2.9	0.263
				20	2.9	0.180
				30	2.9	0.169
				40	2.8	0.158
				50	2.9	0.158
				60	2.9	0.157
				70	2.9	0.144
45	5.6	3	0.22	5	2.8	0.433
				10	2.8	0.199
				20	2.8	0.164
				30	2.8	0.147
				40	2.9	0.113
				50	2.9	0.106
				60	2.8	0.106
				70	2.9	0.085
45	5.6	3	0.44	5	2.5	0.662
				10	2.9	0.179
				20	2.9	0.086
				30	2.9	0.082
				40	2.9	0.056
				50	2.9	0.062
				60	2.8	0.045

θ	Fr	H/D	R	X/D	Y/D	$\Delta C_m/\Delta C_0$
45	5.6	3	0.44	70	2.9	0.047
45	5.6	10	0.11	5	6.4	0.506
				10	9.9	0.252
				20	9.7	0.181
				30	9.9	0.160
				40	9.9	0.132
				50	9.9	0.122
				60	9.9	0.099
				70	9.9	0.096
45	5.6	10	0.22	5	4.9	0.500
				10	6.4	0.208
				20	9.9	0.120
				30	9.8	0.073
				40	9.8	0.068
				50	9.7	0.066
				60	9.9	0.064
				70	9.9	0.053
45	5.6	10	0.44	5	3.1	0.578
				10	5.0	0.163
				20	6.3	0.073
				30	8.0	0.040
				40	9.7	0.043
				50	9.9	0.042
				60	9.8	0.035
				70	9.9	0.035
45	5.6	15	0.11	5	6.1	0.498
				10	9.0	0.177
				20	14.9	0.113
				30	14.4	0.108
				40	14.8	0.096
				50	14.9	0.102
				60	14.9	0.087
				70	14.9	0.088
45	5.6	15	0.22	5	4.0	0.608
				10	6.5	0.253
				20	8.4	0.062
				30	14.7	0.066
				40	14.8	0.048
				50	14.9	0.043
				60	14.9	0.033
				70	14.9	0.035
45	5.6	15	0.44	5	3.4	0.618

θ	Fr	H/D	R	X/D	Y/D	$\Delta C_m/\Delta C_0$
45	5.6	45	0.44	10	4.3	0.206
				20	5.8	0.099
				30	7.2	0.068
				40	11.0	0.043
				50	12.0	0.035
				60	14.9	0.024
				70	14.9	0.017
45	13.5	3	0.11	5	2.8	0.574
				10	2.9	0.406
				20	2.9	0.290
				30	2.9	0.282
				40	2.9	0.260
				50	2.9	0.251
				60	2.9	0.259
				70	2.9	0.239
45	13.5	3	0.22	5	2.7	0.570
				10	2.9	0.306
				20	2.9	0.176
				30	2.9	0.160
				40	2.9	0.153
				50	2.9	0.163
				60	2.9	0.127
				70	2.9	0.127
45	13.5	3	0.44	5	1.6	0.416
				10	2.7	0.306
				20	2.8	0.245
				30	2.9	0.171
				40	2.9	0.135
				50	2.9	0.123
				60	2.9	0.113
				70	2.9	0.104
45	13.5	10	0.11	5	5.4	0.660
				10	7.8	0.326
				20	9.4	0.172
				30	9.8	0.199
				40	9.8	0.137
				50	9.9	0.137
				60	9.2	0.120
				70	9.9	0.132
45	13.5	10	0.22	5	3.4	0.552
				10	6.2	0.298
				20	9.3	0.123
				30	9.4	0.121

θ	Fr	H/D	R	X/D	Y/D	$\Delta C_m/\Delta C_0$
45	13.5	10	0.22	40	9.8	0.104
				50	9.7	0.083
				60	9.5	0.071
				70	9.9	0.072
45	13.5	10	0.44	5	1.7	0.446
				10	3.3	0.237
				20	4.2	0.169
				30	4.9	0.108
				40	6.4	0.080
				50	8.8	0.080
				60	8.9	0.073
				70	9.8	0.067
45	13.5	15	0.11	5	5.2	0.578
				10	9.1	0.343
				20	14.1	0.155
				30	13.9	0.099
				40	14.2	0.110
				50	14.7	0.122
				60	14.6	0.097
				70	14.2	0.092
45	13.5	15	0.22	5	3.7	0.537
				10	5.6	0.273
				20	8.4	0.138
				30	10.9	0.096
				40	13.8	0.092
				50	14.5	0.074
				60	14.6	0.080
				70	14.7	0.070
45	13.5	15	0.44	5	3.3	0.411
				10	4.3	0.284
				20	4.7	0.145
				30	4.8	0.108
				40	7.0	0.088
				50	7.5	0.072
				60	7.8	0.053
				70	14.8	0.046
45	25.0	3	0.11	5	2.9	0.930
				10	2.9	0.507
				20	2.9	0.358
				30	2.9	0.310
				40	2.9	0.280
				50	2.9	0.246
				60	2.9	0.223

θ	Fr	H/D	R	X/D	Y/D	$\Delta C_m/\Delta C_0$
45	25.0	0	0.11	70	2.9	0.217
45	25.0	3	0.22	5	2.9	0.784
				10	2.9	0.475
				20	2.9	0.252
				30	2.9	0.221
				40	2.9	0.186
				50	2.9	0.160
				60	2.9	0.152
				70	2.9	0.135
45	25.0	10	0.11	5	6.4	0.633
				10	9.5	0.385
				20	9.8	0.305
				30	9.9	0.237
				40	9.9	0.204
				50	9.9	0.199
				60	9.9	0.181
				70	9.9	0.172
45	25.0	10	0.22	5	3.4	0.707
				10	7.8	0.293
				20	9.4	0.200
				30	9.5	0.156
				40	9.9	0.134
				50	9.8	0.113
				60	9.9	0.106
				70	9.9	0.102
45	25.0	15	0.11	5	7.2	0.697
				10	9.5	0.357
				20	14.2	0.232
				30	14.7	0.202
				40	14.9	0.190
				50	14.9	0.184
				60	14.8	0.169
				70	14.9	0.163
45	25.0	15	0.22	5	5.5	0.649
				10	7.7	0.288
				20	9.0	0.163
				30	11.9	0.112
				40	13.0	0.095
				50	14.0	0.083
				60	14.3	0.070
				70	14.9	0.065
90	5.6	3	0.11	5	2.8	0.322

θ	Fr	H/D	R	X/D	Y/D	$\Delta C_m/\Delta C_0$
90	5.6	3	0.11	10	2.9	0.231
				20	2.9	0.191
				30	2.9	0.204
				40	2.9	0.222
				50	2.9	0.232
				60	2.9	0.208
				70	2.9	0.186
90	5.6	3	0.22	5	2.9	0.324
				10	2.9	0.183
				20	2.9	0.162
				30	2.9	0.131
				40	2.9	0.082
				50	2.9	0.063
				60	2.9	0.065
				70	2.9	0.060
90	5.6	3	0.44	5	2.9	0.236
				10	2.9	0.137
				20	2.9	0.092
				30	2.9	0.070
				40	2.9	0.052
				50	2.9	0.043
				60	2.9	0.034
				70	2.9	0.032
90	5.6	10	0.11	5	9.8	0.180
				10	9.9	0.154
				20	9.7	0.121
				30	9.9	0.116
				40	9.9	0.097
				50	9.9	0.090
				60	9.9	0.097
				70	9.9	0.096
90	5.6	10	0.22	5	7.0	0.184
				10	9.8	0.146
				20	9.9	0.078
				30	9.9	0.073
				40	9.9	0.063
				50	9.9	0.050
				60	9.9	0.043
				70	9.9	0.039
90	5.6	10	0.44	5	3.9	0.228
				10	5.1	0.154
				20	6.9	0.073
				30	7.3	0.060

θ	Fr	H/D	R	X/D	Y/D	$\Delta C_m/\Delta C_0$
90	5.6	10	0.44	40	9.5	0.056
				50	9.9	0.050
				60	9.9	0.033
				70	9.9	0.031
90	5.6	15	0.11	5	9.0	0.173
				10	14.4	0.146
				20	14.5	0.134
				30	14.9	0.113
				40	14.9	0.104
				50	14.8	0.101
				60	14.9	0.085
				70	14.9	0.080
90	5.6	15	0.22	5	7.3	0.207
				10	9.9	0.139
				20	14.3	0.094
				30	14.3	0.077
				40	14.9	0.055
				50	14.9	0.040
				60	14.9	0.043
				70	14.9	0.034
90	5.6	15	0.44	5	4.0	0.281
				10	4.2	0.151
				20	7.8	0.106
				30	8.5	0.104
				40	11.3	0.076
				50	12.9	0.050
				60	14.9	0.045
				70	14.9	0.047
90	13.5	3	0.11	5	2.8	0.346
				10	2.9	0.264
				20	2.9	0.225
				30	2.9	0.210
				40	3.0	0.210
				50	2.9	0.227
				60	2.9	0.243
				70	2.9	0.237
90	13.5	3	0.22	5	2.9	0.361
				10	2.9	0.263
				20	2.9	0.267
				30	2.9	0.216
				40	2.9	0.200
				50	2.9	0.187
				60	2.9	0.148

θ	Fr	H/D	R	X/D	Y/D	$\Delta C_m/\Delta C_0$
90	13.5	3	0.22	70	2.9	0.139
90	13.5	3	0.44	5	2.9	0.348
				10	2.9	0.245
				20	2.9	0.183
				30	2.9	0.133
				40	2.9	0.103
				50	2.9	0.103
				60	2.9	0.080
				70	2.9	0.085
90	13.5	10	0.11	5	9.7	0.196
				10	9.8	0.179
				20	9.9	0.126
				30	9.9	0.114
				40	9.7	0.134
				50	9.9	0.120
				60	9.7	0.113
				70	9.7	0.095
90	13.5	10	0.22	5	6.0	0.220
				10	8.6	0.188
				20	9.6	0.119
				30	9.5	0.108
				40	9.7	0.102
				50	9.9	0.093
				60	9.9	0.082
				70	9.9	0.082
90	13.5	10	0.44	5	3.2	0.277
				10	3.4	0.206
				20	6.0	0.154
				30	5.1	0.090
				40	6.4	0.099
				50	7.7	0.090
				60	9.8	0.077
				70	9.7	0.069
90	13.5	15	0.11	5	10.6	0.158
				10	12.7	0.130
				20	14.8	0.065
				30	14.5	0.072
				40	14.7	0.050
				50	14.9	0.052
				60	14.6	0.050
				70	14.9	0.049
90	13.5	15	0.22	5	7.0	0.269

θ	Fr	H/D	R	X/D	Y/D	$\Delta C_m/\Delta C_0$
90	13.5	15	0.22	10	8.7	0.145
				20	12.1	0.107
				30	13.6	0.077
				40	14.2	0.086
				50	14.4	0.070
				60	14.6	0.050
				70	14.9	0.045
90	13.5	15	0.44	5	3.1	0.392
				10	5.6	0.220
				20	5.9	0.130
				30	7.0	0.083
				40	9.1	0.090
				50	9.5	0.074
				60	10.1	0.062
				70	11.5	0.037
90	25.0	3	0.11	5	2.9	0.556
				10	2.9	0.390
				20	2.9	0.322
				30	2.9	0.295
				40	2.9	0.267
				50	2.9	0.240
				60	2.9	0.218
				70	2.9	0.211
90	25.0	3	0.22	5	2.9	0.434
				10	2.9	0.322
				20	2.9	0.248
				30	2.9	0.215
				40	2.9	0.180
				50	2.9	0.162
				60	2.9	0.140
				70	2.9	0.122
90	25.0	10	0.11	5	9.9	0.357
				10	9.9	0.259
				20	9.9	0.227
				30	9.8	0.205
				40	9.7	0.193
				50	9.8	0.180
				60	9.9	0.167
				70	9.9	0.156
90	25.0	10	0.22	5	9.0	0.273
				10	9.5	0.200
				20	9.9	0.119
				30	9.8	0.107

θ	Fr	H/D	R	X/D	Y/D	$\Delta C_m/\Delta C_0$
90	25.0	10	0.22	40	9.6	0.083
				50	9.9	0.080
				60	9.8	0.070
				70	9.9	0.067
90	25.0	15	0.11	5	14.5	0.298
				10	14.7	0.244
				20	14.9	0.202
				30	14.9	0.158
				40	14.9	0.137
				50	14.9	0.127
				60	14.9	0.105
				70	14.9	0.093
90	25.0	15	0.22	5	8.3	0.272
				10	9.0	0.162
				20	11.5	0.092
				30	12.5	0.080
				40	13.5	0.074
				50	14.5	0.068
				60	14.8	0.078
				70	14.5	0.068